UNITED STATES
NAVAL POSTGRADUATE SCHOOL

VISCOELASTIC FRACTURE
AN EXPOSITORY TREATMENT OF POLYMER FAILURE

by

Gerald H. Lindsey

1 November 1967

NAVAL POSTGRADUATE SCHOOL
Monterey, California

Rear Admiral R. W. McNitt, USN
Superintendent

R. F. Rinehart
Academic Dean

ABSTRACT:

Fracture in viscoelastic materials is discussed here as an extension of elastic fracture. Using continuum theory, three broad approaches are treated in detail, including energy failure surfaces and cumulative damage. Typical experimental work is reported to demonstrate its impact on the theories; however much more experimental work has been omitted than has been included. The attempt and purpose has been to discuss in detail the fundamentals of the subject, and then subsequently build upon that with samplings of experimental results.

The concluding section on the classical works dealing with stress analysis of crack geometries is for the purpose of comparison and unifacation. How these analyses relate to the energy theories is the basis of comparison.

This task was supported by: Navy Department, Naval Ordnance Test Station
Work Request No. 60530

NPS-57LI7111A

1 November 1967

TABLE OF CONTENTS

LIST OF FIGURES

LIST OF FIGURES (Cont.)

LIST OF FIGURES (Cont.)

1. INTRODUCTION

1.1 Preliminaries

Failure prediction is the endpoint of stress analysis, whether the limiting condition is excessive deformation, plastic yield and flow, opening of cracks or holes, or actual separation of a body into two or more pieces. The ideal desired is that upon completion of a stress and deformation analysis, a theory exists by which a simple calculation is made to predict, with accuracy, the failure behavior for an arbitrary geometry and material. Needless to say, such a theory does not exist; in fact, we are probably as far from the ideal in fracture theory as in any branch of solid mechanics. Our knowledge of the actual fracture mechanism with its governing physical laws is little understood. In 1892 Love wrote in his classical book on elasticity that "the conditions of rupture are but vaguely understood." His comment was still valid in 1926 when he published his fourth edition. The interim period up to the present has brought with it a great deal of advancement and insight into the fracture process, but it seems that this advancement does not represent the same rate of success enjoyed by other fields during the same period. There are at least three reasons for this as suggested by Alfrey[1].

(a) Mathematical Difficulty - In stress or strain analysis of either elastic or viscoelastic bodies, the initial, intermediate and final states of the body are described by the same set of continuous parameters and/or variables. If rupture takes place this is no longer true, for a discontinuity has occurred in the response of the material to the applied loads. Opening of the material by a fracture nucleus changes the connectivity of the body, introducing further mathematical complication. In short one cannot begin with an unperforated continuum, load it at the boundary and have the mathematics describe when a hole opens in the body and how it spreads.

Another aspect of the mathematical difficulty is the fact that fracture occurs at the endpoint, or extreme limit of the deformation; thus it often extends beyond the realm of linear theories and may necessitate more sophisticated finite strain or elastic-plastic treatment.

(b) Structural Difficulty - The material properties reflected in the various moduli depend upon the dominant material structure and consequently are reasonably easy to measure. However, the ultimate properties are associated with inhomogeneities, such as non-uniformly distributed flaws. In other words, at failure the non-dominant character of the material, which is very elusive and inherently difficult to study or describe, becomes controlling.

(c) Experimental Difficulty - Closely related to the above, one hundred samples of steel will have tensile moduli that will be extremely close to the same value. However, one hundred samples taken to fracture often differ widely in their ultimate properties. The structural features determining breaking strength are strongly affected by fortuitous and uncontrollably small differences in preparation and testing. Very minor variations in test conditions, sample size, and sample shape, can produce large differences in the effects produced by latent irregularities, flaws and inclusions.

As a consequence of these difficulties, an appropriate failure criterion is quite difficult to establish and apply in conjunction with the stress analysis - notwithstanding the practical engineering requirement that it be done.

There are basically two ways of approaching the fracture problem that are in common use. The first concerns itself with conditions on the molecular level, involving stresses and strains in the chains themselves, as well as bond energies and requirements for breaking the bonds and pulling the chains apart. The other we will term the global, or macroscopic, approach; i.e., from a knowledge of the gross behavior, determine conditions upon which fracture can be predicted without

knowing the local action of molecules.

1.2 Microscopic Approach

Inherent within the first approach is the difficulty of relating the applied loads to such microscopic elements as molecular weight, slip velocities, and degrees of chain freedom. This approach has been pursued extensively by physical chemists. It is important to note that one investigates concurrently the failure threshold and the failure mechanism. For instance, one molecular theory is based upon a weakest link concept while another is founded upon crystallization due to straining. If in any of these theories, failure levels were predicted with accuracy, it would constitute good evidence that this hypothesized failure mechanism was in reality the true mechanism.

The microscopic approach is still in its infancy and not yet functioning as an engineering tool, due to the mathematical complexities of describing complicated chain motion. These difficulties force the analyst to make severe assumptions that frequently do not predict actual faulure phenomena. The great majority of the molecular theories have been formulated for equilibrium conditions only, but recently more and more investigators are attempting to incorporate time and rate effects into their theories. This area of investigation will eventually contribute greatly to the overall knowledge of failure mechanisms, but attention in this article will be devoted to the macroscopic approach.

1.3 Macroscopic Approach

Another point of view commonly applied in the study of fracture can be termed a global approach. The idea is to completely ignore the molecular motions affecting the mechanism of fracture and concentrate upon devising a mathematical theory capable of predicting the occurrence of failure under arbitrary

stress states. Drucker[2] has made some general comments on this subject, which reflect an interesting attitude that is included here in condensed form.

In this continuum approach, even in the simplest of cases, inhomogenieties, time effects, nonlinearities and energy dissipation are ever present facts of life. The incorporation of these effects in any theory is a formidable task even when only small disturbances from equilibrium are considered. If a precise representation is sought, there can be no escape through steady state or equilibrium assumptions. Possible responses of a time and temperature dependent material to arbitrary stress and temperature histories are far too general to be expressed in tractable mathematical terms. This appears to produce an irreconcilable conflict between observed physical behavior and useable mathematical relations to express this behavior. With completeness recognized as impossible, several courses of action are open.

One procedure that is fashionable today is to write the most general mathematical formulations that the author can conceive of in functional form and subsequently manipulate these expressions without ever solving a problem. A second approach looks at broad unifying principles such as those found in thermodynamics, and progress has definitely been made via this method. Still another procedure is to start from strong idealizations of physical reality and develop the simplest theory containing the basic physical idea. Successful theories that would fall in this category are linear elasticity, Levy-Mises plasticity theory, linear viscoelasticity, etc. The fact that no elastic perfectly-plastic material exists does not detract from the fact that these elements of behavior exist in all metals. It is at this stage of progression that fracture mechanics now stands, and theories that at least include the basic elements of fracture are being sought.

Interestingly enough, all of the methods in current use for viscoelastic fracture are extensions of similar methods developed for the fracture of metals. Therefore their history has a common core, and it is appropriate to consider it briefly as a foundation is built for further discussion of macroscopic fracture theory. Irwin[3] has provided such an account that is more than sufficient for this study.

1.4 Historical Development

The classical beginning of studies on fracture is taken as Leonardo da Vinci's tests on the strength of wire. His sketches of apparatus and test results are all preserved with ample annotations and his investigations in the late 1400's showed a definite dependency of strength on the length of test specimen. On the other hand Galileo (1564- 1642) delved into the mathematical aspects of fracture with his investigations on the strength of cantilever beams. He stated that the strength of a member in tension should depend only upon the cross-sectional area and not upon the length. His analytical approach dominated engineering design for many years.

Later in the 1600's, Mariotte (1620-1684) proposed that a specimen would fail when the fractional elongation reached a given limit. This introduced the use of maximum limit theories that are extensively used today with maximum normal stress, shear stress, energy, etc. Actually the shear stress criterion didn't come until the next century when Coulomb (1736-1806) introduced it as his preference for predicting strength both in tension and compression, where added strength would be expected due to sliding friction.

The 1800's brought more experimental work and further verification of da Vinci's dependency of strength on specimen size, but the next great milestone in fracture theory related to stress analysis around cracks. It was the solution by Inglis[4] in 1913 of the stress field surrounding an elliptical cavity in an infinite two-dimensional sheet. This result later paved the way for Griffith to introduce an entirely new concept in fracture mechanics.

Inglis' model is pictured in Fig. 1 where only one axis of stress is applied.

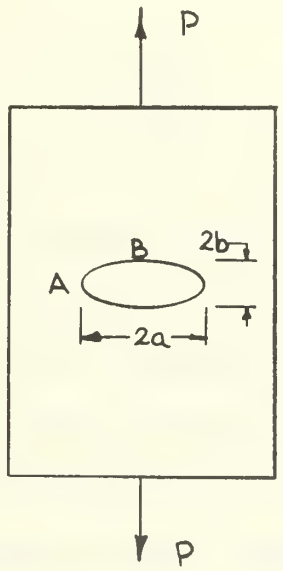

Fig. 1 Inglis Model - Infinite Sheet with Elliptical Hole

Results of the calculation, which are quite lengthy and involved, especially since they are in the unfamiliar elliptical coordinates, are all that are included here. The expression for the hoop stress at the surface of the ellipse at location A, which is the critical component, is given by

$$\sigma = P\left[1 + 2\frac{a}{b}\right] \qquad (1)$$

at B

$$\sigma = -P \qquad (2)$$

2. FRACTURE CRITERIA

In general, there are three principal fracture criteria used in viscoelastic fracture analysis today, and each one of them will be discussed in detail. They are the energy balance, the fracture surface and cumulative damage. They will be treated in that order, and the Griffith theory will be developed from conservation of energy following Lindsey[7].

2.1 Energy Method

From the laws of mechanics it is known that energy must be balanced during the fracture process, and although this is not what Griffith did, his results can be obtained in this way. A simple, yet meaningful, way to apply conservation of energy to the fracture process is to study the behavior of the classical two-dimensional sheet possessing an internal cylindrical crack, as solved by Inglis. It is not necessary to consider all of the details in the field stresses, strains or displacements in order to discover the physical process involved; in fact, a great deal can be learned by treating the specimen as a black box. This is a useful tool used by Orowan[8] primarily because of the mathematical simplicity and ease with which physical aspects of the problem can be grasped and intuitively followed; yet it includes the essentials that are necessary to get a true picture of the fundamental processes.

The cracked sheet configuration to be used is shown in Fig. 2, where F is the total applied boundary force and δ is the boundary displacement over the entire end of the specimen. The cracked sheet can be considered as a linear spring whose stiffness is a function of the internal crack length. By observing only

the boundary forces and displacements, without regard to the changes occurring locally in the interior, energy diagrams can be drawn of the fracture processes under various loading conditions.

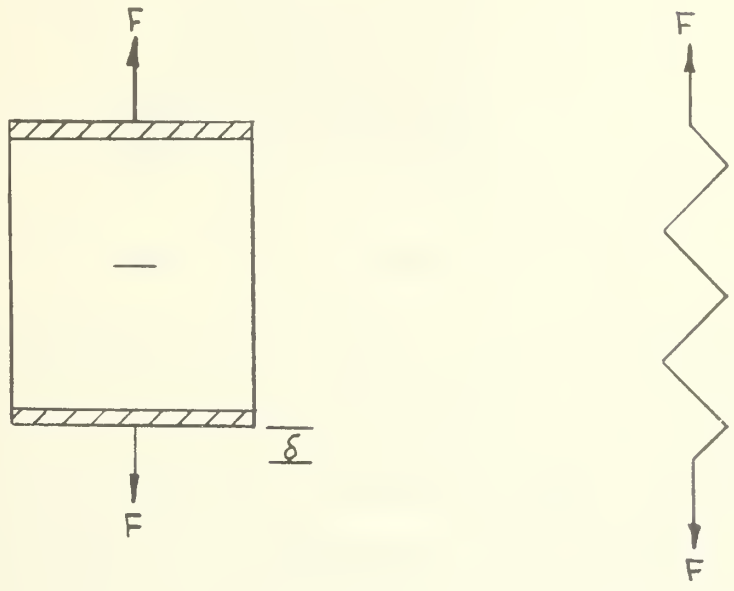

Fig. 2 Cracked Sheet Model

2.1.1 Fixed Force Loading

First consider the spring or black box to be loaded to incipent fracture and further assume that the boundary force is kept constant during the entire course of the fracture. The equilibrium energy state of the body just prior to crack extension will be compared to an equilibrium state after the crack has run an arbitrary distance. For such a situation the force displacement diagram has the appearance of Fig. 3.

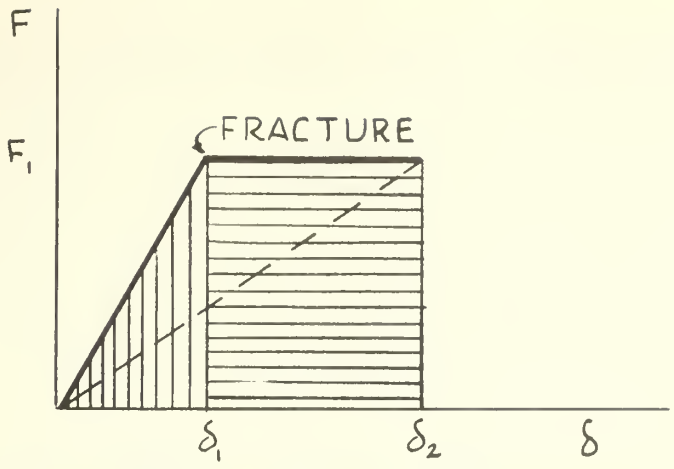

Fig. 3 Energy Diagram - Fixed Force

The strain energy before or at fracture is given by the triangle with vertical shading, while the work done at the boundary due to the crack extending is represented by the rectangle with horizontal shading. As the crack extends, portions of the sheet in the neighborhood of the crack that were previously restrained are now free to move and this motion carries to the boundary where work is done on the body by the constant forces acting there. Using the spring analogy, the internal constituents have been altered and the stiffness of the spring has been reduced. If the specimen were to be unloaded it would follow a path down the dotted line, where the slope is associated with the new crack length. Therefore the strain energy of the sheet after fracture is represented by the triangular area under the dashed line, which clearly demonstrates an increase in the strain energy of the sheet due to fracture under fixed force loading. To apply the conservation law to this situation, it will be assumed that the material is non-dissipative; i.e., there are no losses of energy except that which goes into the creation of surface, and the propagation of the crack is slow enough to neglect any inertial effects. The concept of surface energy or interface energy, is one that is undergoing examination by the chemists and is still somewhat nebulous.

Herein S is taken to include energy required to break bonds, readjustment of surface atoms, heat loss, etc. In other words, it is a dissipation term including all energy lost from the body while making the surface. The expression for energy conservation is formulated by equating U_1, representing the strain energy before fracture, plus the work done during fracture, δW, to the strain energy after fracture, U_2, plus the energy dissipated in forming new surface, δS

$$U_1 + \bar{\delta}W = U_2 + \bar{\delta}S \tag{5a}$$

forming an incremental equation

$$\Delta U - \bar{\delta}W + \bar{\delta}S = 0 \tag{5b}$$

formulating the expressions for each term we have

$$\tfrac{1}{2} F_1(\delta_2 - \delta_1) - F_1(\delta_2 - \delta_1) + \bar{\delta}S = 0 \tag{6a}$$

or

$$\bar{\delta}S = \tfrac{1}{2} F_1(\delta_2 - \delta_1) = \Delta U\Big|_{\Delta F = 0} \tag{6b}$$

Equation (6b) shows for a linear system that half of the work done at the boundary is dissipated in creation of surface, and the other half is stored in the body and recoverable.

2.1.2 Fixed Grip Loading

Turning now to fixed grip loading, which is the other most commonly used loading condition, the specimen is extended to incipient fracture and the boundary displacements are held constant by a rigid fixture. Although this

configuration is the most commonly discussed in the literature in speaking of the energetics of fracture, confusion has arisen on this point too. For instance, Starr[9] strongly refuted Griffith's original work in the open literature shortly after it was published on the basis that the strain energy terms were not representing the real physical process; however Starr was speaking of results of a fixed grip test while Griffith, although he never stated it explicitly, was dealing with a fixed force configuration. There is considerable difference in the two, which becomes obvious with this simplified model but which remains obscure without it. Because the fixed grip arrangement facilitates easier visualization as to where the energy is going, it is the one normally selected to explain fracture in the literature and textbooks. (See Timoshenko[10].) As the crack extends, under fixed boundary displacements, the internal stiffness decreases as before, but the specimen in such a state of loading is constrained to follow a different path as shown in Fig. 4.

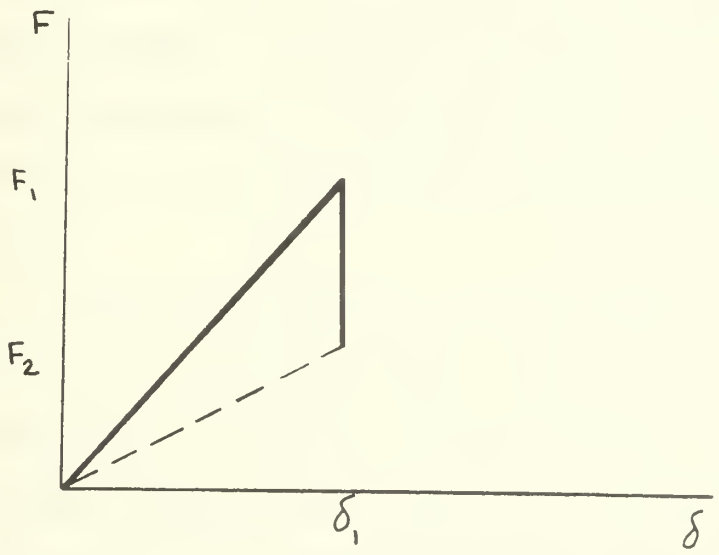

Fig. 4 Energy Diagram - Fixed Grip

In this instance the strain energy decreases, and all energy required for the new surface must come from the strain energy in the body, since there is no work done at the boundary. The energy balance of equation (5b) becomes

$$\Delta U + \bar{\delta} S = 0 \tag{7a}$$

which from Fig. 4 becomes

$$\bar{\delta} S = \tfrac{1}{2} \delta_1 (F_1 - F_2) = -\Delta U \Big|_{\Delta\delta = 0} \tag{7b}$$

Some discussion has arisen about whether the strain energy in a cracked sheet is greater or less than its uncracked counterpart, and as the preceding discussion has demonstrated, it depends upon the basis of comparison. If the two sheets are compared with the same boundary displacements, then the uncracked sheet contains the greater strain energy; however, if the basis of comparison is a given load at the boundary, the situation is reversed and the cracked sheet possesses the greater strain energy. Although Griffith never did state which fracture problem he was actually solving, he did speak of the increase in energy of the cracked sheet over the uncracked one and all his work dealt with this energy difference. In order to be correct he therefore had to be working a fixed force problem.

It is convenient for computation and for later comparisons to cast the energy equation into a differential form. This will be accomplished by dividing the equation by an increment of crack length and taking the limit as the change in crack length approaches zero. Implicit within this operation is the assumption that each term in the equation can be written as a continuous function of crack length, which can only be done if the flaw hypothesis is made. This results from the fact that the fracture point of a specimen with a residual crack

is actually the point of initiation of the propagation phase, and the energy terms can be represented as continuous functions of crack length. On the other hand, if there is no macroscopic flaw and fracture originates at a sub-continuum level, then the energy terms are not continuous functions of crack length, and the incremental equations must be used. The differential form of the conservation law becomes

$$\frac{dU}{dc} - F\frac{d\delta}{dc} + \gamma\frac{dA}{dc} = 0 \qquad (8)$$

where $S = \gamma A$ (assumption)

γ = the energy density required to create new surface

A = the area of the new surface

F = the boundary force

δ = the boundary displacement

Up to this point equation (8) is a necessary condition for fracture within the bounds of the assumptions made, but it is not known whether it is a sufficient condition or not. Certainly it is required that energy be conserved in the fracture process, and any fracture condition that violates equation (8) is definitely wrong; however, whether or not fracture is predicted by it remains to be seen. In other words, whether it can be demonstrated that it is both a sufficient condition as well as a necessary one is yet to be undetermined.

2.1.3 Comparison of Boundary Conditions

The two loading conditions considered here are actually the two extremes in the loading spectrum and are by far the most common, if not the only ones, mentioned in the literature. They are also the ones that investigators

attempt to achieve in the laboratory, and for this reason the critical levels that they predict should be compared. Plotting both cases on the same diagram in a general way provides a means of comparison.

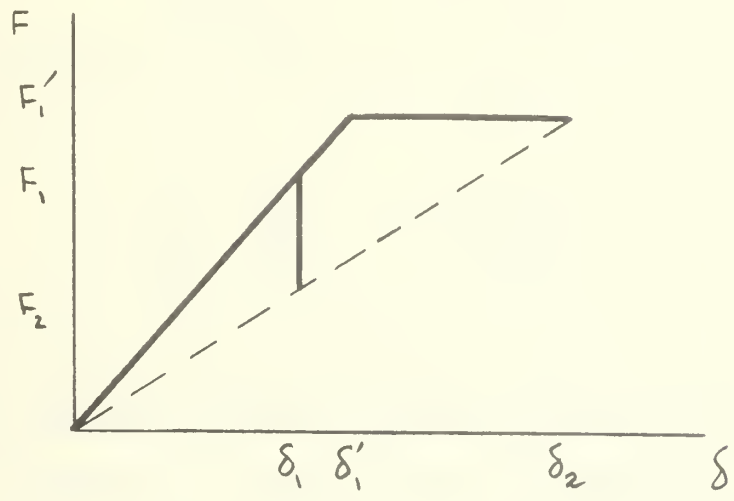

Fig. 5 Energy Diagram - Comparison

The fact that the fixed force loading is depicted with the higher fracture load does not detract from the generality of comparison because F_1' and F_1 are arbitrary points in the plane, and either could be taken to be the larger. Writing equation (8) for fixed force conditions

$$\frac{1}{2} F_1' \left.\frac{\partial \delta}{\partial c}\right|_{\substack{F \\ \delta=\delta_1'}} - F_1' \left.\frac{\partial \delta}{\partial c}\right|_{\substack{F \\ \delta=\delta_1'}} + T \left.\frac{\partial A}{\partial c}\right|_F = 0 \qquad (9)$$

where F is held constant, and the derivative is evaluated at $\delta = \delta_1'$.

Now for fixed grip

$$\frac{1}{2} \delta_1 \left.\frac{\partial F}{\partial c}\right|_{\substack{\delta \\ F=F_1}} + T \left.\frac{\partial A}{\partial c}\right|_\delta = 0 \qquad (10)$$

where δ is held constant, and the derivative is evaluated at $F = F_1$. By making

the physically reasonable assumption that the energy dissipated in the formation of surface would be the same regardless of the boundary conditions, the relationship between the two cases is obtained

$$-F_1' \left.\frac{\partial \delta}{\partial c}\right|_{\substack{F \\ \delta=\delta_1'}} = \delta_1 \left.\frac{\partial F}{\partial c}\right|_{\substack{\delta \\ F=F_1}} \tag{11a}$$

Inserting the constitutive law based on the spring analogy, $F = E_c \delta$, into this equation gives

$$\frac{F_1'^2}{E_c^2} \frac{dE_c}{dc} = \delta_1^2 \frac{dE_c}{dc} \tag{11b}$$

However from Fig. 5, it is seen that $\delta_1^2 E_c^2 = F_1^2$ and consequently $F_1' = F_1$.

This conclusion that both loading conditions produce the same potential fracture level is similar to a result obtained by Orowan[8] with a slightly different technique. Actually he proved that the energy available for fracture was the same in the two cases; however this converse proof requires the assumption that the fracture stress be the same in both loadings. It becomes a matter of personal preference as to which is the most fundamental assumption. Having established that the two limit conditions in the loading spectrum predict the same critical fracture levels, it is reasonable to assume that the in-between loading conditions, where both the surface forces and the surface displacements change during fracture would produce the same critical level for a linear system. Actually these are the conditions that are probably produced in the laboratory as an approximation to fixed force or fixed grip loading.

With these results from the conservation law, it is appropriate to proceed to a consideration of other energy methods; namely, the potential energy functional, which historically has been the most commonly used. The energy

functionals are often more convenient to work with, and they provide a sound method for ultimately examining the stability of the crack in an attempt to evaluate whether equation (8) is a sufficient condition for fracture. Consequently we will now proceed to examine an extended form of the potential energy and evaluate it in light of fundamental principles just discussed.

2.1.4 Extended Potential Energy

The discussion of fracture within the framework of potential energy must begin with Griffith's work on brittle fracture of glass[5,6]. These two classical papers put forth an entirely new concept in fracture analysis and stand as an ingenious contribution to the field. The basic idea is given by Griffith himself on page 165 of reference 5:

> "In view of the inadequacy of the ordinary hypotheses, the problem of the rupture of elastic solids has been attacked from a new standpoint. According to the well-known theorem of minimum energy, the equilibrium state of an elastic solid body deformed by specified surface forces is such that the potential energy of the whole system is a minimum. The new criterion of rupture is obtained by adding to this theorem the statement that the equilibrium position, if equilibrium is possible, must be one in which rupture of the solid has occurred, if the system can pass from the unbroken to the broken condition by a process involving a continuous decrease in potential energy.
>
> In order, however, to apply this extended theorem to the problem of finding the breaking loads of real solids it is necessary to take account of the increase in potential energy which occurs in the formation of new surfaces in the interior of such solids. It is known that, in the formation of a crack in a body composed of molecules which attract one another, work must be done against the cohesive forces of the molecules on either side of the crack. This work appears as potential surface energy, and if the width of the crack is greater than the very small distance called the radius of molecular action, the energy per unit area is a constant of the material, mainly, its surface tension."

This is Griffith's hypothesis of an extended energy theorem and is subsequently formulated on the basis of two assumptions; first, that the potential energy can be extended to include surface energy effects, and second, that such an extended functional will seek a minimum based on variations of geometries as opposed to variations of displacements. He continues on page 166 to state a theorem in support of the first of these assumptions:

> "The calculation of the potential energy is facilitated by the use of a general theorem which may be stated thus: in an elastic solid body deformed by specified forces applied at its surface, the sum of the potential energy of the applied forces and the strain energy of the body is diminished or unaltered by the introduction of a crack whose surfaces are traction free."

The proof of the theorem is included in the paper and credit is given to Mr. C. Wigley for its authorship.

> "This theorem may be proved as follows: it may be supposed, for the present purpose, that the crack is formed by the sudden annihilation of the tractions acting on its surface. At the instant following this operation, strains, and therefore the potential energy under consideration, have their original values; but in general, the new state is not one of equilibrium. If it is not a state of equilibrium, then by the theorem of minimum energy, the potential energy is reduced by the attainment of equilibrium; if it is a state of equilibrium the energy does not change. Hence the theorem is proved."

It is not felt that this constitutes a proof, for it is based on theorems established through variations in field variables such as displacement rather than changes in geometry like opening cracks; however the hypothesised reaction of the body to the formation of new surface sounds reasonable, does not run contrary to intuition and appears to be an acceptable method for extending the potential energy functional.

In order to translate the ideas into symbols, a sign must be affixed to the surface energy term. This will be reasoned* by first considering the classical potential energy functional V[11]

$$V = U - P \tag{12}$$

where U is the strain energy and P is the so-called potential energy of the boundary forces. For linear systems, it is easy to show that $P = 2U$; (for example, see Love[12]), thus $V = -U$. During fracture under a fixed force loading condition, the potential energy will decrease due to the increase in the strain energy, but when fracture occurs, part of the increase in strain energy is dissipated in the formation of new surface; consequently, the potential energy does not decrease by the full value of U, rather by the difference, U - S. The extended potential energy $\bar{V}$ then becomes

$$\bar{V} = -(U-S) = U - P + S \tag{13}$$

Let us now compare the potential energy at two neighboring states, $\bar{V}_1$ just prior to fracture and $\bar{V}_2$ just after,

$$\bar{V}_2 - \bar{V}_1 = \Delta\bar{V} = \Delta U - \Delta P + \delta S \tag{14}$$

A diagram of fracture under fixed force loading, exhibiting the various terms of equation (14) is shown in Fig. 6 where P_1 is represented by vertical shading, and P_2 is the sum of both shaded areas. From the diagram then it is clear that $\Delta P = \delta W$ (compare with Fig. 3) in the energy equation (5), which is the crux for the establishment of the fracture criterion, for a variation of the extended

---

* It is not certain what the original argument was. The two papers are quite vague in many respects.

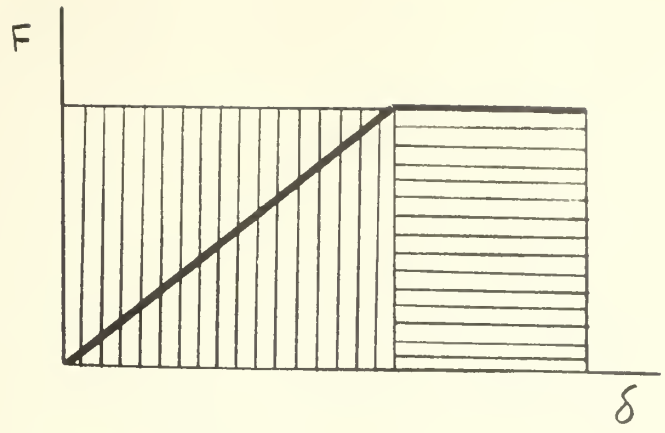

Fig. 6 Potential Energy Diagram

potential energy, where the crack length is the variation parameter, becomes

$$\delta \bar{V} = \left[\frac{\partial U}{\partial c} - \frac{\partial P}{\partial c} + T \frac{\partial A}{\partial c} \right] \delta c \qquad (15)$$

By a comparison with the energy equation (8) it is apparent that $\delta \bar{V} = 0$ is identically the same as requiring the energy to be conserved. This is a significant result, for it establishes in a rational manner from fundamental principles one of the assumptions that Griffith made without explanation or justification, that fracture would occur when the extended potential energy reached a minimum. In fact it is difficult at this point to see why this is so, but later examinations of stability will clarify the result.

2.1.5 Extended Complementary Energy

If a similar comparison is made between the extended potential energy for fixed grip loading and the energy balance made for the same conditions, it is seen that the two do not coincide and that the two conditions are not the same. It is, therefore, concluded that the extended potential energy is not the correct

functional for fixed grip loading. However an analogy can be made between the types of loading and the correct functional, for in the case of fixed force loading, where the force is held constant and the displacements are varied, it was found that the potential energy was the proper function; therefore it would appear appropriate that for the fixed grip condition where the displacements are held constant and the forces are varying that complementary energy would be a fertile area to investigate. It turns out that this is true.

For a linear system subjected to infinitesimal strains, the complementary energy functional is given by[11]

$$V^* = U - \int_{\Sigma_\delta} F_i \delta_i \, d\sigma \tag{16}$$

where U = strain energy

F_i = surface fractions

δ_i = surface displacements

$d\sigma$ = surface element

Σ_δ = portion of surface where displacements are specified

Pursuing arguments similar to those used for extending potential energy, the complementary energy may be extended to

$$\bar{V}^* = \bar{U} - Q + S \tag{17}$$

where

$$Q = \int_{\Sigma_\delta} F_i \delta_i \, d\sigma$$

Upon examination of the fixed grip loading condition, for which Q does not change with crack length c, the first variation of $\bar{V}^*$ is

$$\delta \bar{V}^* = \left[\frac{\partial U}{\partial c} + \frac{\partial S}{\partial c} \right] \delta c \tag{18}$$

Comparing this with the appropriate energy equation (7), it is seen that the two expressions are identical if the first variation of the extended complementary energy functional with respect to the crack length is set equal to zero.

Thus the two limit cases have been successfully associated with an appropriate energy functional, whose first variations when set equal to zero yields the same critical value as the conservation of energy for the same conditions.

2.1.6 Energy Applied to Fracture of Glassy Polymers

In the previous section pure brittle fracture was discussed where the material must be completely linear throughout the specimen all of the way to fracture. Few materials possess this quality, but one that comes as close as any is glass. Griffith performed tests upon it and demonstrated a measure of correlation with his theory.

In an effort to extend this concept to polymeric materials, the logical place to begin appears to be with glassy polymers. They come the closest to being brittle, and with their glass transition temperatures being so high, the viscoelastic rate effects would be expected to be minimized. Berry[13] initiated tests in this area on Polymethyl Methacrylate (PMM) with a specimen that bore only a slight resemblence to the Inglis sheet, but which theory he used to interpret the experimental data. He used a uniaxial tensile bar with an edge saw-cut. He then wedged the saw-cut to form a crack. Finally he removed the material containing the saw-cut, leaving an edge crack in a tensile bar. (See Fig. 7).

These specimens were pulled to rupture, and the failure stress as a function of crack length was found to obey the inverse square root law of brittle

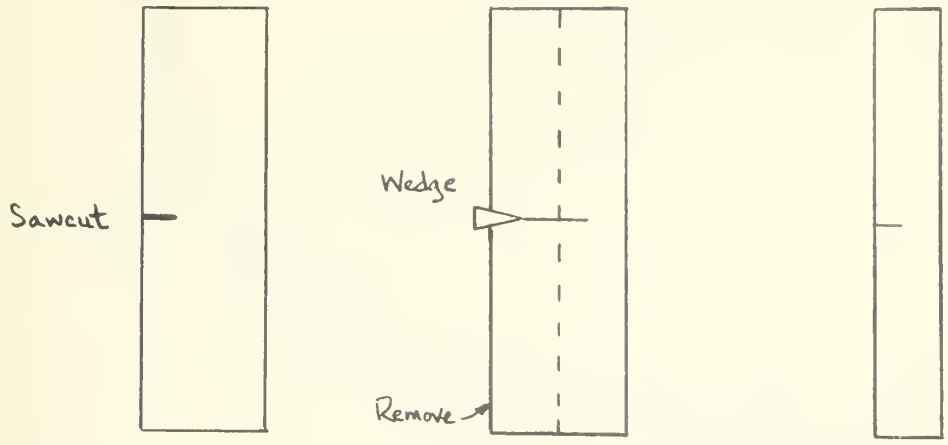

Fig. 7 Berry Specimen

fracture theory (see Fig. 8). The rate of testing was varied by one decade with no noticeable affect on fracture behavior. From these experiments the surface energy density was measured and found to be $3.0 \pm 0.8 \times 10^5$ ergs/cm^2. This compares favorably with some other investigators (for instance Bueche[14]), but it is rather large when compared to a theoretical calculation. Computing a maximum theoretical surface energy required to separate two planes of atoms based on perfect alignment of chains and the energy of carbon-carbon bonds, a value of 450 ergs/cm^2 is obtained, giving a descrepancy factor of 10^3.

In the same experiments, Berry[15] noted color patterns on the fracture surface, as had other investigators[16], and this was postulated to be a thin layer of highly oriented molecules, possessing a different refractive index. The colors were found to change as the length of the crack increased, indicating that the energy required to produce the orientation was not constant but was a function of crack length or crack velocity.

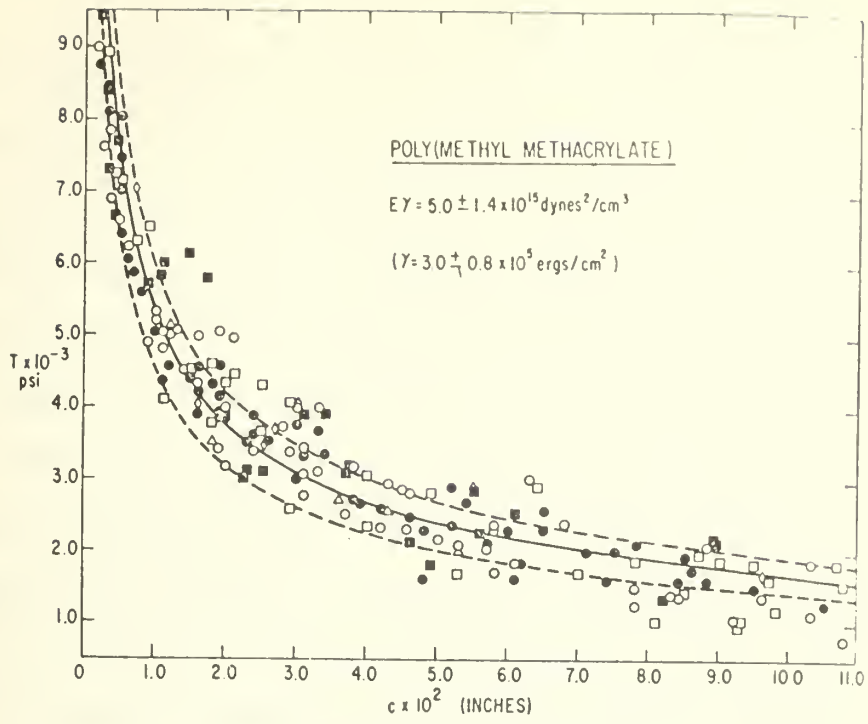

Fig. 8 Berry Results

Berry[17] repeated these experiments on Polystyrene (PS) and found the same verification of the inverse square root dependency of fracture load on crack size down to cracks of the order of 0.05 in., where it leveled off rather than giving a higher strength (see Fig. 9).

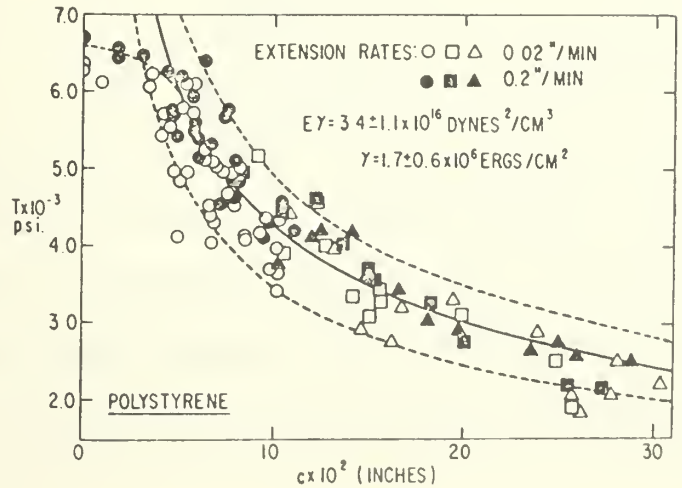

Fig. 9 Tensile Strength vs. Crack Size

The reason for this being that .05 in. is in the range of the effective flaw size of an uncracked specimen, which was measured at 0.043 in. This is measured by pulling an uncracked specimen to find the critical load, and then assuming the Griffith Theory is correct, compute the flaw size producing failure. For comparative purposes PMM followed an inverse square root law down to 0.004 in., and the inherent flaw size was measured to be 0.002 in.

The surface energy density was measured to be $1.7 \pm 0.06 \times 10^6$, which is an order of magnitude larger than PMM. Because γ is larger for PS than PMM, the strength of PS is greater for cracks of the same size; however due to the larger inherent flaw size in PS, its uncracked strength is lower. The larger flaw size was involved with the tendency of PS to craze in areas of high stress.

Subsequent investigations by Kambour[18] described crazes as not being true cracks, but they are sharply bounded regions containing a polymer filling which interconnects the bulk polymer. The filler is high in void content and the altered structure possesses a different refractive index. A method is reported by Kambour[19] for measuring void content and refractive index, η_c in the craze in the interior of the bulk polymer. The results showed:

PMM	$\eta_c = 1.38$ $\eta_{bulk} = 1.49$	Void = 40%
PS	$\eta_c = 1.33$ $\eta_{bulk} = 1.60$	Void = 40%

Kambour[20] has further shown that the colors on the fracture surface observed by Berry is a thin layer of craze material. He carefully produced some planar fractures by a cleavage wedge in a disk of PMM. By coating the surface with a liquid of high refractive index, he artificially produced the situation of the craze in a bulk polymer and made the same measurements as referred to above.

The value for the fracture surface was $\eta = 1.32 \pm 0.01$. As a check the sample was annealed at 95°C and retested and all interference fringes disappeared. With this correlation, it was concluded that the fracture surface layer, like the craze, is an expanded polymer structure with a void content of 40%, the formation of which would explain at least part of the discrepancy between the theoretical and measured surface density.

The layer thickness has also been measured by Kambour[21] with interference fringe techniques. A 40X microscope was used to evaluate the fringes, and the thickness was determined through the relationship,

$$\left(n+\tfrac{1}{2}\right)\lambda = 2\eta d \cos\phi$$

where

λ = wavelength of light used

η = refractive index

d = layer thickness

ϕ = angle of incidence of light

n = fringe order

Variations in thickness were observed as experiments were run with the cracks stopped and restarted repetatively. In the stop band, which was consistently 25μ long, the fracture surface layer was found to be thicker than the portion of the layer just preceding the stop band. In the stop band the thickness averaged 6800A, while the layer on the surface preceding the band decreases in thickness upon approaching it, and at the edge averages 5500A. This thickness is taken to be a function of velocity, which in turn will make γ velocity dependent. Where the crack is growing with essentially zero velocity, the layer averages 6800A, and it

is in this region that the Griffith theory has its closes applicability.

The effects of sub-surface crazing has not yet been evaluated; i.e., microscopic crazing throughout the specimen in regions of high stress. This would contribute to the energy needed to form new surface, but the area involved would not be known. This would make measurement of γ geometry dependent since the amount of sub-surface crazing would depend upon the stress field.

Similar measurements have been made on nine different glassy polymers now with the result that all but polyvinyl chloride failed via the crazing mechanism in a brittle-type of fracture up to the glass transition temperature. Above that point (about 90°C) no crazing is detected and no residual surface layer is formed, but below that temperature fracture in glassy polymers can accurately be described as the formation and subsequent breaking of crazes.

Berry[22] has reported results of an investigation of void content and void formation in the craze. The spatial and size distribution has been found to be random throughout the craze volume. The sizes ranged over wide values down to the resolution of the electron microscope. Berry offers the following explanation for the void formation: he states in effect, that the optical effects indicate a high degree of molecular orientation, which in turn demands a large local elongation of the sample with a corresponding reduction in cross-section. However, the thickness of the region in which the effect is noted is very small compared with the cross-section. Because the thin layer is constrained by the substrate, effectively no reduction in cross-section is possible and the material is in a state of triaxial tension. Void formation is thus a natural consequence.

In summary, it appears that based on the experimental evidence available thus far, glassy polymer fracture can be predicted with a modified Griffith theory. The mechanism seems summarily to be, first the build up of stress about a

microscopic flaw, which causes an orientation of the chains. This produces a localized triaxial stress field with consequent production of voids and the formation of crazed material. This coalesces and grows to a critical size where it precipitates fracture according to the energy prediction.

2.1.7 Energy Applied to Fracture of Rubber

The British Rubber Producers Research Association has sponsored a significant amount of work on the application of energy principles to rubber fracture. In a series of articles[23-30] over a ten year period they rather throughly explored the subject. The initial paper by Rivlin and Thomas investigated the applicability to rubber of the concept of surface energy as used by Griffith. They selected three specimens of widely different geometries and took as the fracture definition the point at which a crack ran catastrophically. Since the deformations were large they measured the work input required to strain the specimen to fracture and then plotted it versus initial crack length. The slopes of the curves were then taken to evaluate the carry-over of the Griffith result

$$\frac{\partial U}{\partial c} = \gamma t$$

where

γ = surface energy density

t = specimen thickness

The resulting values for γ from the three tests gave 1.2×10^7, 1.2×10^7 and 1.4×10^7 ergs/cm^2 respectively.

The experiments were repeated, the only difference being the threshold of failure was taken as the first observable sign of tearing. The crack was inked and observed under microscope. The first sign of fresh material was taken as

failure. The value for T for these tests was 3.7×10^6 erg/cm^2. They emphasize that this quantity δ is not twice the surface energy of a crack or fracture surface, but the work expended irreversibly per unit of surface area to create it.

The subsequent papers in the series discussed many facets of the above equation like the strain concentration at the tip of the tear. Finally a review of the whole project including the effects of temperature and strain rate on tear energy was published by Greensmith et. al.[31].

2.1.8 Energy Applied to Holes and Cavities (Linear Theory)

The elastic energy method has also been applied to spherical cavities as well as line cracks. Williams and Schapery[32] considered a spherical cavity in an infinite medium subjected to hydrostatic tension. Because of the symmetry it is possible to use a nonlinear theory applying the same energy balance as used in cracks. Before doing this the principles will be demonstrated as they are applied in a linear theory. Figure 10 shows the model and a classical solution[33] for the stress field, where the outer boundary is spherical of radius b is given by

$$\sigma_r = \frac{p b^3 (r^3 - a^3)}{r^3 (b^3 - a^3)} \qquad \sigma_t = \frac{p b^3 (2r^3 + a^3)}{2r^3 (b^3 - a^3)} \qquad (19)$$

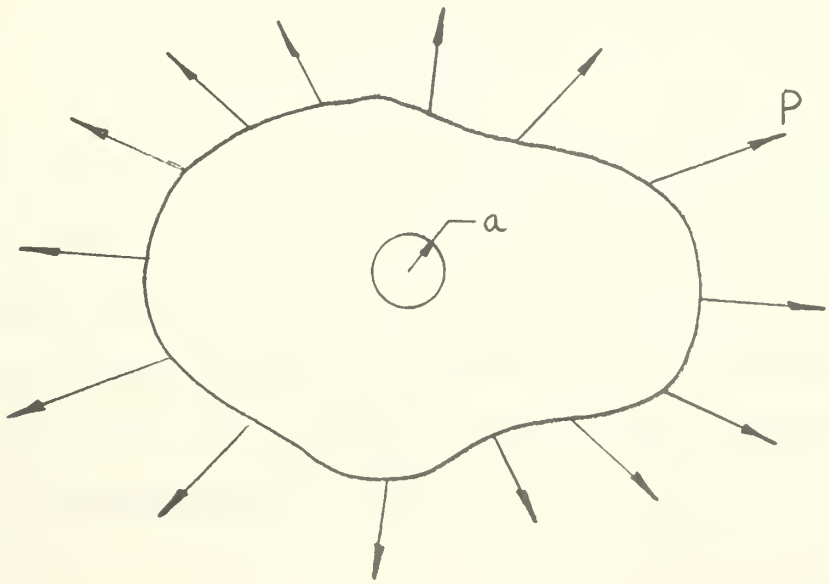

Fig. 10 Idealized Model of Spherical Flaw in a Hydrostatic Field

The corresponding strains for an incompressible material become

$$\varepsilon_r = \frac{1}{E}\left(\sigma_r - \sigma_t\right) \qquad \varepsilon_t = \frac{1}{2E}\left(\sigma_t - \sigma_r\right) \tag{20}$$

Forming a strain energy density function and integrating over the body we have

$$U = \frac{1}{2}\int_V \tau_{ij}\,\varepsilon_{ij}\,dV = \frac{\pi}{2E}\,p^2\left[\frac{1}{a^3} - \frac{1}{b^3}\right]^{-1} \tag{21}$$

In order to obtain the critical rupture pressure, the energy criterion of equation (8) is invoked

$$\frac{\partial}{\partial a}\left(U - S\right) = 0 \tag{22}$$

where for a linearly elastic material P = -2U. S represents the surface energy, which is given by a product of the cavity area times the surface energy density γ , and a is a measure of the flaw growth. In this instance when $b >> a$, equation (22) becomes

$$\frac{\partial}{\partial a}\left[\frac{3\pi}{2E}\,p^2 a^3 - 4\pi a^2 \gamma\right] = 0 \tag{23}$$

which yields a critical pressure of

$$P_c = \frac{4}{3}\sqrt{\frac{E\gamma}{a}} \tag{24}$$

This gives the typical inverse square root dependency of critical rupture stress on initial flaw radius. In fact, the defining equation of (24) varies only slightly for the entire spectrum of flaw geometries. Sneddon[34] and Sack[35] obtained the inverse square root dependency for "penny-shaped" cracks in hydrostatic fields, which is very similar to the Griffith result for the line crack in a two-dimensional sheet.

A summary table shows the quantitative similarity for representative geometries

Geometry	Sheet with Line Crack (Griffith)	Cylindirical Cavity	Penny-shaped Crack (Sneddon)	Spherical Cavity
Critical Stress	$\sqrt{\frac{2}{\pi}\frac{E\gamma}{a}}$	$\sqrt{\frac{E\gamma}{2a}}$	$\sqrt{\frac{2\pi E\gamma}{a}}$	$\frac{4}{3}\sqrt{\frac{E\gamma}{a}}$

Williams[36] has discussed this similarity and uses it to investigate the more complicated phenomenon of viscoelastic fracture.

It should be noted that this analysis, through the manner in which the energy terms were formulated, inherently assumes a radial mode of propagation for the fracture surface; i.e., the flaw grows spherically in a manner similar to ablation. This may place a limitation on the information gained, but a similar situation arises for the 'penny-shaped" crack, which also is confined to propagate radially in a planar mode. Only experimentation can provide the means for evaluating these assumptions and determining what portion or portions of the fracture process can be analyzed by them.

2.1.9 Energy Applied to Holes and Cavities (Nonlinear Theory)

The spherical symmetry in this problem makes it possible to extend the infinitesimal deformation fracture analysis to include effects of finite deformations. This is seldom possible, although Gent and Lindley[37] did use the model of a spherical cavity in an infinte medium and investigated the strains at the cavity using a maximum strain criterion. Schapery and Williams[38] used a nonlinear theory for the same problem and coupled it with an energy criterion to predict fracture. This is a particularly interesting approach for polymeric

materials where large strains are the rule; furthermore, it provides an opportunity to see how large strains affect the inverse square root dependency of initial flaw size.

The presence of deformations exceeding the limits of infinitesimal theory produces many ramifications in the mechanics of the energy analysis: First, the matter of loading requires a more careful definition to fit the actual conditions both experimentally and theoretically, for with finite strains the change in area of the bounding surfaces is accounted for and there becomes a distinction between fixed force and fixed stress conditions. This difference will manifest itself in almost every quantity previously calculated and will affect the outcome of the conclusions drawn on the basis of the infinitesimal theory.

Second, this same matter of the differences between the deformed and the undeformed area produces questions about the manner in which surface energy is handled in the governing expressions. Normally in these computations, a surface energy is computed as if it were a variable of state; i.e., as if the existing surface possessed a given surface energy as opposed to only speaking of changes in the surface, or energy required to create surface. The actual computation is then made by differentiating this quantity with respect to the crack length. However additional consideration must be given when the surface of interest is significantly altered by deformation before fracture occurs, i.e., the original surface changes in area but does not rupture. This deformation is accounted for in the stress analysis of the body and in the energy expressions, but the correct manner in which it influences the surface energy may be debatable.

Third, the classical potential energy theorem has been shown to apply regardless of the magnitude of strain. For example, Green and Zerna[39] derived the theorem for large strains, and the form of the expression is found to be identical with the linear theory if proper attention is given to the definition of stress and strain. By examining Fig. 11, which depicts a loading history and subsequent fracture under fixed-force conditions for a general non-linear body, it is seen that δP of the potential energy expression[15] is still equal to δW of the conservation equation (5b). As a result, the first variation of the extended potential energy, with proper stress and strain definition, still remains as a valid stability criterion for large strains also.

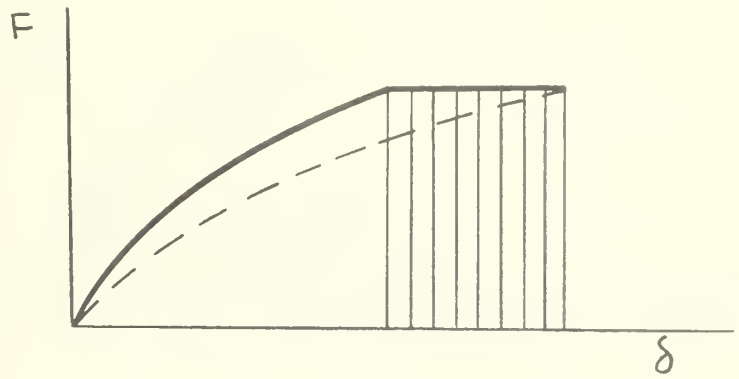

Fig. 11 Force-Deflection Curve

Fourth, the complementary energy functional for finite strains has been formulated by Levinson[40] in terms of the Lagrange stress and strain tensor. The Lagrange stress tensor is an unsymmetric tensor associated with base vectors in the undeformed body, whose intensity is measured in terms of the undeformed area. The Lagrange strain tensor is simply the displacement gradient. Levinson was able to obtain a complementary energy principle, which differs in form from the infinitesimal functional only by a change in sign. With regard to this he states, "This is because it is customary to give the infinitesimal theorem

as a minimum principle, (for stable equilibrium) whereas its derivation by the Legendre transformation would lead to a maximum principle whose function would agree in sign." Thus, the first variation of $\bar{V}^*$ set equal to zero applies for finite strains also, since it checks energy conservation laws if proper care is given to stress and strain definition.

Fifth, the fracture stress for the different loading conditions is no longer the same when non-linearities are considered, whether they be finite or infinitesimal. This can be shown through a comparison of the energy equations for the limit cases of fixed force and fixed grip (see Fig. 12).

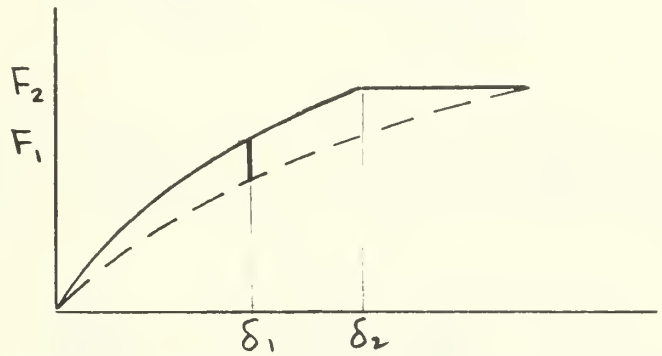

Fig. 12 Comparison of Failure Under Fixed-Force and Fixed Displacement Boundary Conditions

For purposes of illustration, assume the force deflection equation to be

$$F = k(c)f(\delta) \tag{25}$$

The strain energy is still equal to the work done on the body

$$U = \int F\,d\delta = k(c)\int f(\delta)\,d\delta = k(c)\,g(\delta) \tag{26}$$

or

$$U = F\,\frac{g(\delta)}{f(\delta)} = F\,h(\delta) \tag{27}$$

The energy expressions from equation (5b) become

$$\left\{ F \frac{dh}{d\delta}\left(\frac{d\delta}{dc}\right)_F - F\left(\frac{d\delta}{dc}\right)_F + \gamma\left(\frac{dA}{dc}\right)_F \right\}_{F=F_2} = 0 \qquad \text{(Fixed Force)}$$

(28)

$$\left\{ h(\delta)\left(\frac{dF}{dc}\right)_\delta + \gamma\left(\frac{dA}{dc}\right)_\delta \right\}_{\delta=\delta_1} = 0 \qquad \text{(Fixed Grip)}$$

Since

$$\gamma\left(\frac{dA}{dc}\right)_F = \gamma\left(\frac{dA}{dc}\right)_\delta$$

Then

$$\left\{ F\left(\frac{dh}{d\delta} - 1\right)\left(\frac{d\delta}{dc}\right)_F \right\}_{F=F_2} = \left\{ h(\delta)\left(\frac{dF}{dc}\right)_\delta \right\}_{\delta=\delta_1} \qquad (29)$$

But

$$\frac{dh}{d\delta} = 1 - \frac{g(\delta)}{f^2(\delta)} \frac{df}{d\delta} \qquad (30)$$

Substituting equations (25) and (30) into (29)

$$\left\{ -F \frac{g(\delta)}{f^2(\delta)} \frac{df}{d\delta}\left(\frac{d\delta}{dc}\right)_F \right\}_{F=F_2} = \left\{ h(\delta) f(\delta) \frac{dk}{dc} \right\}_{\delta=\delta_1} \qquad (31)$$

Returning to the equivalent constitutive law, equation (25), a relationship between $\frac{d\delta}{dc}$ and $\frac{dk}{dc}$ can be found

$$\left\{ \frac{dF}{dc} \right\}_F = 0 = k \left\{ \frac{df}{dc} \right\}_F + f \frac{dk}{dc}$$

which, when substituted in equation (31) and simplified, gives

$$F_2 = \frac{h(\delta_1)}{h(\delta_2)} F_1 \qquad (32)$$

The conclusion which follows is that in general for non-linear systems, the fracture stress depends upon the form of the stress-strain law as well as the boundary loads, and the specific cases must be analyzed. For instance, if $f(\delta) = \delta^{1/n}$ the critical stresses coincide, but the nature of the system must always be examined to make certain. This could possibly explain some discrepancies in polymeric fracture data, for in the instance of typical material representations such as Neo-Hookean or Mooney-Rivlin, the critical loads will not coincide because of the form of the constitutive law.

Following Schapery and Williams[38], Lindsey[41] has computed the critical fracture stress for both a Neo-Hookean (NH) and a Mooney-Rivlin (MR) material to provide not only a comparison between the two non-linear stress-strain laws, but also with the infinitesimal theory. The strain energy function for both can be represented by

$$W = \frac{E}{6}\left[(I_1-3) + (1-f)(I_2-3)\right] \qquad I_3 = 1 \tag{33}$$

where f = 1 gives NH, and $0 \leq f < 1$ is MR. Following Levinson[42] the relation between the hydrostatic tensile pressure, p, applied at infinity and the stretch ratios of the inner boundary a and outer boundary b is

$$\frac{P}{\mu} = \frac{f}{2}\left[\left(\frac{1}{\lambda_b^4} - \frac{1}{\lambda_a^4}\right) + 4\left(\frac{1}{\lambda_b} - \frac{1}{\lambda_a}\right)\right] - (1-f)\left[\left(\frac{1}{\lambda_a^2} - \frac{1}{\lambda_b^2}\right) - 2\left(\lambda_a - \lambda_b\right)\right] \tag{34}$$

From incompressibility

$$b_o^3 - a_o^3 = b^3 - a^3 \tag{35}$$

where a_0, b_0 denote undeformed measures of the radii. This can be rewritten as

$$a_o^3\left(\lambda_a^3 - 1\right) = b_o^3\left(\lambda_b^3 - 1\right) \tag{36}$$

or

$$\lambda_b = \left[1 + \left(\frac{a_o}{b_o}\right)^3 (\lambda_a^3 - 1)\right]^{1/3} \tag{37}$$

However for an infinite medium $a_0/b_0 << 1$; furthermore, $a/b_0 = \left(\frac{\lambda_a a_o}{b_o}\right) << 1$

From the binomial expansion

$$\lambda_b^n = 1 + \frac{n}{3}\left(\frac{a_o}{b_o}\right)^3 \left(\lambda_a^3 - 1\right) + \cdots \tag{38}$$

Substituting equation (38) into equation (34) the pressure relation simplifies to

$$P = \frac{E}{b} f \left[S - \frac{4}{\lambda_a} - \frac{1}{\lambda_a^4}\right] - \frac{E}{3}(1-f)\left[\frac{1}{\lambda_a^2} - 2\lambda_a + 1\right] \tag{39}$$

As was previously discussed, the altered or extended form of the potential energy functional can also be used for finite deformations. Of course the boundary conditions remain as constant pressure during fracture and the potential of the surface forces is no longer twice the strain energy as in the linear theory. All three energy terms must now be individually computed and inserted into the governing energy equation (15)

$$\frac{\partial}{\partial a_o}\left[U - P + S\right] = 0 \tag{40}$$

where U = strain energy

P = potential of surface forces

S = surface energy

The strain energy is computed through the defining integral

$$U = \int_{b_o}^{b} 4\pi p b^2 db = \int_1^{\lambda_b} 4\pi p b_o^3 \lambda_b^2 d\lambda_b \tag{41}$$

Using equation (38) to express the integral in terms of the extension ratio at the flaw cavity, equation (41) becomes

$$U = 4\pi b_o^3 \int_1^{\lambda_a} p \lambda_a^2 \left(\frac{a_o}{b_o}\right)^3 d\lambda_a \tag{42}$$

where the fact that $a_0/b_0 << 1$ has been used to simplify the expression. Substituting the expression for p, equation (39), and integrating

$$U = \frac{4}{3}\pi a_o^3 E\left[(1-f)\frac{\lambda_a^4}{2} + \left(\frac{7f-2}{6}\right)\lambda_a^3 - f\lambda_a^2 - 1 + f\lambda_a + \frac{f}{2\lambda_a} - \frac{(7f-5)}{6}\right] \tag{43}$$

External work is a much simpler term to compute due to the fact that p is now held constant.

$$P = 4\pi p b_o^2 (b - b_o) = 4\pi p b_o^3 (\lambda_b - 1) \tag{44}$$

Using equation (38) once again

$$P = \frac{4}{3}\pi p a_o^3 (\lambda_a^3 - 1) \tag{45}$$

One of the new facets of the problem alluded to previously is encountered at this point. Before rupturing, the cavity surface may undergo a large change in surface area, which would be considered as a stretching of the molecular structure, with all input energy remaining recoverable. At the critical point, energy will be dissipated by the formation of new surface, and although the cavity is deformed considerably, the surface energy density should be referred to the cavity surface before deformation. The reason being that γ, the surface energy density, is an artifice that relates molecular activity to continuum activity. Consequently it is the number of molecules present on the surface that is of concern in computing fracture energies. This remains constant during the deformation and therefore

$$S = 4\pi a_o^2 \gamma \tag{46}$$

Substituting equations (43), (45) and (46) into the energy equation of (40) and performing the differentiation, with p held constant, we obtain

$$\lambda_a^8 + \frac{2f}{1-f}\lambda_a^6 - \frac{3+2k}{1-f}\lambda_a^4 + 2\lambda_a^2 + \frac{f}{1-f} = 0 \qquad (47)$$

This expresses the critical condition for fracture in terms of the stretch ratio at the cavity and a material parameter $k = \frac{6\gamma}{Ea_o}$. The simplist case is for the NH material when f = 1, then the critical condition is[38]

$$\lambda_a^6 - \left(\frac{3}{2}+k\right)\lambda_a^4 + \frac{1}{2} = 0 \qquad (48)$$

A check of this polynomial reveals that there is only one positive, real root greater than one, so no complicated interpretations arise. Of course once the critical extension ratio is known, the critical pressure can be computed from equation (39), and for completeness, the expression for the tangential hoop stress is given.

$$\sigma_t = \mu\left[f + \lambda_a^2(1-f)\right]\left[\lambda_a^2 - \frac{1}{\lambda_a^4}\right] \qquad (49)$$

2.1.10 Comparison of Linear and Nonlinear Theory

All of these quantities have been plotted collectively for comparison in Figs. 13-15. There is a noticeable variation in almost every quantity, as for instance the ultimate extension of the cavity surface for NH bodies is increased considerably over MR bodies for $\log \frac{6T}{Ea_0}$ greater than 0.50, while the reverse relation holds for the hydrostatic field stress p. In this case, p for the NH body approaches an asymptote of $\frac{5E}{6}$, while MR exhibits behavior characteristic of the infinitesimal theory, and as a result these two curves diverge

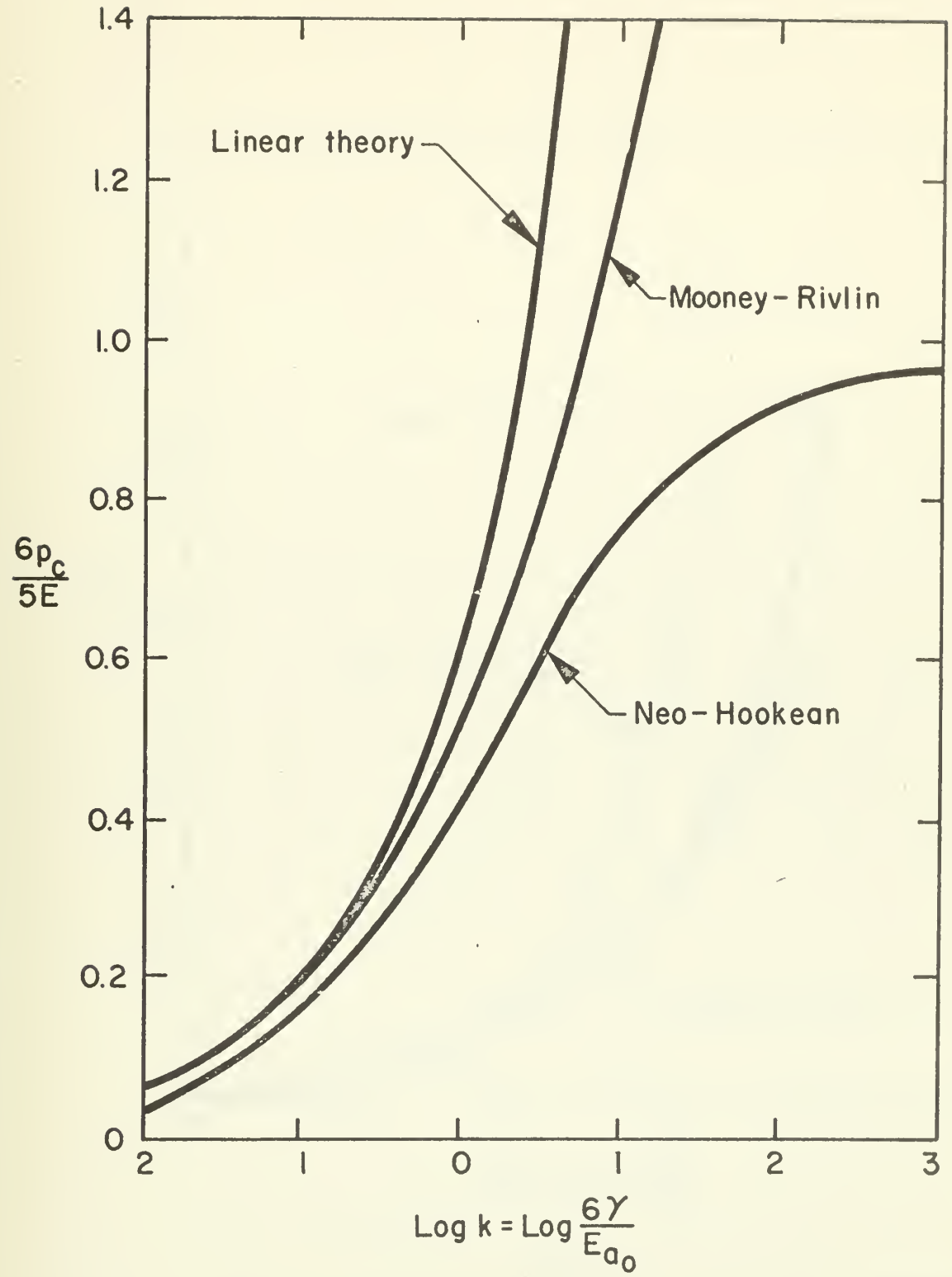

FIG. 13
CRITICAL HYDROSTATIC PRESSURE CONDITION FOR INSTABILITY OF A SPHERICAL CAVITY.

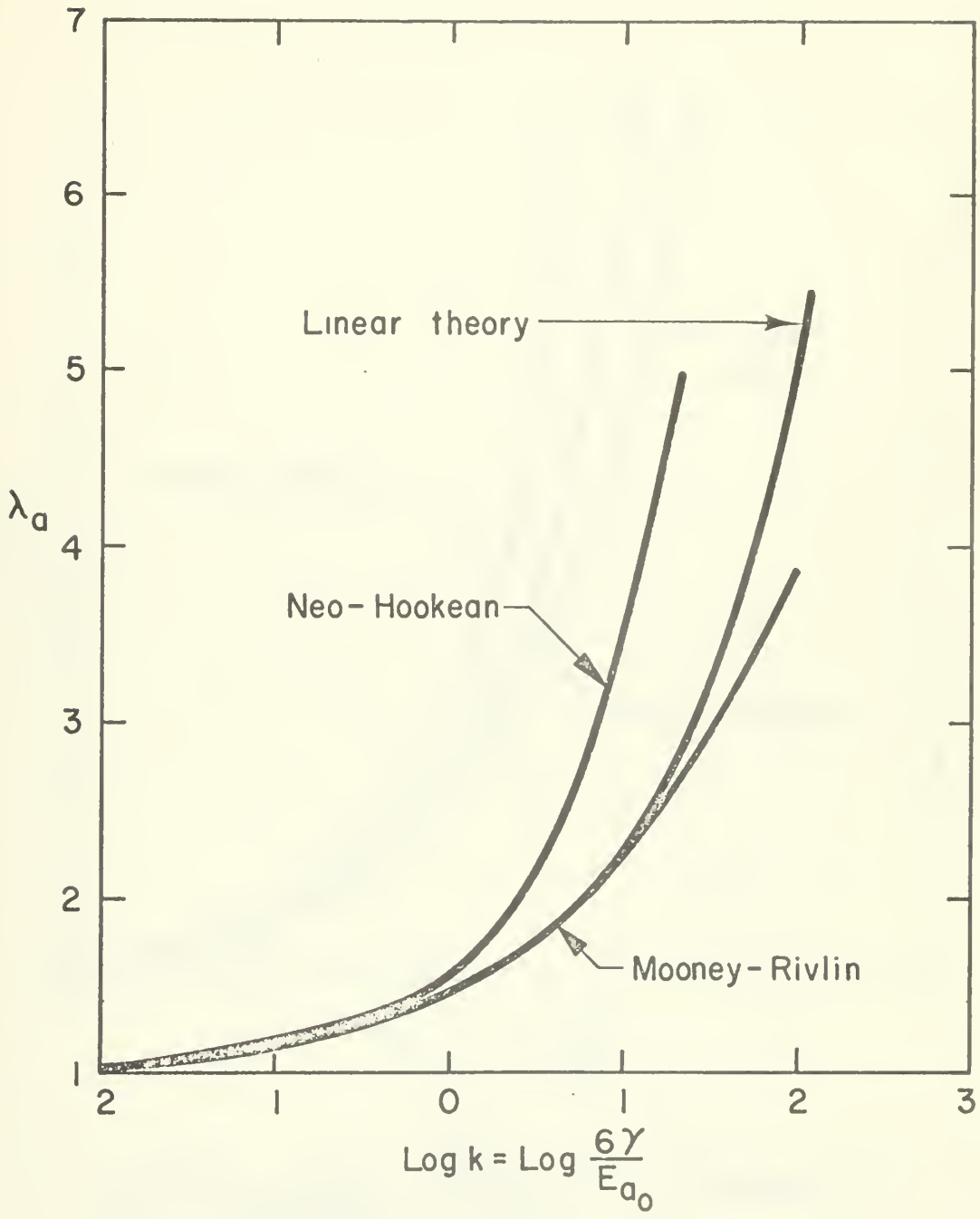

FIG. 14
CRITICAL EXTENSION RATIO AT THE SURFACE FOR INSTABILITY OF A SPHERICAL CAVITY.

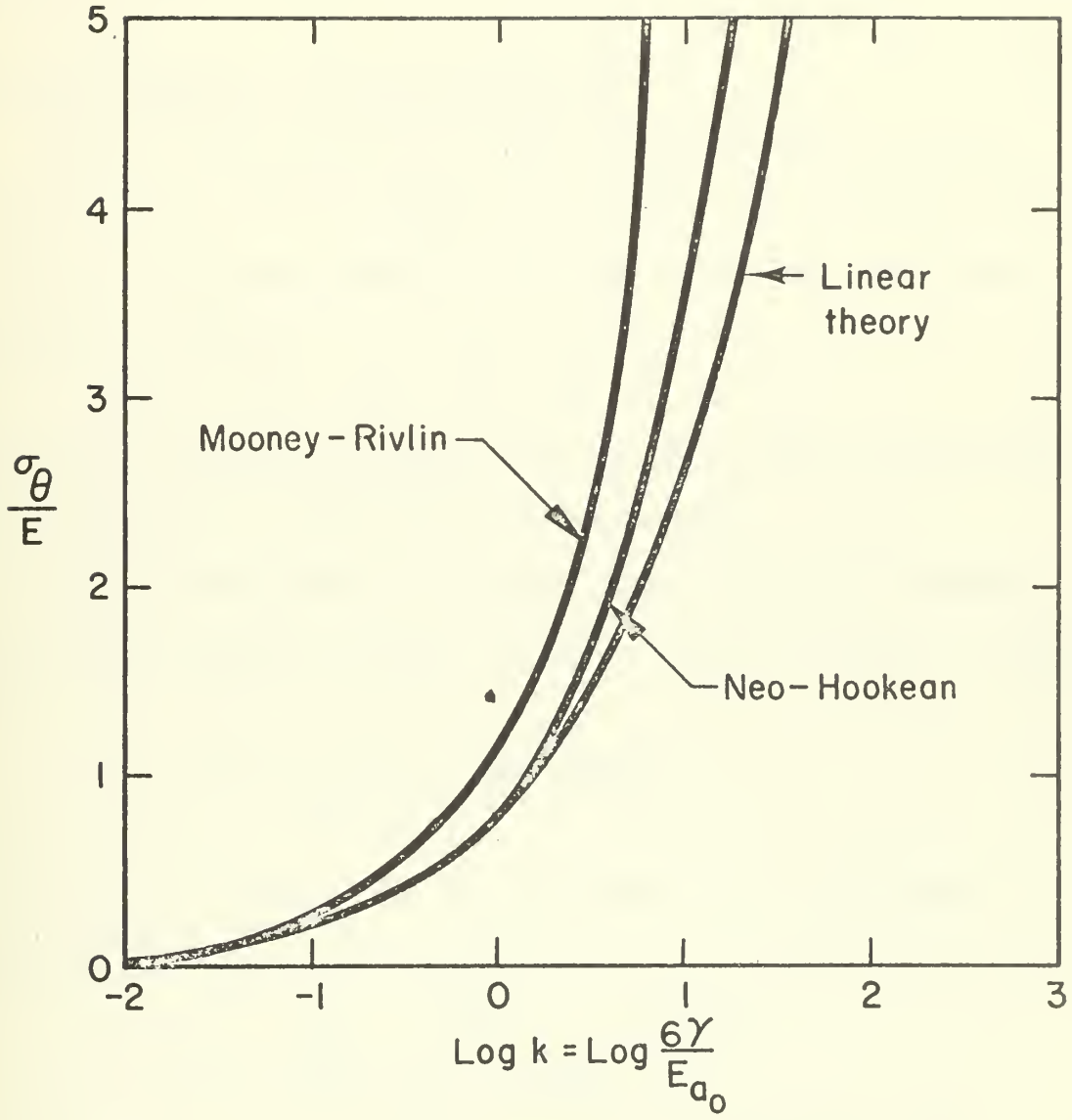

FIG. 15
CRITICAL HOOP STRESS FOR INSTABILITY OF A SPHERICAL CAVITY.

rapidly. However for both NH and MR the inverse square root dependency on a_0 is reduced by considering finite strains. In spite of this reduction, there still remains a strong influence of a_0 on p_c.

2.1.11 Energy Applied to Dissipative Materials

Williams[36] has extended the energy balance concept to include viscoelastic materials. In this instance it is appropriate to work with the time derivative of the energy equation, or the power equation. Neglecting kinetic energy, it becomes

$$\dot{U} + \dot{D} - \dot{W} + \dot{S} = 0$$

where the symbols have the same definitions as equation (5b), the dots denote total time derivative and D represents energy dissipated.

The first two terms are the energy stored and energy dissipated respectively, which together represent the input work up to fracture. Designating this by Y

$$Y = \int_u \int_s \vec{T}_i \, ds \, du_i$$

where $\vec{T}_i$ = surface traction s = surface area u_i = displacement.

Converting to a time derivative

$$\dot{Y} = \frac{d}{dt} \int_t \int_s \vec{T}_i \frac{du_i}{dt} \, ds \, dt$$

Relating the surface tractions to the internal stress components, $\vec{T}_i = \tau_{ij} \nu_j$,

$v_i = \frac{du_i}{dt}$

$$\dot{Y} = \frac{d}{dt} \int_t \int_s \tau_{ij} \nu_j v_i \, ds \, dt$$

Converting the surface integral to a volume integral,

$$\dot{Y} = \frac{d}{dt}\int_t \int_V \left[\tau_{ij,j} v_i + \tau_{ij} v_{i,j}\right] dV\, dt$$

However $\tau_{ij,j} = 0$ from equilibrium and $v_{i,j} = \dot{\varepsilon}_{ij} + \dot{\omega}_{ij}$

$$\dot{Y} = \frac{d}{dt}\int_t \int_V \left[\tau_{ij}\dot{\varepsilon}_{ij} + \tau_{ij}\dot{\omega}_{ij}\right] dV\, dt$$

Since τ_{ij} is symmetric and ω_{ij} is antisymmetric, $\tau_{ij}\omega_{ij} = 0$

$$\dot{Y} = \frac{d}{dt}\int_t \int_V \tau_{ij}\dot{\varepsilon}_{ij}\, dV\, dt$$

The rate of work done during fracture for a constant load is given by

$$\dot{W} = \int_s \dot{T}_i \dot{u}_i\, ds$$

and surface energy becomes

$$\dot{S} = \frac{d}{dt}\int_s \gamma\, ds$$

Williams computes these terms for a spherical cavity in a hydrostatic tensile field subjected to constant stress, constant strain, constant stress rate and constant strain rate. From these he computes time to fracture for the spherical cavity, assuming a radial propagation mode similar to ablation. For instance for a spherical cavity in an infinite medium subjected to a step stress, the critical stress is given by

$$\sigma_c = \frac{4}{3}\sqrt{\frac{\gamma/a_o}{2D_{crp}(t_o) - D_g}}$$

where Dcrp is the creep compliance, Dg is the glossy compliance, and t_o is the time to failure. This can be compared to the elastic case of equation (24),

especially for $t_o \rightarrow 0$, in which case

$$\sigma_c = \frac{4}{3}\sqrt{\frac{E_4 \gamma}{a_o}}$$

This application has been extended to plane stress and plane strain by Burton and Noel[75] for application to cylindrical cavities.

2.2 Failure Surfaces

In general materials may be subjected to six stress components, three normal and three shearing. Only three of these are independent, and the stress state can always be resolved into an axis system where the stress state is defined by three principal stresses. Inasmuch as there are three orthogonal components, they may be used as an axis system in what will be termed principal stress space. This coordinate system divides the space into octants, as shown in Fig. 16, where only four are drawn for the sake of clarity. Values of the failure stress can be plotted to create a failure surface, some part of which will occupy a portion of each octant (Fig. 17).

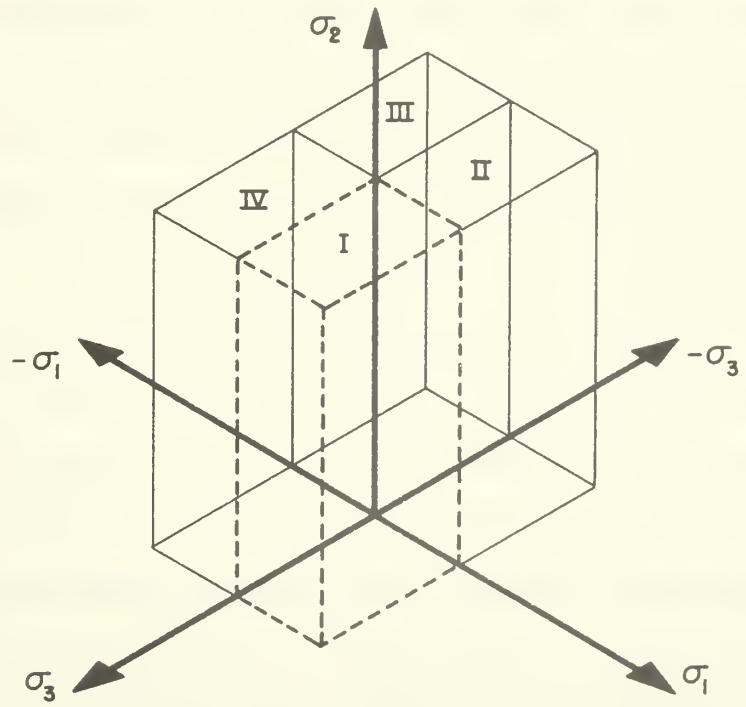

Fig. 16 Principal Stress Space

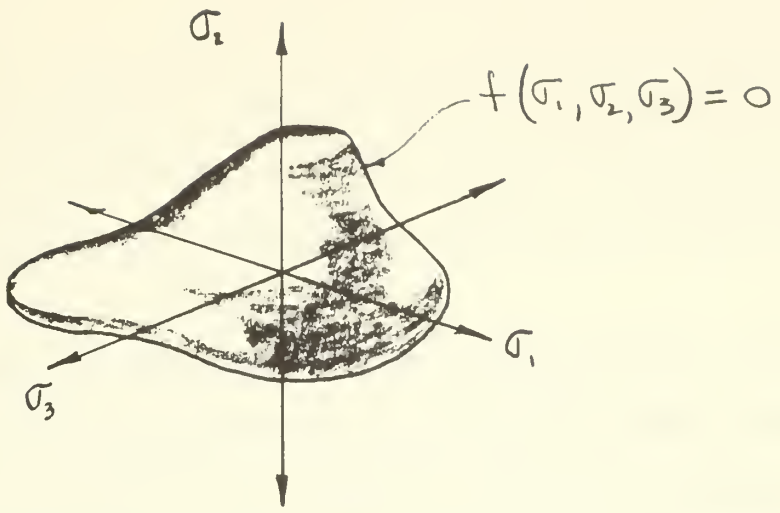

Fig. 17 General Failure Surface

Mathematically the surface is described by

$$f(\sigma_1, \sigma_2, \sigma_3) = 0 \tag{50}$$

In its most elementary form, when fracture depends upon the instantaneous stress alone, failure is described in terms of a surface that is assumed to exist in stress space. As an element in a body is loaded, the state of stress for each increment describes a path, as σ_i takes on new values. When the path remains within, i.e., on the origin side of the failure surface, the element is considered "safe" from failure. Fracture occurs when the stress path contacts the failure surface. The strength of this method lies in the fact that generally it is not practical, and frequently impossible to achieve exact duplication of engineering stress fields by laboratory techniques, for instance the myriad of varieties in a solid propellant rocket motor. This concept is being used presently by various investigators to extrapolate or interpolate laboratory data to motor conditions. A mathematical description of the failure surface concept depicts failure properties of the propellant in terms of the isochronal and isothermal loci of ultimate properties in either stress or strain space. Providing that the general shape (functional form) of this failure surface can be determined by a few

discriminately chosen laboratory tests, the failure condition for any configuration of propellant grain can be reliably predicted. This is theoretically possible even though the exact state or conditions are not duplicated by the laboratory tests.

Before discussing the characteristics of failure surfaces, attention is called in passing to the comprehensive survey of failure criteria presented in the work of Blatz, Ko, and Zak[43] where some 24 criteria are discussed, and to the more recent survey by Kruse[44] of laboratory techniques for solid-propellant characterization.

2.2.1 Failure Theories in Principal Stress Space

The failure surface means of representation gives tha analyst a technique for visualizing regions of failure and safety. It also provides a means of visualizing the region of applicability of the various failure theories that have been proposed. Nadai[45] enumerates, for example, several different theories in common use. Each criterion defines some particular functional of the stress field, the value of which is to be determined empirically. When the appropriate functional is exceeded, the associated fracture takes place. Six common ones are listed below:

a. Maximum principal stress

b. Maximum principal strain

c. Maximum principal stress difference (shear)

d. Maximum principal strain difference

e. Maximum total strain energy

f. Maximum distortional strain energy

Each of these fracture theories can be plotted in principal stress or strain space as has been done for the first one in Fig. 18

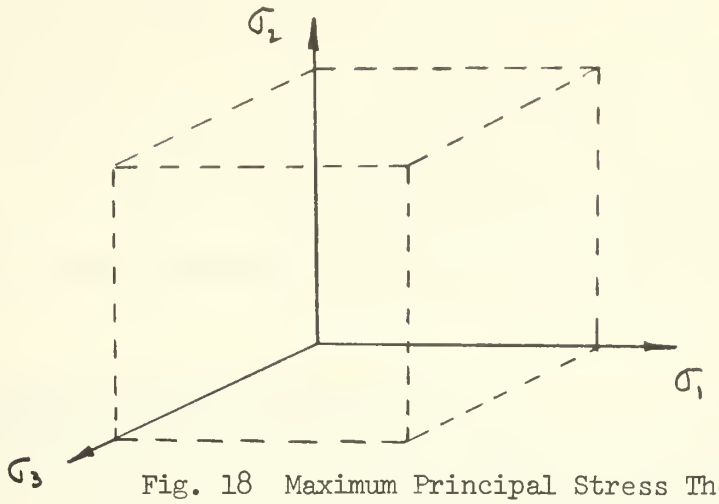

Fig. 18 Maximum Principal Stress Theory

No general criterion such as those listed above has enjoyed much success over a broad range of materials or conditions; consequently the fialure surface generally has to be constructed from extensive testing. It is appropriate to tabulate the various possible stress combinations in the different octants.

Octant	1	2	3	Number of Positive Stresses
I	+	+	+	3
II	+	+	-	2
III	-	+	-	1
IV	-	+	+	2
V	+	-	+	2
VI	+	-	-	1
VII	-	-	-	0
VIII	-	-	+	1

By virture of equivalence of the three principal axes, it is noted that there are four categories of octants characterized by the number of stresses of the same sign. Thus octants II, IV and V are similar, and octants III, VI and VIII are similar. This means that for an isotropic material only four octants need to be tested. If in addition, it is known that the compressive properties are the same as the tensile properties, then only two octants need be tested.

2.2.2 Symmetry About the Hydrostatic Line

Deductions can be made as to the general shape of the failure surface through symmetry. The equivalence of the three principal axes means that they are invariant to the group of rotations in the body; i.e. which principal stress direction in the body is selected to coincide with σ_1, σ_2, σ_3, is arbitrary. The hydrostatic line (locus of points making equal angles with the coordinate axes in octants I and VII) becomes an axis of symmetry, and fracture in hydrostatic tension or hydrostatic compression become extremums; i.e. they are limit points on the failure surface. (See Fig. 19).

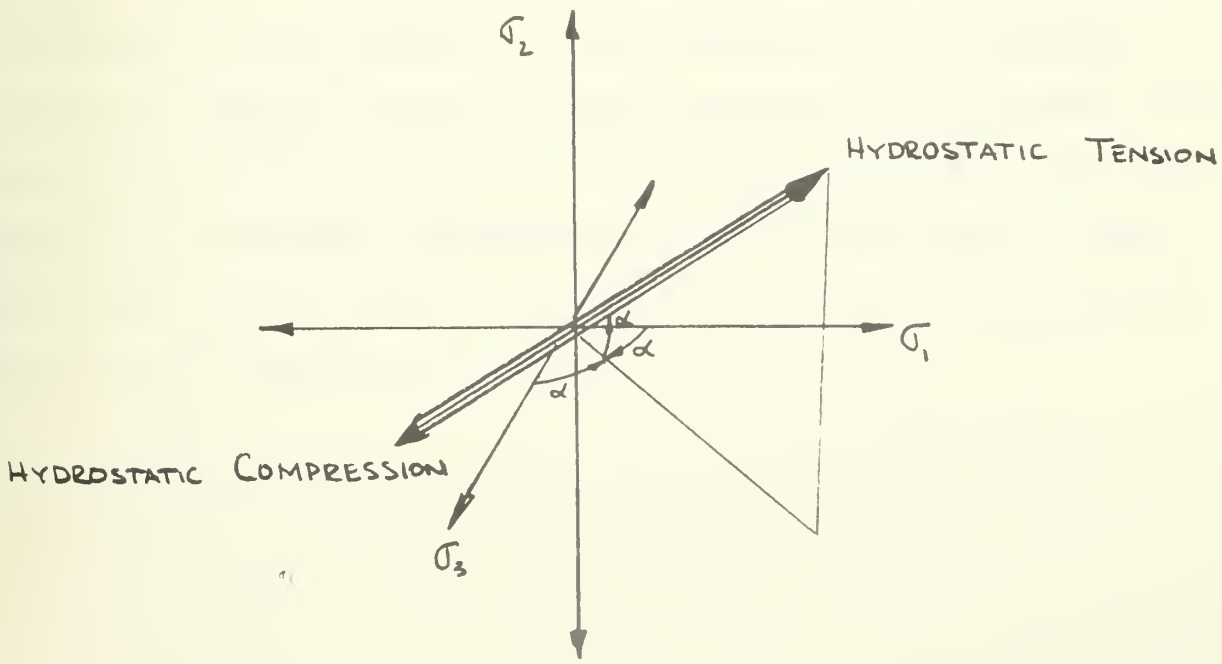

Fig. 19 Locus of Hydrostatic Tension and Compression in Principal Stress Space

Now although there are many obvious similarities between hydrostatic tension and compression, there is a great deal of difference in the manner in which materials respond to these two environments fracture-wise. The theory cannot demonstrate that there will be a difference in the actual configuration of the failure surface; however it has been found through experiment that there are significant differences. Bridgman[46] has shown that in combined stress states involving high levels of hydrostatic pressure, none of the standard failure criteria of maximum principal stress, maximum principal strain, etc. postulated from tensile results are accurate. He has investigated many stress states that cover several of the octants and has noted large changes in the levels of ultimate strains and ultimate stresses in these other octants when compared to the +++ octant. Bridgeman[47] has also discussed the fact that it is necessary before rupture can occur to have what he terms an energy release mechanism, or more simply, a place for the material to go so that energy can be used to create new surface. Reflection upon this point leads to the conclusion that in pure hydrostatic compression fracture could never occur and the ultimate strength would be infinite. However, slight perturbations from this field would provide enough anti-symmetry to allow fracture to occur at realistic levels. Therefore in hydrostatic compression the failure surface possesses a cusp at infinity, which would be in strong contrast to the same situation in tension where there is an energy release mechanism, and fracture can occur at finite values. It then follows that tension and compression produce quite different surfaces and their behavior are not inverses of each other.

2.2.3 Further Symmetry Conditions[48]

Assuming material isotropy, if a path $\sigma_1', \sigma_2', \sigma_3'$ from the origin leads to failure at the point $\sigma_{1f}, \sigma_{2f}, \sigma_{3f}$ then a path $\sigma_1'', \sigma_2'', \sigma_3''$ where $\sigma_1'' = \sigma_2'$; $\sigma_2'' = \sigma_1'$ (where σ_1' and σ_2' have been interchanged) performed at the same conditions would fail at $\sigma_{2f}, \sigma_{1f}, \sigma_{3f}$. The locus of failure points; i.e., the failure surface is therefore symmetrical with respect to the plane $\sigma_1 = \sigma_2$. Upon looking down the hydrostatic line, cross-sections of the failure surface are planes parallel to the so-called π plane (Fig. 20). The lines LN NM LM are intersections of the π plane with the coordinate planes, and the contour of the failure surface is symmetrical about LL', MM' and NN'. (All lines shown are in the π plane except for the coordinate axes.) As a result of the symmetry, a single failure point, such as the uniaxial tension points L, M, N may be plotted three times; therefore it is only necessary to consider stress states whose vectors lie in one of the six characteristic segments.

The actual contour such as LR or LS can be determined by performing a discrete number of tests for a given segment.

2.2.4 Convexity

Of particular note are the implications of the symmetry condition together with the concept of convexity upon the possible configuration of the equilibrium fracture surface. A curve in a plane is said to be convex* if the points of any chord lie entirely to one side of the curve. A convex surface, in

---

* An alternate definition for a convex curve in a plane states "A curve such that any straight line cutting the curve cuts it in just two points." This definition is applicable only to closed curves, however.

turn, is one in which any plane section is a convex curve. As will be seen, it is most advantageous when convexity can be associated with a failure surface.

As discussed by Blatz, Ko, and Zak[43], based upon the thermodynamic arguments of Coleman, the failure surface in principal stretch space is convex. For the failure surfaces in principal stress space all experience points to the fact that it too is convex. With convexity augmenting the symmetry conditions, upper and lower bounds upon the fracture surface can be established which approach each other as the number of tests increase. With reference to Fig. 21, based on uniaxial tensile date only (points L, M, N), any convex curve with the symmetry described previously must lie inside the triangle M'L'N' (upper bound) and outside the triangle M L N (lower bound). Although this can be shown mathematically, the reader may convince himself readily by attempting to construct a convex symmetric curve, any portion of which lies outside the region described.

The bounds shown in Fig. 21, based on tensile data alone, admit a wide range of possible failure criteria and do little to locate the failure locus precisely. This provides a rational explanation as to why it has been possible for so many different multiaxial failure criteria to have appeared in the literature. However, with additional tests, more useful bounds arise, e.g., through the diametral compression test, the points labeled D are established in Fig. 22. These together with uniaxial tests T (with a suitably chosen superimposed time-dependent hydrostatic pressure so that points T and D are in the same plane) considerably narrow the spectrum of admissible failure contours*.

---

* An admissible contour may be defined as any convex curve through the failure points possessing the symmetry imposed by material isotropy.

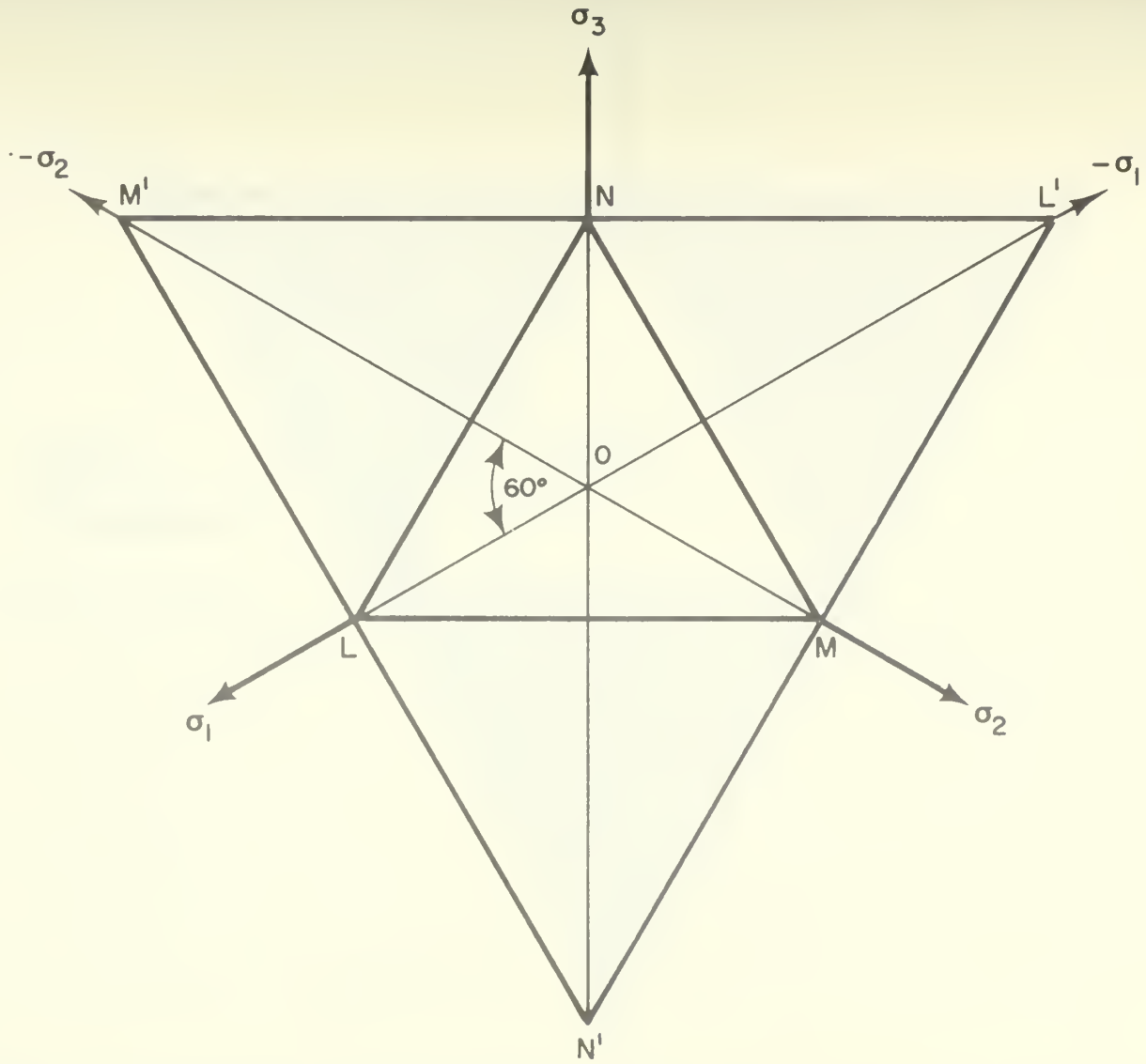

FIG. 20 SYMMETRY OF FAILURE SURFACE CONTOURS PARALLEL TO THE π PLANE

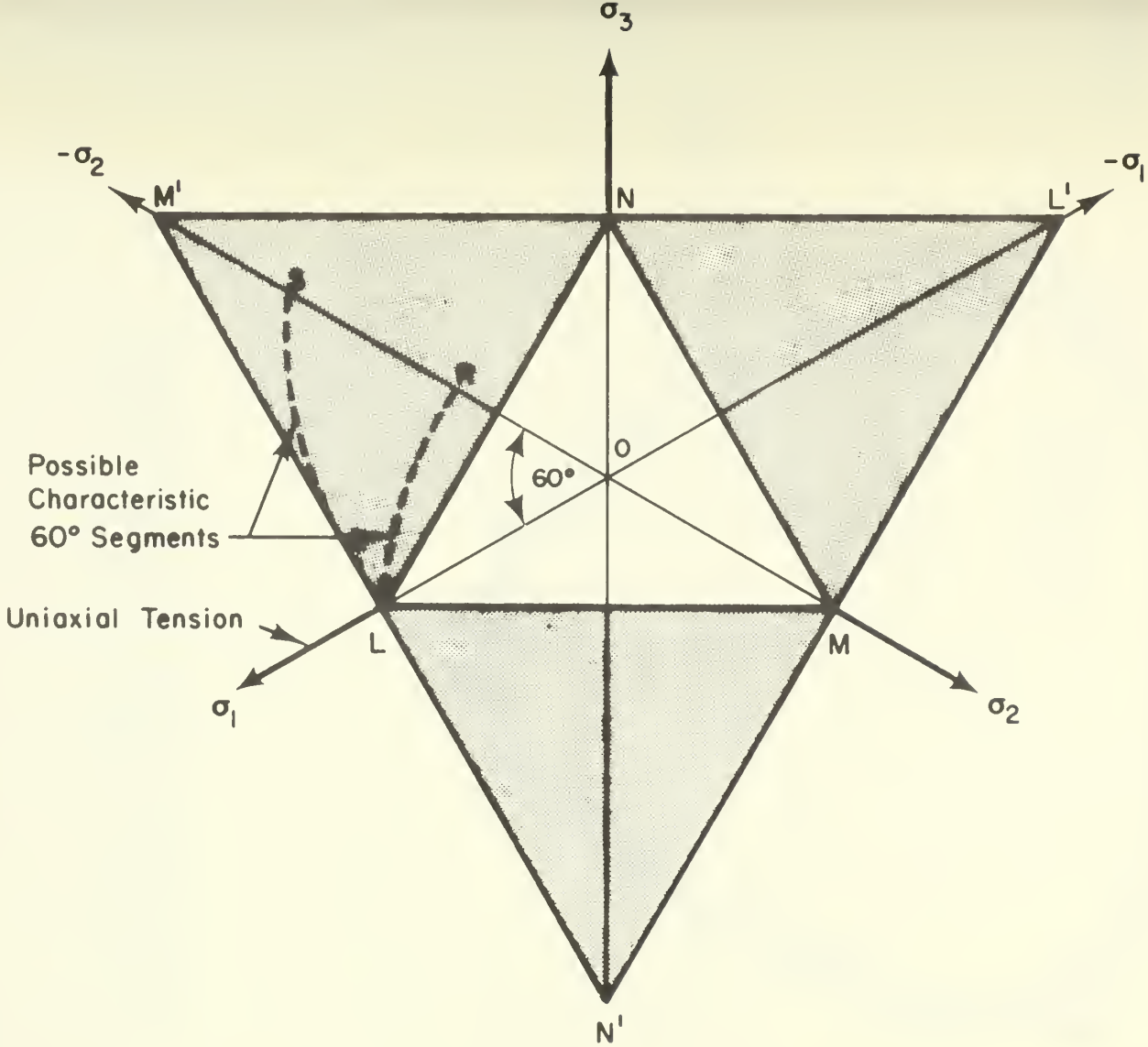

FIG. 21 SPECTRUM OF ADMISSIBLE FAILURE CONTOURS PARALLEL TO THE π PLANE ($\sigma + \sigma + \sigma = 0$), GIVEN TENSILE (POINTS L, M, N) ONLY.

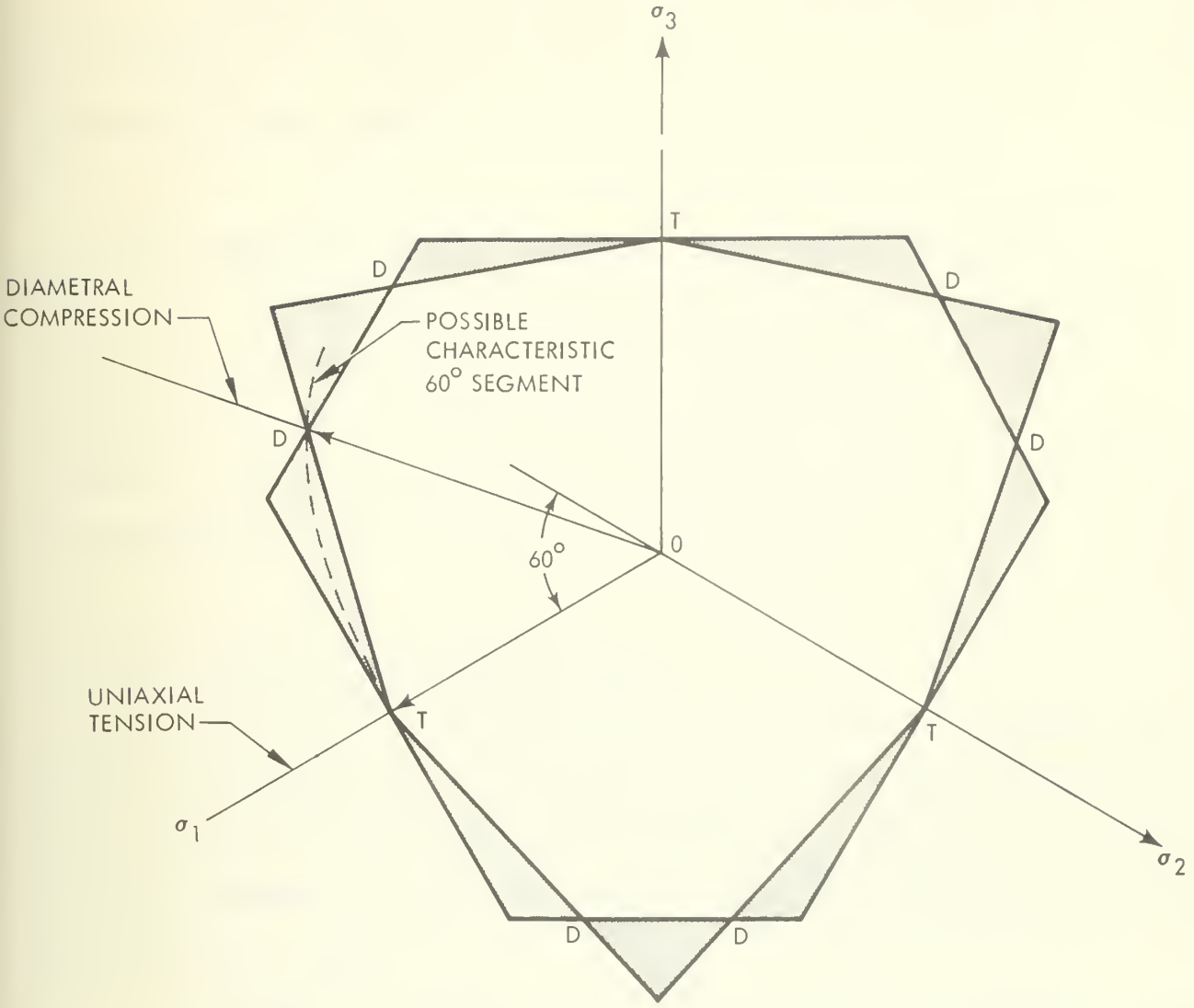

Fig. 22 Spectrum of Admissible Failure Contours Parallel to the π Plane ($\sigma_1 + \sigma_2 + \sigma_3 = 0$), Given Tensile (Point T) and Diametral Compression (D) Data

If in addition the biaxial-strip test is performed, again in the presence of a suitably chosen time-dependent hydrostatic pressure, the spectrum of admissible contours is further narrowed as shown (qualitatively in Fig. 23).

2.2.5 Appearance of a Typical Surface in the Failure Spectrum

In summary, a characteristic 60° segment of the associated failure surface (Fig. 24) is expected to be a surface situated about the axis, possessing (by material isotropy) three planes (through the coordinate axes) of symmetry. Intersections with planes in stress space parallel to the π plane are expected to be convex and similar to one another.

2.2.6 Time Dependent Failure Surfaces

In general, viscoelastic failure properties are not invariant with respect to strain history. The time dependency associated with the viscoelastic nature of the propellant binder network gives rise to a multiplicity, or spectrum, of failure surfaces in stress space, where each surface represents constant strain-rate, isothermal behavior.

The onset of fracture in a viscoelastic body is determined by mechanical geometric variables, as well as the entire history of manufacture and storage. Considering only materials with identical production histories, initially in a stress- and strain-free condition, then in tests under a variety of loading conditions fracture will depend only on the thermomechanical states described by the quantities $\sigma_{ij}(t)$, $\varepsilon_{ij}(t)$, $\dot{\varepsilon}_{j}(t)$, T up to the time of fracture. Because fracture depends not only upon the instantaneous value of these variables, but also upon all the preceding values, the criterion for fracture is expressable as

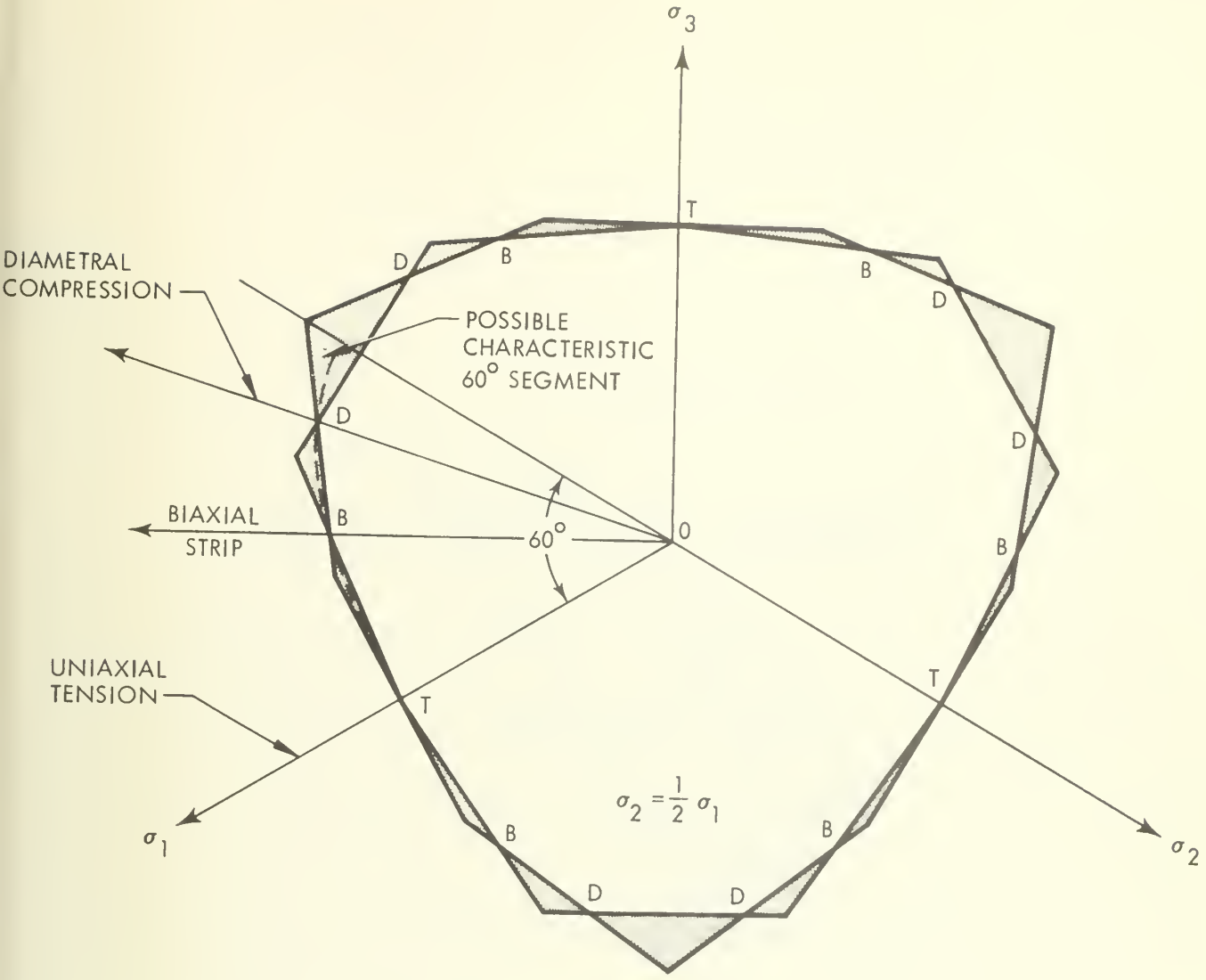

Fig. 23 Spectrum of Admissible Failure Contours Parallel to the π Plane ($\sigma_1 + \sigma_2 + \sigma_3 = 0$), Given Tensile (Point T), Biaxial Strip (B), and Diametral Compression (D) Data Points

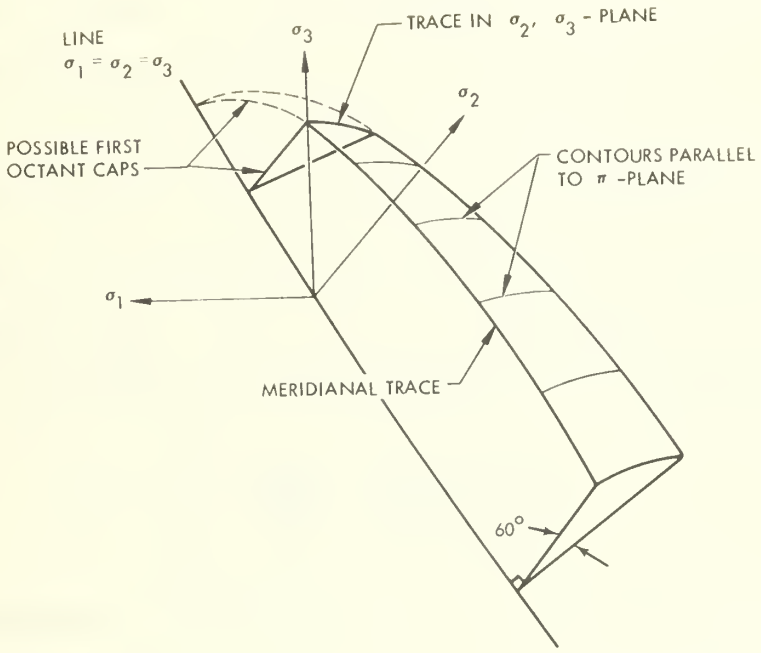

Fig. 24 Characteristic 60° Segment of a Typical Member of the Failure Surface Spectrum in Principal Stress Space

a functional. As stress, strain, and strain rate are not independent variables but are expressable as functionals of each other, the failure criterion can be represented by

$$F\left[\sigma_{ij}^{f}, \varepsilon_{ij}\right] = 0 \tag{51}$$

where F is a function of the stress components σ_{ij}^{f} at the instant of failure and a functional of strain. Formulations equivalent to equation (51) are also possible in principal strain space.

The functional form of equation (51) can be refined further by recognizing that the strain history of loading has both time-history and path-history dependence as the same path can be traversed at different rates. Following Pipkin and Rivlin[49] the strain history $\varepsilon_{ij}(\tau)$ $(-\infty < \tau \leq t)$ is described by specifying the strain path and the rate of traversal. The arc length, s, along the path is defined as

$$s = \int_{-\infty}^{t} \left(\frac{d\varepsilon_{ij}}{d\tau}\,\frac{d\varepsilon_{ij}}{d\tau}\right)^{\frac{1}{2}} d\tau \tag{52}$$

and ε_{ij} is described by its dependence on s, in the form $\varepsilon_{ij}(s)$ $(0 \leq s \leq S)$. Therefore equation (51) becomes

$$F\left[\sigma_{ij}^{f}, \varepsilon_{ij}, s(t-\tau)\right] = 0 \tag{53}$$

as the rate of traversal is known from s(t).

This functional form when translated into words would represent failure surfaces in a six dimensional stress space possessing a nested set of shells, describing failure for different strain rates. How the six different strain rates enter is also not clear; therefore at this stage, the general time-dependent failure surface is not an applicable tool.

One exception for viscoelastic materials is the equilibrium failure surface that in addition to being time and temperature independent is also believed to be path independent as suggested by its psuedo-elastic characteristics. At sufficiently low loading rates, the integral laws of linear viscoelasticity reduce to Hooke's Law. This equilibrium behavior has already been observed in uniaxial tests. Therefore, the dependence of F upon rate need not be included when equation (53) is associated with the equilibrium surface. For inviscid behavior therefore,

$$F\left[\sigma_{ij}^{f},\ \varepsilon_{ij}\right] = 0 \tag{54}$$

Further, as Hooke's Law is path independent, F is not influenced by intermediate values of strain, but only upon the strain at failure which is expressible in terms of σ_i^f. Therefore, the functional form of equation (54) reduces simply to a function of the failure stresses, i.e.,

$$F\left(\sigma_{ij}^{f}\right) = 0 \tag{55}$$

which represents uniquely a surface in principal stress space.

2.2.7 Failure Envelope

The idea of a failure envelope is similar in name and in practical usage to a failure surface, but in fundamental concept it is completely different. It is included here for completeness. Smith[50] discovered experimentally that if the failure points for uniaxial tension are plotted on a stress-strain graph, a unique locus is obtained for a wide range of strain histories.

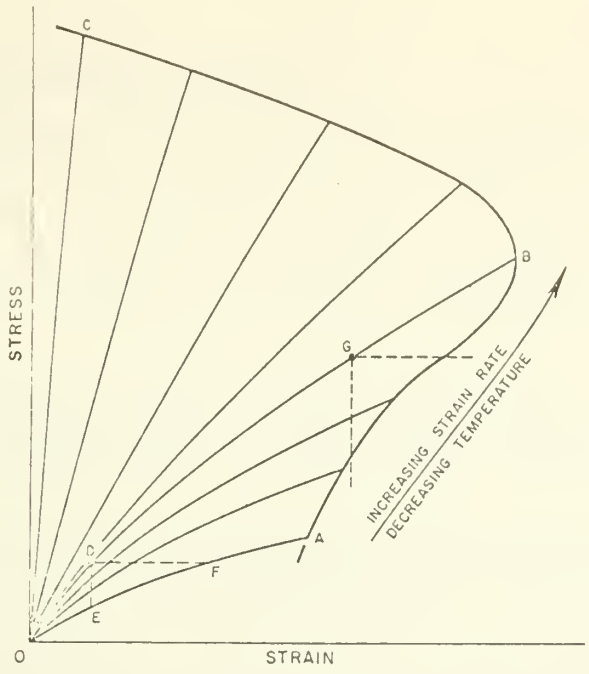

Fig. 25 Schematic Representation of the Failure Envelope

Williams[51] has pointed out that the uniqueness of the envelope holds up well as long as the strain histories are monotonic. Thus prediction of fracture in uniaxial tension for time dependent materials subjected to arbitrary strain histories is feasible but not of too great a practical interest, since most stress fields arising in engineering structures are more complex.

Methods for biaxial and triaxial fracture predictions based on analogies with uniaxial specimens have been designed. For instance, an approach to failure currently in use by some of the propellant industry is based upon the uniqueness of the uniaxial failure envelope and the concept of equivalent uniaxial stress and strain. This criterion has the advantage of incorporating all components of stress and strain, and although accounting for variable strain rates does not

employ the cumulative damage technique.

It is suggested, therefore, that a (variable rate) stress-strain path be super-imposed on the uniaxial failure envelope to determine when failure occurs. For multiaxial states of stress, the equivalent uniaxial stress is defined by

$$\sigma_e = \frac{\sqrt{2}}{2}\left[(\sigma_1-\sigma_2)^2 + (\sigma_2-\sigma_3)^2 + (\sigma_3-\sigma_1)^2\right]^{\frac{1}{2}} \tag{56}$$

Calculated at a given point of the grain, it may be plotted against the equivalent uniaxial strain

$$\varepsilon_e = \frac{\sqrt{2}}{2(1+\nu)}\left[(\varepsilon_1-\varepsilon_2)^2 + (\varepsilon_2-\varepsilon_3)^2 + (\varepsilon_3-\varepsilon_1)^2\right]^{\frac{1}{2}} \tag{57}$$

If the profile lies completely within the envelope, the grain may be considered safe from failure at the point in question. The method need not be restricted to bore strains but can include, for example, slot roots as well.

The quantities σ_e and ε_e have been constructed to reduce to σ_i and ε_i (i = 1, 2, and 3), respectively, for the case of uniaxial tension in the i-direction.

The quantity σ_e is also variously known as the generalized stress or the effective stress[52] and is related to the second invariant of the stress deviation tensor J_2 and the octahedral shear stress τ_{oct} through

$$J_2 = \frac{1}{3}\sigma_e^2 = \frac{3}{2}\tau_{oct}^2 \tag{58}$$

It can be shown that σ_e is related appropriately to ε_e through

$$\sigma_e = E\varepsilon_e \tag{59}$$

Landel and Fedors[53] have proffered a more general version of the failure envelope where they have incorporated many polymers on the same plot. By plotting reduced data through normalizing the variables on the basis of crosslink density, they have shown that a universal failure envelope can be generated. Supporting their contention with a large quantity of experimental data, they further find the envelope to be analytically described by the Martin, Roth Stieler[54] equation for elastomers.

They also examine failure data in terms of three dimensional plots of stress, strain and time. This more general look at the problem becomes awkward and loses its effectiveness because the path of the time dependent material becomes important again in predicting failure.

2.3 Fracture Experiments

In order to supply the extensive data needed to use these theories to predict fracture in any given stress state, numerous experiments are needed. The design and selection of fracture experiments is based upon the ability to create a specimen that will produce fracture in an area of known stress. It is desirable that this stress field be constant over a sizeable area, so that no large gradients confuse the interpretation of experimental results. Obviously it must be a configuration that is amenable to accurate stress analysis, so that values of the local stress and strain are available. All of these constraints severely limit the possibilities, but a few standard failure tests have emerged and are being used successfully.

Another theoretical consideration relating to fracture experiments is the inherent statistical nature of material rupture. This is attributed to the fact that fracture initiation is a very localized phenomenon, originating from minute defects in the material. Since these are statistically distributed in the fabrication process, failure will be statistical when ultimate properties are evaluated.

The phenomenon is amenable to statistical representation, and the probability distribution functions are readily obtainable if enough samples are tested. The limiting factors are usually time and money; otherwise the failure properties can be quite accurately defined.

2.3.1 Test Methods[27]

The uniaxial, biaxial, and triaxial failure test methods routine used for viscoelastic characterization are as follows:

A. Uniaxial tension - Joint Army-Navy-Air Force (JANAF) and filleted bonded-end samples (class A)

(1) Constant strain rate

(2) Constant load

(3) Constant strain

B. Uniaxial shear - double shear samples

(1) Constant strain rate

(2) Constant load

(3) Constant strain

C. Biaxial compression - disc samples

(1) Constant crosshead speed

D. Biaxial tension - strip samples

(1) Constant strain rate

(2) Constant load

(3) Constant strain

E. Pressurized tensile - bonded end samples and shear sample

(1) Constant strain rate

F. Triaxial tension - poker chip sample

(1) Constant strain rate

G. Large amplitude dynamic tension - bonded end samples

H. Analogue motor thermal test - steel case

I. Analogue motor pressurization test - fiberglass case.

These tests have been reduced to practice and when conducted over a sufficiently broad time and temperature test spectrum, yield adequate information for evaluation of an empirical failure criteria useful for establishing grain structural limits.

2.3.2 Unixial Tension

Tensile failure characterization is obtained by testing milled JANAF specimens with plastic gauges per the ICRPG mechanical behavior manual (section 4.3.5). Filleted tab end samples (class A) are used for all engineering work, but JANAF (class B) samples with plastic gauges are still tested for comparative purposes. Constant load and constant strain tests are conducted with class A bonded-end samples to establish endurance limits for cumulative damage analysis.

2.3.3 Biaxial Compression

The diametral compression test is performed by compression of a propellant disc until rupture occurs at the center of the specimen (Fig. 26). Compressive stress and strain at the center of the sample are evaluated from the Instron load and crosshead displacement (section 4.5.1 of ICRPG mechanical behavior manual).

The vertical compressive stress (σ_y) at the center of the sample is given by

$$\sigma_y = \frac{-6F_y}{td}$$

where F_y = compressive force

t = sample thickness

d = sample diameter

The tensile stress (σ_x) along the horizontal axis reaches a peak at the center of the sample

$$\sigma_x = \frac{2F_y}{td}$$

The horizontal strain (ε_x) at the center of the sample is calculated from

$$\varepsilon_x = \frac{2(1+3\nu)}{(1-\nu)(2-\pi)+(1+\nu)} \frac{U}{d}$$

where U is the total deformation along the horizontal axis, and Poisson's ratio is normally assumed to be 0.5.

Shear stress along the horizontal axis is a maximum at 45° to the axis and reaches a peak at the center of the sample as

$$\tau_{xy} = \frac{4F_y}{td}$$

The test is carried out at a constant crosshead speed. The vertical force, F_y, and the total diameter change, U, are measured during the test and used to

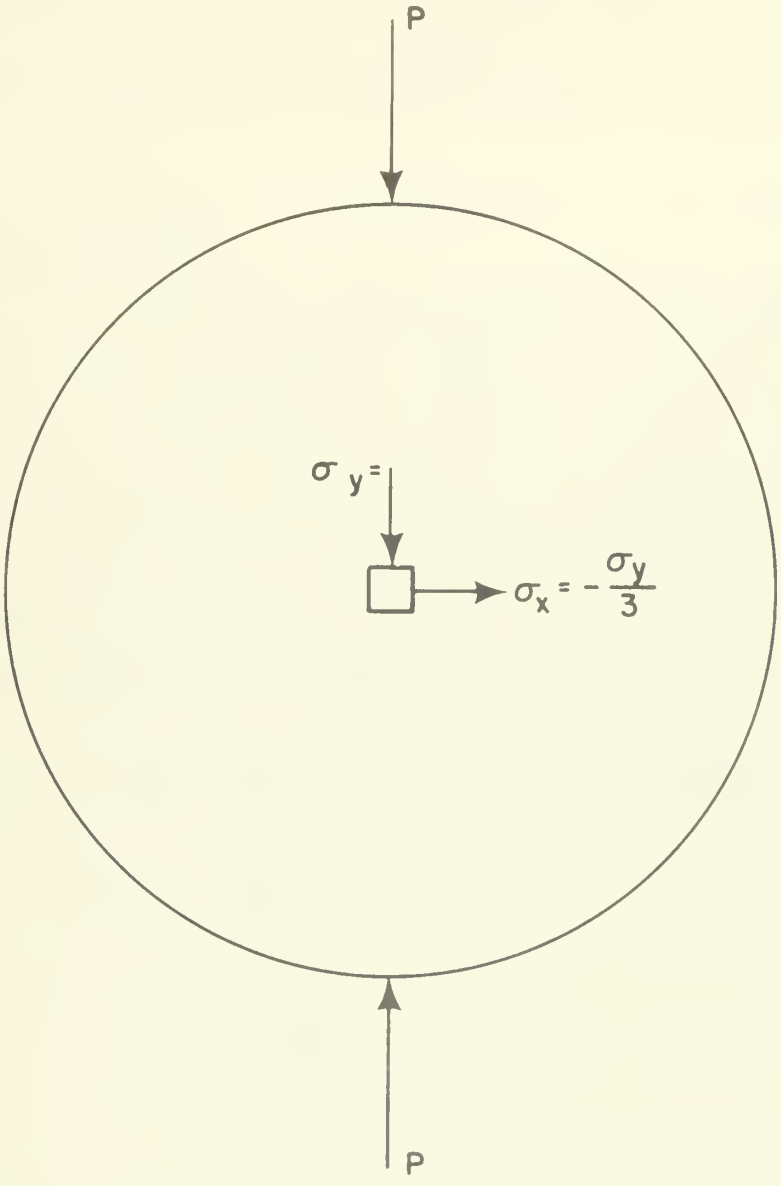

FIG. 26 DIAMETRAL COMPRESSION

calculate stress and strain at rupture.

Failure occurs by cracking at the center of the specimen. The failure mode may be either tensile or shear depending on the test material and temperature. This combined tension-compression stress and strain field at the center of the circular disc is very similar to that in a pressurized rocket motor.

2.3.4 Biaxial Tension

A biaxial strip test specimen consists of a thin plate of propellant that is wide with respect to height and clamped along the edges, as shown in Fig. 27. Samples are tested by pulling at a constant crosshead rate on the Instron tester. The stress and strain distribution at the propellant center for any sample width-to-diameter ratio is given by Williams and Schapery[55].

The stress and strain at the center of the sample geometry are given by the following equations, if Poisson's ratio is assumed to be one-half:

$$\sigma_x = \frac{F}{A} \qquad \text{vertical,}$$

$$\sigma_y = \frac{\sigma_x}{2} \qquad \text{horizontal,}$$

$$\varepsilon_x = \frac{\Delta l}{l_o} \qquad \text{vertical, and}$$

$$\varepsilon_y = 0 \qquad \text{horizontal.}$$

The stress ratio at the center of the sample is 2:1. Failure of the strip biaxial sample usually occurs by cracking in the central region of the strip where the stress field is reasonably uniform. Constant load and constant strain tests are conducted to establish biaxial endurance limits for cumulative damage and long term storage analysis.

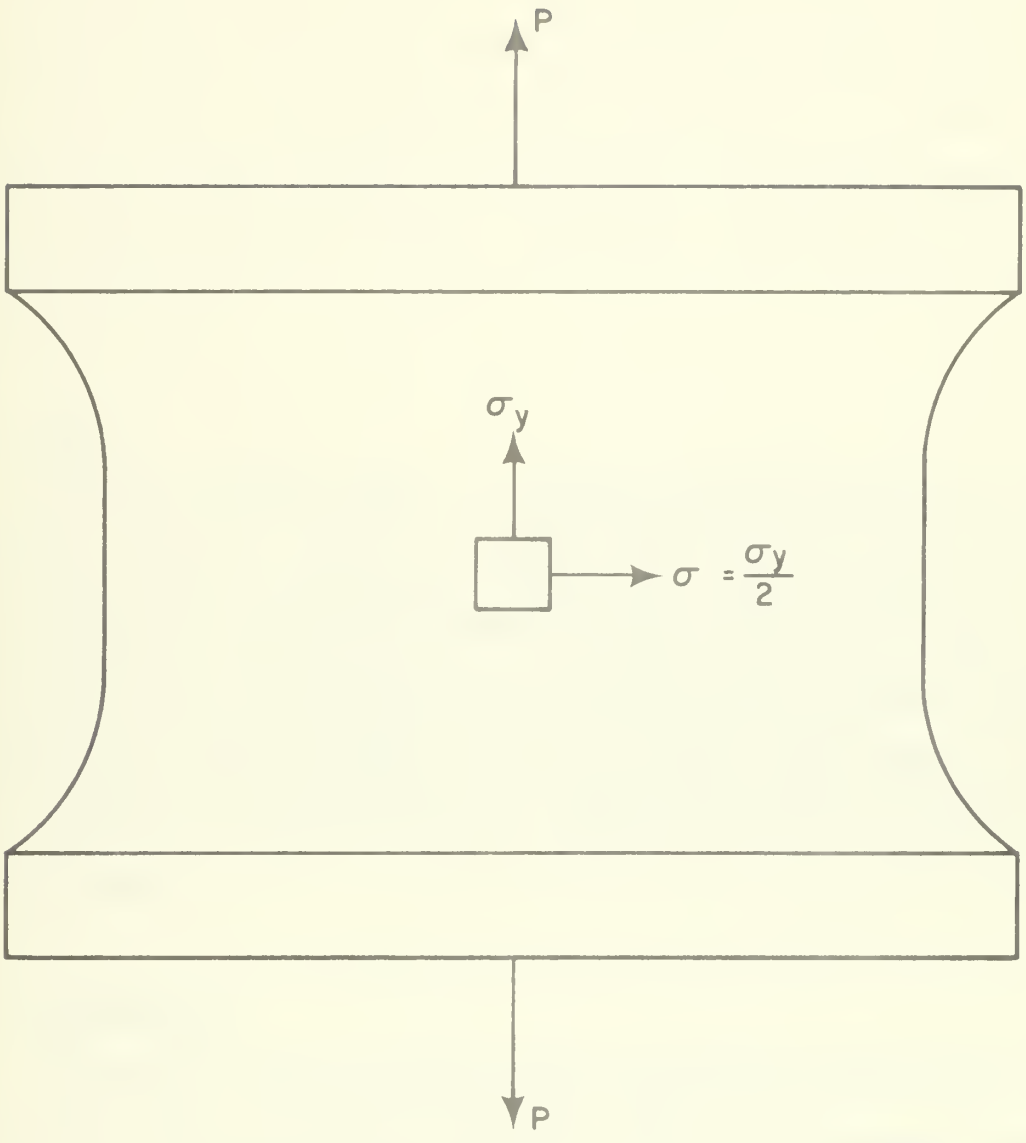

FIG. 27 BIAXIAL STRIP

2.3.5 Pressurized Tension

Tensile stress and strain failure properties improve when measured under pressure. Data reported by Siron and Duerr[56] and Farris[57] both show definite increases in strain at maximum load and maximum stress for increasing pressure. Pressurized tensile failure data for a CTPB propellant is presented in Fig. 28. The extent of improvement in failure properties is believed to be related to the dilatational behavior of the propellant, since those propellants which dewet excessively show the largest improvement in failure properties when tested under pressure.

2.3.6 Shear

Propellant shear behavior is evaluated by testing the double shear specimens shown in Fig. 29. Samples are prepared by casting propellant into appropriate prelined metal fixtures designed for shear evaluation. Failure of the shear sample occurs by cracking parallel to the shearing direction in the weakest region of the liner-propellant bond area. Shear stress limits are usually one-third to one-half of the tensile failure limits, while shear strains normally exceed tensile limits.

2.3.7 Triaxial Test

A hydrostatic tensile stress field is generated experimentally using the so-called poker chip test, which derives its name from the specimen geometry (section 4.5.5 of the ICRPG mechanical behavior manual). In this test a thin circular disc of propellant is bonded between rigid plattens and pulled perpendicular to the large surface (Fig. 30). Sample deformation is accurately measured during the test with three linear variable differential transformers to ensure that the sample deformation is uniform. Propellant failure stress limits measured under

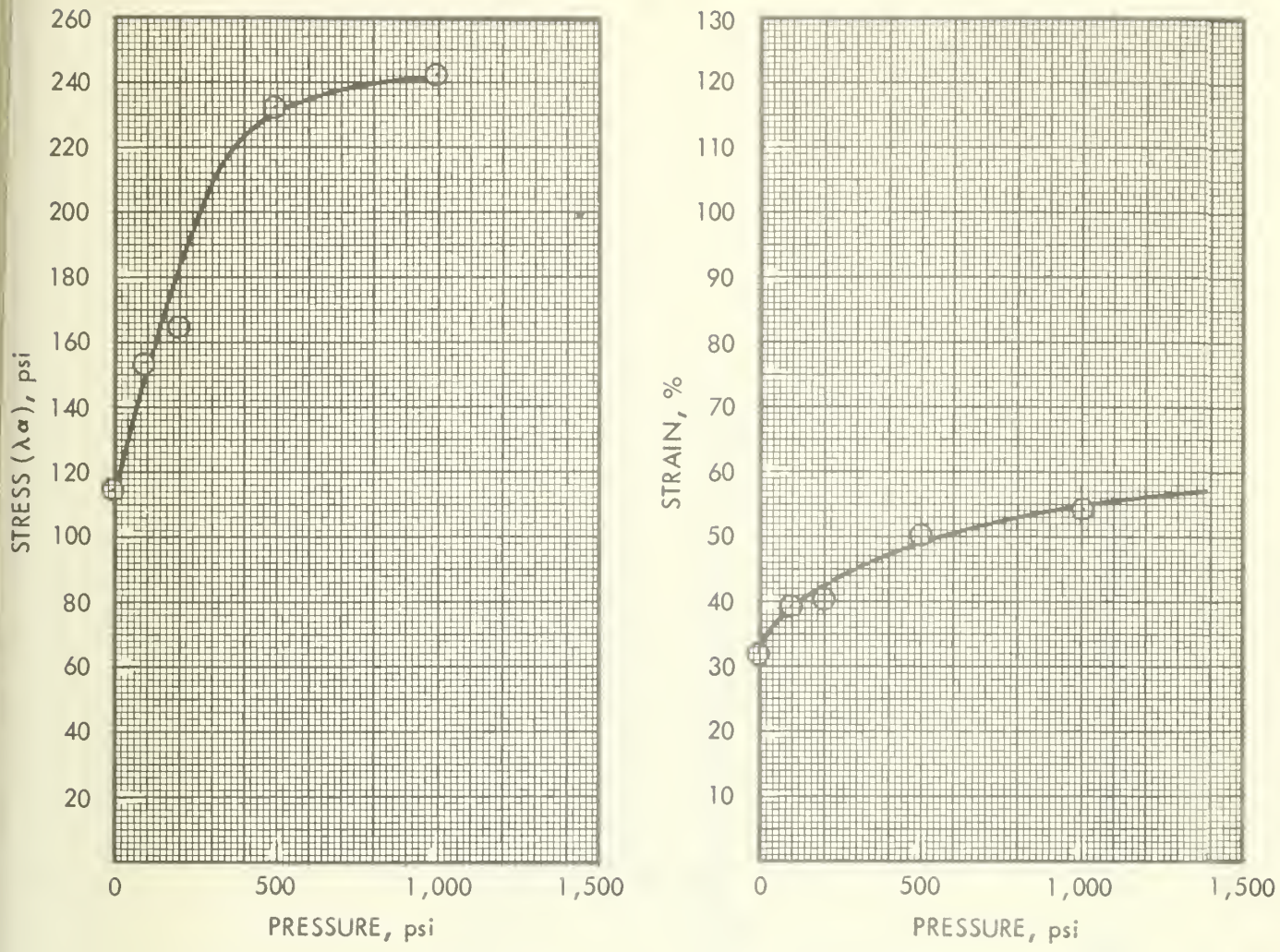

Fig. 28 Effect of Pressure on the Stress and Strain Limits of a CTPB Propellant

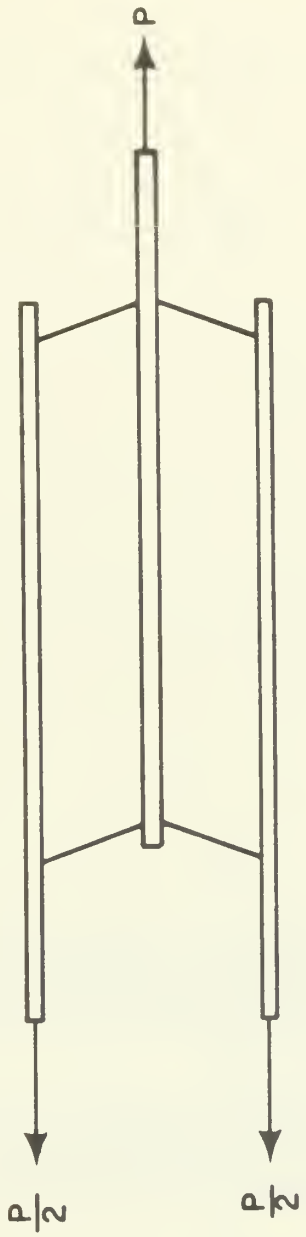

FIG. 29 DOUBLE LAP SHEAR

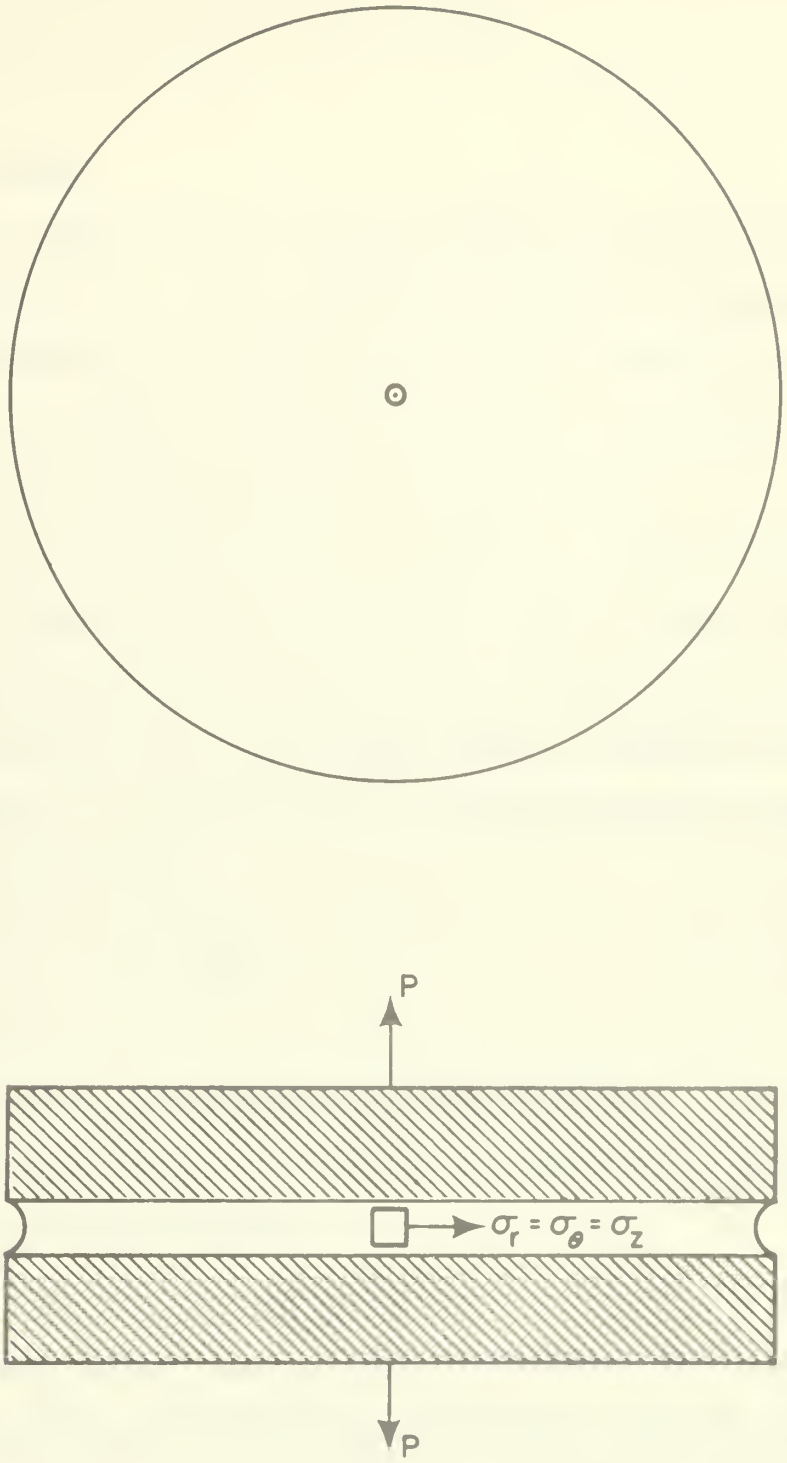

FIG. 30 POKERCHIP TEST

triaxial tension usually equal or exceed uniaxial stress data, while triaxial strains are much less than uniaxial strain limits.

2.4 Cumulative Damage

"What fatigue damage is, how it can be measured, and how it grows as a result of the stress experienced ... are questions that cannot be adequately answered today."[58] This statement in a recent review article on damage accumulation in metals reveals the continuing difficulty encountered in coping with fatigue, even in materials whose research history is long-standing.

In propellant, the question of how to analyze for fatigue failure, or the more general problem of how to account for arbitrary loading history, remains unresolved. Methods presently used refer to the original idea of Miner[59] that material damage occurs for load applications smaller in magnitude than that required for failure. He postulated that for cyclic loading the damage would accumulate in a linear fashion

$$\sum_i \frac{n_i}{N_i} = D \tag{60}$$

where

n_i = number of cycles at a given stress level,

N_i = number of cycles to failure at a given stress level, and

D = accumulated damage.

Each term of the sum represents a fraction of the total life at a given fraction of the total life at a given stress level; when these fractions sum to one, the damage has theoretically become great enough to produce rupture of the component.

In a comprehensive study of design and analysis of solid propellant rocket grains, Williams[60,61] suggested that a carryover of Miners' Law to viscoelastic

materials might be in order. He made a correlation between the time that a viscoelastic specimen is subjected to a given strain rate and the number of cycles a metallic specimen is exposed to a given stress. This resulted in an expression that predicted time to failure if the damage accumulation law was known. Taking it to be linear where no differentation is made for order of loading, the incremental damage is given by

$$\Delta D_i = \frac{\Delta t_i}{t_{fi}} \tag{61}$$

where

Δt_i = time at ith loading

t_{fi} = time to failure at ith loading, and

ΔD_i = incremental damage

Whether or not the linear relationship is acceptable depends upon the characteristic of a given material, but most preliminary reports have shown it not to be completely accurate. However, at this stage of development, nonlinear theories involve such complications that it is deemed wise to approximate real behavior with a linear law. This assumption reduces the computation of damage level to simple addition of the individual damage terms as they stand,

$$\sum_i \Delta D_i = \sum_i \frac{\Delta t_i}{t_{fi}} \tag{62}$$

Even more importantly, it makes the extension in the limit to an integral quite straightforward

$$\int_0^D dD = \int_0^t \frac{dt}{t_f} \tag{63}$$

Bills[62] has shown that time to failure t_f is linearly related to stress level for logarithmic plots, where the history is one of constant load to failure (see Fig. 31). Tests at UTC have shown a similar result for cyclic loading, as

given in Fig. 32, which can be fit with analytic expressions that are readily manageable in engineering calculations. Fitting the curve of Fig 32

$$\text{Log}\,\sigma = m\,\text{Log}\,\frac{t}{a_T} + \text{Log}\,C \tag{64}$$

Matching the slope and intercept at Log $(t_f/a_T) = 0$,

$$\left(\frac{t_f}{a_T}\right)^{-m} = \frac{\sigma}{\sigma_o} \tag{65}$$

Therefore,

$$t_f^{-1} = \frac{1}{a_T}\left(\frac{\sigma}{\sigma_o}\right)^A \tag{66}$$

where A = 1/m. Substituting into equation (63), an expression similar to Bills, constant load is obtained

$$D = \frac{1}{a_T \sigma_o}\int_0^t \sigma^A\, dt \tag{67}$$

This equation will give the time to failure for a given stress level history by setting D = 1 and integrating; however, since fracture is observed to be a statistical quantity, there will be statistical variations of the experimentally observed failures about unity. This presents no problem in uniaxial tensile bars, but it does become expensive in more complicated tests. The means of incorporation of statistical descriptions into the analysis is clear, but the only limiting factor is the economic one which controls the number of tests allowed to define the probability distribution functions.

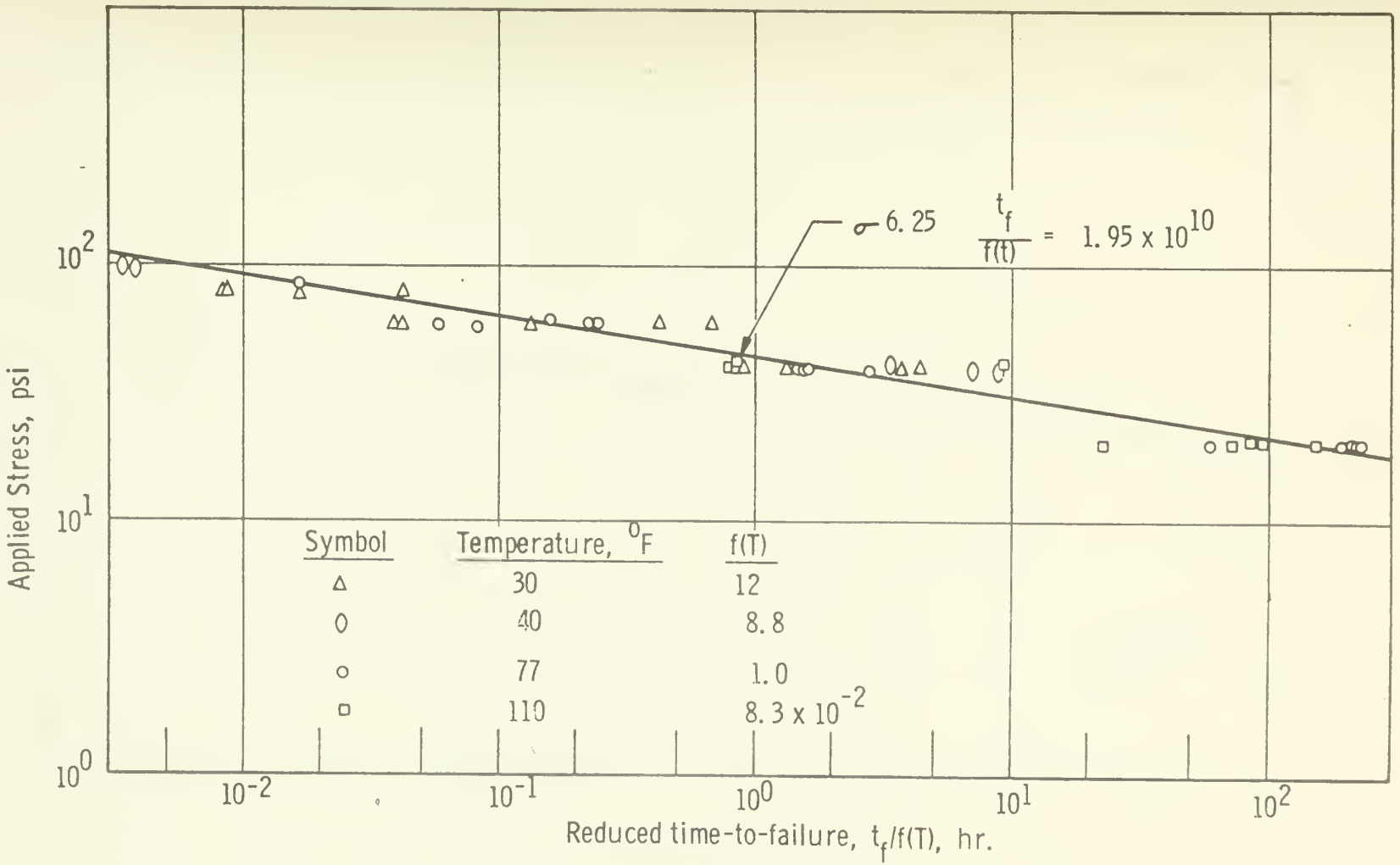

Fig. 31 Master Plot of Applied Stress vs. Reduced Time-to-Failure for Bond Specimens

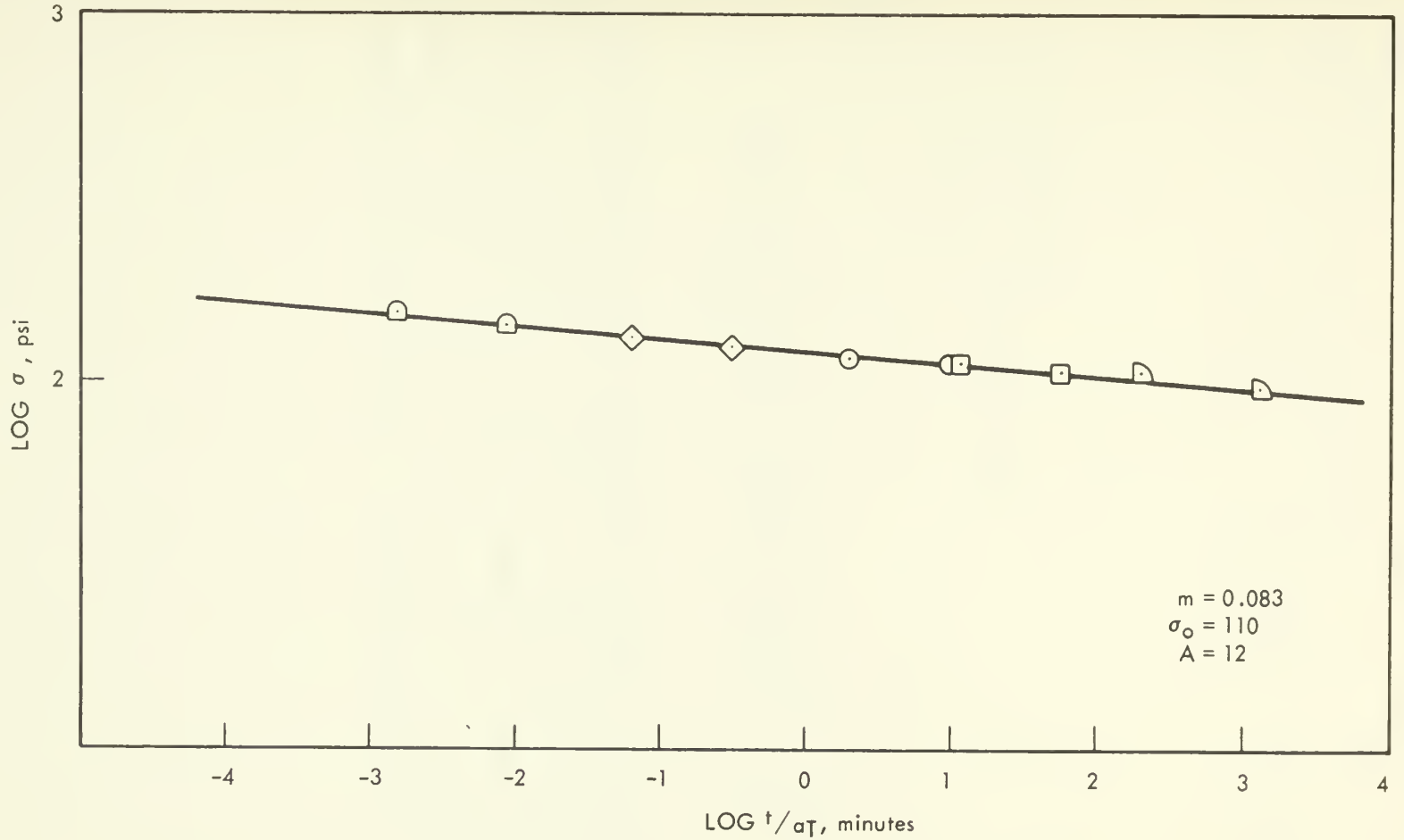

Fig. 32 Stress vs. Time to Rupture Data for a Cyclic Strain Test Mode

The linear assumption can be carried one step further and used in the calculation of failure for bodies subjected to more than one mode of loading. It seems reasonable that the order of loading would be immaterial when considering different types of loading and how they interact

$$\sum_i \Delta D_i = \sum_i \left[\frac{\Delta t_i}{t_{fi}}\right]_L + \sum_i \left[\frac{\Delta t_i}{t_{fi}}\right]_F + \sum_i \left[\frac{\Delta t_i}{t_{fi}}\right]_R \quad (68)$$

where

L = constant load,

F = fatigue or cyclic load, and

R = constant rate.

In the limit,

$$D = \frac{1}{a_T} \int_0^t \left[\alpha \sigma_L^A + \beta \sigma_F^B + \gamma \sigma_R^C + \cdots\right] dt \quad (69)$$

This linear theory will allow a prediction of failure, either deterministic or statistical, for any arbitrary combination of loads. Such calculations can be made and tested for uniaxial and biaxial specimens to evaluate the validity of the assumptions. Having a measure of the accuracy of the prediction, a realistic combined load situation could be formulated and applied to rocket motors.

Stress Concentrations

Obtaining the stress field around holes and cracks is a complicated task normally involving large and complex expressions, but one of the early efforts in this direction yielded an elegent solution. It was made in 1898 by Kirsch[63]. He obtained the solution for a tensile member with a central circular hole, which was a very significant building block in fracture mechanics. Because it relates significantly to a later solution, the rudiments of the solution will be included here.

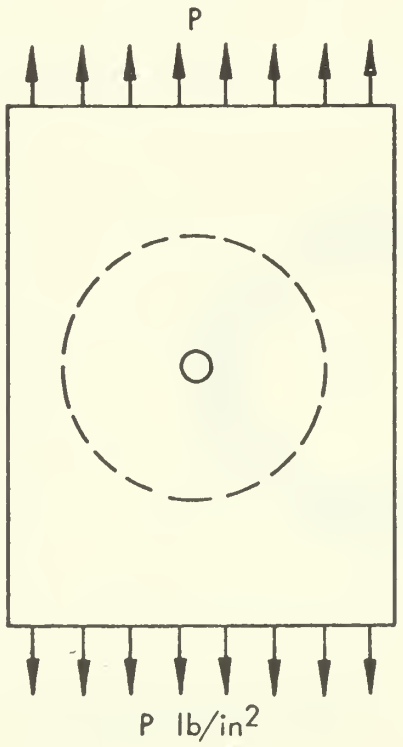

Inside radius = a

Outside radius = r_o

Fig. 33 Tensile Specimen with Central Hole

Kirsch employed the principal of St. Venant and assumed that at some radius $r = r_o$ the effect of the hole would be negligible; furthermore, disallowing the influence of the other boundaries, he took the sheet to be infinite. The solution of the problem then proceeds by transforming the stress conditions at $r = r_o$, which are $\sigma_y = P$, $\sigma_x = \tau_{xy} = 0$, into cylindrical coordinates. This transformation gives

$$\sigma_r(r_o) = \frac{P}{2}\left[1 - \cos 2\theta\right] \tag{70a}$$

$$\tau_{r\theta}(r_o) = \frac{P}{2} \sin 2\theta \tag{70b}$$

The problem is then decomposed into two parts as shown in Fig. 34 where the appropriate boundary conditions are given for each.

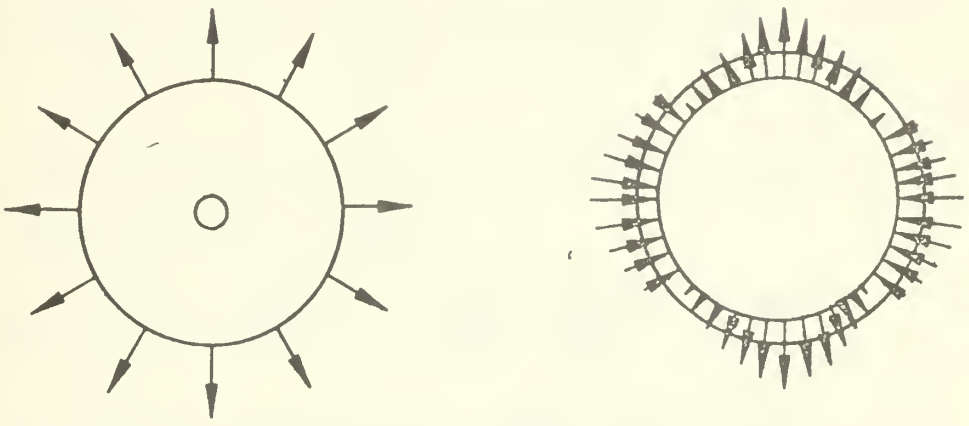

Fig. 34 Decomposition of Problem

The first has the classical solution of

$$\sigma_r = \frac{P}{2} \frac{r_o^2}{r_o^2 - a^2} \left[1 - \frac{a^2}{r^2} \right] \tag{71a}$$

$$\sigma_\theta = \frac{P}{2} \frac{r_o^2}{r_o^2 - a^2} \left[1 + \frac{a^2}{r^2} \right] \tag{71b}$$

$$\tau_{r\theta} = 0$$

The second solution is found through the use of the Airy stress function ϕ,

$$\nabla^4 \phi = 0 \tag{72}$$

by assuming

$$\phi = f(r) \cos 2\theta \tag{73}$$

An ordinary differential equation is obtained for f(r) when equation (73) is substituted into equation (72). Solving for ϕ

$$\phi = \left[A + Br^2 + \frac{C}{r^2} + Dr^4 \right] \cos 2\theta \tag{74}$$

The boundary conditions provide four simultaneous equations for the constants, and the complete solution is given by

$$\sigma_r = \frac{P}{2} \left[\left(1 - \frac{a^2}{r^2} \right) - \left(1 - 4\frac{a^2}{r^2} + 3\frac{a^4}{r^4} \right) \cos 2\theta \right] \tag{75a}$$

$$\sigma_\theta = \frac{P}{2} \left[\left(1 + \frac{a^2}{r^2} \right) + \left(1 + 3\frac{a^4}{r^4} \right) \cos 2\theta \right] \tag{75b}$$

$$\tau_{r\theta} = \frac{P}{2} \left[\left(1 + 2\frac{a^2}{r^2} - 3\frac{a^4}{r^4} \right) \sin 2\theta \right] \tag{75c}$$

This very significant solution in the evolution of fracture mechanics is outlined here to show two things. First that even for this most simple geometry

the expressions are algebraically involved and require manipulations that are somewhat tedious. Any steps taken toward a more complicated geometry result in a significant increase in tedium. Secondly, this general method of solution was the one followed by Inglis[4] when he solved the same problem with an elliptical hole.

Inglis Solution

Following the details of the Inglis solution as we did the circular hole is too involved for consideration here, but the procedure was the same only with elliptical coordinates. The resulting hoop stress is given by

$$\sigma_{\eta\eta} = \frac{P[\sinh 2\xi + \cos 2\beta - e^{-2\xi}\cos 2(\beta-\eta)]}{\cosh 2\xi - \cos 2\eta} \qquad (76)$$

where ξ = elliptical coordinate

η = hyperbolic coordinate

β = angle of inclination of applied load to the ellipse

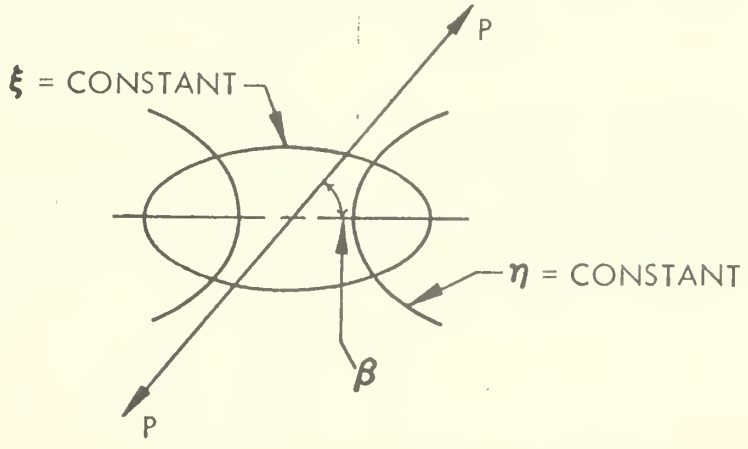

Fig. 35 Coordinate System

On the surface of the ellipse, which is specified by $\xi = \xi_o$, all of the quantities in equation (76) can be expressed in terms of the semi-major and minor axes a and b. The particular location of interest on the surface of the hole is specified by η, which functions in a manner very similar to θ in polar coordinates. For instance the tip A is specified by $\eta = 0$ and location B is given by $\eta = \frac{\pi}{2}$.

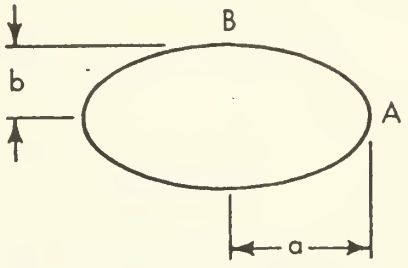

Fig. 36 Hole Dimensions

When these quantities are substituted into equation (76) and simplified, the hoop stresses at the hole are

$$\sigma_{\eta\eta}(A) = P\left[1 + \frac{2a}{b}\right] \tag{77a}$$

$$\sigma_{\eta\eta}(B) = -P \tag{77b}$$

An alternative form for the hoop stress in terms of radius of curvature at the tip has been popular. For this location on the ellipse, the radius of curvature is given by

$$R = -\frac{b^2}{a} \tag{78}$$

Substituting into expression (77), the hoop stress becomes

$$\sigma_{\eta\eta}(A) = P\left[1 + 2\sqrt{\frac{a}{R}}\right] \qquad (79)$$

This expression for the stress at the tip of the ellipse can be used to examine stresses at the tip of a crack. Equation (79) shows the local stress is higher, the longer the crack, and the sharpness of the crack also directly influences the local tip stress. The limit as $R \longrightarrow 0$ represents a mathematically sharp crack, producing a theoretically infinite stress at the tip. This has persisted up to the present time with additional analyses coming forth in the interm to both strengthen and refute the idea of a singularity.

Harking back to the Griffith energy theory, no light is shed on the discussion because even though this solution which contains a singularity was used, it yields a finite energy expression when integrated over the volume. Thus, the critical applied load P_{cr} is finite but from equation (79) the local stress is still infinite for a vanishing radius of curvature.

Neuber's Solution

Neuber's solution, similar in some respects to Inglis', adds evidence to the existence of a singularity. His treatise[64] on notch stresses is exhaustive in its coverage of the area and is somewhat complementary to the one previously discussed. In this instance it is the hyperbolae that are maintained as stress free boundaries and the mathematics become very involved.

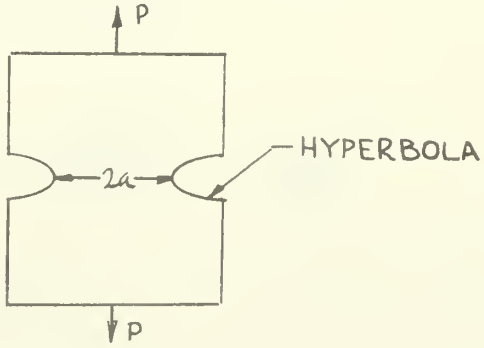

Fig. 37 Neuber's Notch Model

Neuber is able to generate stress functions to satisfy the stress free boundaries for a variety of loading conditions and geometries. For symmetrical notches subjected to tension, he found

$$\sigma_{\xi\xi} = \frac{A \cosh\xi \cos\eta}{\sinh^2\xi + \cos^2\eta}\left[2 + \frac{\cos^2\eta_0 - \cos^2\eta}{\sinh^2\xi + \cos^2\eta}\right] \tag{80}$$

where η_0 = value of η on hyperbolic notch

A = arbitrary constant

For tensile loading

$$A = \frac{P \sin\eta_0}{\eta_0 + \sin\eta_0 \cos\eta_0} \tag{81}$$

In terms of radius of curvature at the tip of the notch

$$R = \frac{a}{\tan^2\eta_0} \tag{82}$$

where 2a is the distance separating the notch tips. Equation (80) now becomes, in Neuber's form

$$\sigma_{\xi\xi} = \frac{2\left(\frac{a}{R}+1\right)P\sqrt{\frac{a}{R}}}{\left(\frac{a}{R}+1\right)\tan^{-1}\sqrt{\frac{a}{R}} + \sqrt{\frac{a}{R}}} \tag{83a}$$

Clearing the numerator for limiting purposes

$$\sigma_{\xi\xi} = \frac{2P}{\sqrt{\frac{R}{a}}\tan^{-1}\sqrt{\frac{a}{R}} + \frac{R}{a+R}} \tag{83b}$$

In the limit as $R \longrightarrow 0$, $\sigma_{\xi\xi} \longrightarrow \infty$, and the theory predicts a singularity in the same way that Inglis' solution did.

Williams Solution

Williams,[65] while investigating the stress field at the attachment boundary of swept wings, obtained a solution for plates with angular corners, both in bending and in stretching. These solutions can be adopted to find the details at a crack tip for comparison with Inglis and Neuber, by letting $\alpha = 180^{\circ}$.

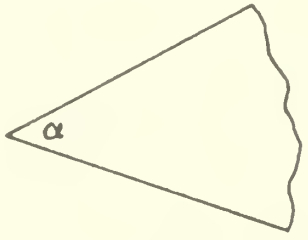

Fig. 38 Angular Corner of Plate

Considering the two sides as stress free and the other boundaries to be loaded in some resonable but unspecified way, Williams obtained a solution in terms of coordinates referenced to the crack tip (Fig. 39)

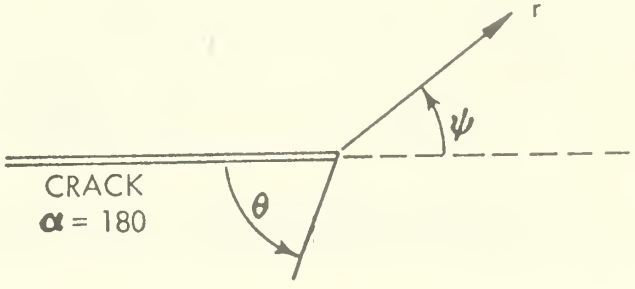

Fig. 39 Crack Geometry

This corresponds to a mathematically sharp crack like the preceding analysis, which applied only to a continum where atomic forces, spacings, etc. are not a consideration. The problem then is to solve $\nabla^4 \chi$. Using the biharmonic theorem[66], let

$$\chi = \phi_1 + r^2 \phi_2 \tag{84}$$

where

$$\nabla^2 \phi_1 = \nabla^2 \phi_2 = 0$$

Assuming a separable solution for the harmonic equation

$$\phi_1 = R(r)\,T(\theta) \tag{85}$$

gives

$$\phi_1 = \left[Ar^p + Br^{-p}\right]\left[C \sin p\theta + D \cos p\theta\right] \tag{86}$$

where p^2 is the separation constant. The same solution can be used for ϕ_2, with q^2 as the other separation constant,

$$\begin{aligned}\chi = &\left[Ar^p + Br^{-p}\right]\left[C \sin p\theta + D \cos p\theta\right] \\ &+ \left[Er^{q+2} + Fr^{-q+2}\right]\left[G \sin q\theta + H \cos q\theta\right]\end{aligned} \tag{87}$$

To simplify this expression somewhat, a look is taken at one of the boundary conditions $\left[\sigma_\theta\right]_{\theta=0} = \dfrac{\partial^2 \chi}{\partial r^2} = 0$

$$\begin{aligned}0 = &D\left[p(p-1)\,Ar^{p-2} + p(p+1)\,Br^{-p-2}\right] + \\ &H\left[(q+2)(q+1)\,Er^{q} + (-q+2)(-q+1)\,Fr^{-q}\right]\end{aligned} \tag{88}$$

If D and H are set equal to zero, other troubles are contracted later, so two options are open: (1) let q = p - 2 and relate A and E, or (2) let q = p + 2 and relate B and F. Arbitrarily selecting the first alternative,

$$q = p-2 \qquad \text{and} \qquad B = F = 0 \tag{89}$$

This will now satisfy the boundary conditions if A, D, E and H are appropriately

related. Simplifying and renaming constants

$$\chi = r^p \left[a \sin p\theta + b \cos p\theta + c \sin (p-2)\theta + d \cos (p-2)\theta \right] \quad (90)$$

To fit this into Williams[67] notation, let $p = \lambda + 1$

$$\chi = r^{\lambda+1} \left[a \sin (\lambda+1)\theta + b \cos (\lambda+1)\theta + c \sin (\lambda-1)\theta + d \cos (\lambda-1)\theta \right] \quad (91a)$$

$$\chi = r^{\lambda+1} F(\theta, \lambda) \quad (91b)$$

The stress components become

$$\sigma_\theta = \frac{\partial^2 \chi}{\partial r^2} = r^{\lambda-1} \left[\lambda(\lambda+1) \right] F(\theta, \lambda) \quad (92a)$$

$$\tau_{r\theta} = -\frac{1}{r} \frac{\partial^2 \chi}{\partial r \partial \theta} + \frac{1}{r^2} \frac{\partial \chi}{\partial \theta} = -r^{\lambda-1} \lambda F'(\theta, \lambda) \quad (92b)$$

Requiring σ_θ and $\tau_{r\theta}$ to vanish at $\theta = 0$ and $\theta = 2\pi$, implies that

$$F(0,\lambda) = F'(0,\lambda) = F(2\pi,\lambda) = F'(2\pi,\lambda) = 0 \quad (93)$$

When all of these homogeneous equations are written, the determinant of the coefficients requires

$$\sin 2\pi\lambda = 0 \quad (94)$$

or

$$\lambda_n = \pm \frac{n}{2} \qquad n = 0, 1, 2 \ldots$$

All four boundary conditions can be satisfied by relating a to c and b to d

$$\chi_n = r^{\frac{n}{2}+1} \left\{ c \left[\sin\left(\tfrac{n}{2}-1\right)\theta - \frac{n-2}{n+2} \sin\left(\tfrac{n}{2}+1\right)\theta \right] + d \left[\cos\left(\tfrac{n}{2}-1\right)\theta - \cos\left(\tfrac{n}{2}+1\right)\theta \right] \right\} \quad (95)$$

From this expression, it is seen that stress and strain are proportional to $\frac{n}{2}\left(\frac{n}{2}+1\right) r^{\frac{n}{2}-1}$ and displacements are proportional to $r^{\frac{n}{2}}$. In order for the displacements to be finite, $n \geq 0$, which introduces an anomaly. Obviously, one does not want to admit infinite displacements, but infinite stresses and strains are also uncomfortable. If the restriction is made on physical grounds that strains are finite, then $n \geq 2$. This result though, leaves the stress expressions proportional to positive powers of r only; consequently, the stress decreases as one moves toward the crack tip, which can also be ruled out on physical grounds. The lesser of the two evils seems to be to disallow infinite displacements and allow infinite displacement gradients. Physically, no real crack is mathematically sharp and whatever actual approximation there is to it will quickly produce strains in the region of the tip that are out of the elastic theory and another theory will apply. This will reflect what appears to be the closest duplication of reality within the assumptions upon which the calculations are based.

With the restriction on the eigenvalues specified as $n \geq 0$ the stress function can be represented by a summation

$$\chi = \sum_{0}^{\infty} \chi_n \tag{96}$$

To simplify the expressions, we will consider a loading and geometry that is symmetric about a horizontal line running through the crack. In this instance all of the functions must be even in ψ, and the sin terms can be discarded. In terms of ψ the expressions become

$$\chi_n = r^{\frac{n}{2}+1}\left\{a_n\left[\sin\left(\frac{n}{2}-1\right)(\psi+\pi) - \frac{n-2}{n+2}\sin\left(\frac{n}{2}+1\right)(\psi+\pi)\right]\right.$$
$$\left. + b_n\left[\cos\left(\frac{n}{2}-1\right)(\psi+\pi) - \cos\left(\frac{n}{2}+1\right)(\psi+\pi)\right]\right\} \tag{97}$$

Expanding and dropping sin κ terms,

$$\chi_n = r^{\frac{n}{2}+1}\left\{a_n\left[\sin\left(\tfrac{n}{2}-1\right)\pi\cos\left(\tfrac{n}{2}-1\right)\kappa - \frac{n-2}{n+2}\sin\left(\tfrac{n}{2}+1\right)\pi\cos\left(\tfrac{n}{2}+1\right)\kappa\right]\right. \tag{98}$$
$$\left. + b_n\left[\cos\left(\tfrac{n}{2}+1\right)\pi\cos\left(\tfrac{n}{2}-1\right)\kappa - \cos\left(\tfrac{n}{2}+1\right)\pi\cos\left(\tfrac{n}{2}+1\right)\kappa\right]\right\}$$

Writing out the first few terms

$$\chi = -a_1 r^{3/2}\left[\cos\tfrac{\kappa}{2} + \tfrac{1}{3}\cos\tfrac{3\kappa}{2}\right] + b_2 r^2\left[1-\cos 2\kappa\right] \tag{99}$$
$$+ a_3 r^{5/2}\left[\cos\tfrac{\kappa}{2} - \tfrac{1}{5}\cos\tfrac{5\kappa}{2}\right] + O(r^3) + \cdots$$

The associated stresses are

$$\sigma_r = \frac{a_1}{4r^{1/2}}\left[-5\cos\tfrac{\kappa}{2} + \cos\tfrac{3\kappa}{2}\right] + 2b_2\left[1+\cos 2\kappa\right] + \cdots \tag{100a}$$

$$\sigma_\kappa = \frac{a_1}{4r^{1/2}}\left[-3\cos\tfrac{\kappa}{2} - \cos\tfrac{3\kappa}{2}\right] + 2b_2\left[1-\cos 2\kappa\right] + \cdots \tag{100b}$$

$$\tau_{r\kappa} = \frac{a_1}{4r^{1/2}}\left[-\sin\tfrac{\kappa}{2} - \sin\tfrac{3\kappa}{2}\right] - 2b_2\sin 2\kappa + \cdots \tag{100c}$$

For loading perpendicular to the crack, b_2 can be shown to be zero[67]. Along the line of propagation, $\kappa = 0$, $\sigma_r = \sigma_\kappa = -\frac{a_1}{r^{1/2}}$, $\tau_{r\kappa} = 0$, and there is present a state of equi-biaxial tension regardless of the external loading so long as it is symmetrical. These stresses are principal, and the deformation state at the crack tip is pure dilation.

The corresponding displacements become

$$u_r = \frac{a_1 r^{\frac{1}{2}}}{2\mu}\left[\left(-\frac{5}{2}+\sigma\right)\cos\frac{\kappa}{2} + \frac{1}{2}\cos\frac{3\kappa}{2}\right] \qquad (101a)$$

$$u_\kappa = \frac{a_1 r^{\frac{1}{2}}}{2\mu}\left[\left(\frac{7}{2}-\sigma\right)\sin\frac{\kappa}{2} - \frac{1}{2}\sin\frac{3\kappa}{2}\right] \qquad (101b)$$

where

$$\sigma = \frac{\nu}{1+\nu}$$

One short comment on the solution. The field equations and part of the boundary conditions have been satisfied, but until all of the boundary conditions are met, there is no guarantee of uniqueness. So whether the form of the solution is correct or not cannot be established, but the trends are comparable to those of Inglis and Neuber. The solution is identical in its leading terms with that of Westergaard, and by invoking order conditions at infinity such as finite stresses, the solution becomes identical with Westergaard.

Westergaard's Solution

In 1934 Westergaard[68] published still another solution of the stress field around cracks. He used a complex variable approach based on developments by Carothers, who because of poor communication did a lot of work paralleling

Muskhelishville[69] and Kolassof. Using the Airy stress function, the field equations are represented by

$$\nabla^4 \chi = 0 \tag{102}$$

Any biharmonic function can be represented by

$$\chi = \phi_1 + y\phi_2 \tag{103}$$

where ϕ_1 and ϕ_2 are harmonic. This is why this solution lends itself well to complex variables. Westergaard chose χ such that

$$\chi = \mathrm{Re}\,\bar{\bar{Z}} + y\,\mathrm{Im}\,\bar{Z} \tag{104}$$

where $\bar{\bar{Z}} \equiv \frac{d\bar{\bar{Z}}}{dz}$ $\quad \bar{Z} \equiv \frac{d\bar{Z}}{dz}$ $\quad Z' \equiv \frac{dZ}{dz}$

The associated stresses are given by

$$\sigma_x = \frac{\partial^2 \chi}{\partial y^2} = \mathrm{Re}\,\bar{Z} - y\,\mathrm{Im}\,Z' \tag{105a}$$

$$\sigma_y = \frac{\partial^2 \chi}{\partial x^2} = \mathrm{Re}\,\bar{Z} + y\,\mathrm{Im}\,Z' \tag{105b}$$

$$\tau_{xy} = -\frac{\partial^2 \chi}{\partial x \partial y} = -y\,\mathrm{Re}\,Z' \tag{105c}$$

For an internal crack with an opening between Z = -a and Z = a and subjected to an average uniform tension P at infinity, he chose

$$\bar{Z} = \frac{P}{\sqrt{1 - \frac{a^2}{Z^2}}} \tag{106}$$

Z converges to p for $|z| \to \infty$. For the normal stress of interest along the line of propagation, y = 0

$$\sigma_y = \frac{P}{\sqrt{1 - \frac{a^2}{x^2}}} \tag{107}$$

This expression is valid for $|x| \geq a$, where again there is a singularity at the tip. The displacement field for $|x| < a$ describes an ellipse, so Westergaard has in essence obtained Inglis's solution by another means.

Irwin has shown how Z can be chosen differently so that more of the detail at the crack tip can be ferrated out. For instance

$$\bar{Z} = K_1\sqrt{2Z} \tag{108}$$

produces a discontinuity in displacements. In terms of polar crack coordinates

$$\sigma_x = \frac{K_1 \cos\theta/2}{\sqrt{2r}}\left[1 - \sin\frac{\theta}{2}\sin\frac{3\theta}{2}\right] \tag{109a}$$

$$\sigma_y = \frac{K_1 \cos\theta/2}{\sqrt{2r}}\left[1 + \sin\frac{\theta}{2}\sin\frac{3\theta}{2}\right] \tag{109b}$$

$$\tau_{xy} = \frac{K_1 \cos\theta/2}{\sqrt{2r}}\left[\sin\frac{\theta}{2}\cos\frac{3\theta}{2}\right] \tag{109c}$$

This rather unusual representation of cartesian stress components in terms of polar coordinates is due to the fact that taking fractional powers of Z is much easier in polar coordinates. As can be seen the normal and shear forces vanish on the crack surface, and the stress is singular at the tip. This is very similar to the work done by Williams but not as complete. The equivalence between this solution and the Williams method can be demonstrated by casting everything in polar coordinates. Recall

$$\chi = \mathrm{Re}\,\bar{\bar{Z}} + y\,\mathrm{Im}\,\bar{Z} \tag{110}$$

and

$$\bar{Z} = \sqrt{2}K_1 Z^{1/2}$$

$$\bar{\bar{Z}} = \frac{2}{3}\sqrt{2}K_1 Z^{3/2} + C$$

In polar coordinates

$$\chi = r^{3/2}K_1\sqrt{2}\left[\frac{2}{3}\cos\frac{3\theta}{2} + \sin\theta\sin\frac{\theta}{2}\right] \tag{111}$$

where the constant has arbitrarily been set equal to zero. Using trigonometric sum and difference formulas

$$\chi = \frac{\sqrt{2}\,K_1 r^{3/2}}{6}\left[3\cos\frac{\psi}{2} + \cos\frac{3\psi}{2}\right] \qquad (112)$$

Comparing with the Williams solution, they are identical if

$$a_1 = -K_1/\sqrt{2}$$

Irwin[71] evaluates K_1 by computing the energy change in the body as the crack runs and equates it to surface energy. This gives for plane strain

$$K_1^2 = \frac{2\mu\delta}{\pi(1-\nu)}$$

or for plane stress

$$K_1^2 = \frac{E\delta}{\pi}$$

There are those who strongly disagree with the existence of the stress singularity and G. I. Barenblatt is the most prominent advocate of a finite stress at the crack tip.

Barenblatt's Theory

Barenblatt[70] has written a number of papers on the subject of the finite stress condition in solid mechanics for various geometries and particularly cracks. His approach employs the minimum potential energy theorem to give him the added conditions needed over and above the differential equations and boundary conditions. He speaks of problems in applied physics, such as flow over an airfoil where other conditions are required to obtain a solution. In this instance it is the Kutta-Jakowski condition of finite velocity at the trailing edge.

In order to find this condition, he employs a variational technique and sets it up as follows:

M = Set of undetermined elements (constants or function of variables).

$M + \delta M$ = Variations of these elements.

$\bar{u}$ = Displacement corresponding to the M elements.

$\delta_1 \bar{u}$ = Variation of displacements according to geometric constraints with fixed M.

$\delta_2 \bar{u}$ = Variation of displacements corresponding to δ M.

The potential energy theorem states

$$\delta W - \delta A = 0 \tag{113}$$

where

W = elastic potential, or strain energy

A = Work of external forces

Furthermore,

$$\delta W = \delta_1 W + \delta_2 W \tag{114a}$$

$$\delta A = \delta_1 A + \delta_2 A \tag{114b}$$

where the meaning of the subscripts are defined above. Substituting into equation (113)

$$\delta_1 W - \delta_1 A + \delta_2 W - \delta_2 A = 0 \tag{115}$$

where $\delta_1 W$ and $\delta_1 A$ correspond to variations $\delta_1 \bar{u}$ with fixed M and $\delta_2 W$ and $\delta_2 A$ corresponding to δ M. Since $\delta_1 \bar{u}$ and δ M are independent variations.

$$\delta_1 W - \delta_1 A = 0 \tag{116a}$$

$$\delta_2 W - \delta_2 A = 0 \tag{116b}$$

The first gives the differential equations and boundary conditions, which correspond to an arbitrary set of M. But the M elements are actually specified by the second equation. For a linear system

$$2W = A \tag{117a}$$

$$2\delta W = \delta A \tag{117b}$$

$$2\delta_1 W + 2\delta_2 W = \delta_1 A + \delta_2 A \tag{117c}$$

Due to independence again

$$2\delta_2 W = \delta_2 A \tag{118}$$

Thus with the above

$$\delta_2 W = \delta_2 A = 0 \tag{119}$$

This condition is the crux of the Barenblatt theory; however to the author it does not seem valid. The minimum potential energy theorem is derived on the basis of a variation in the displacement field for a given geometry. In Griffith's[5] paper he also uses the minimum potential energy theorem to determine unstable crack configurations, but he found it necessary to modify the functional by adding a term representing surface energy in order to be correct. Lindsey[7] showed that this modified form is correct on the basis of conservation of energy. Therefore, it appears that equation (119) is not the criterion but should be

$$\delta W - \delta S = 0$$

where S represents surface energy. In this way a much different result is obtained, and the singular term does not vanish.

To continue with the computation of the energy terms anyway, the work done in opening a crack will be computed. The geometry and coordinate system used are shown in Fig. 40.

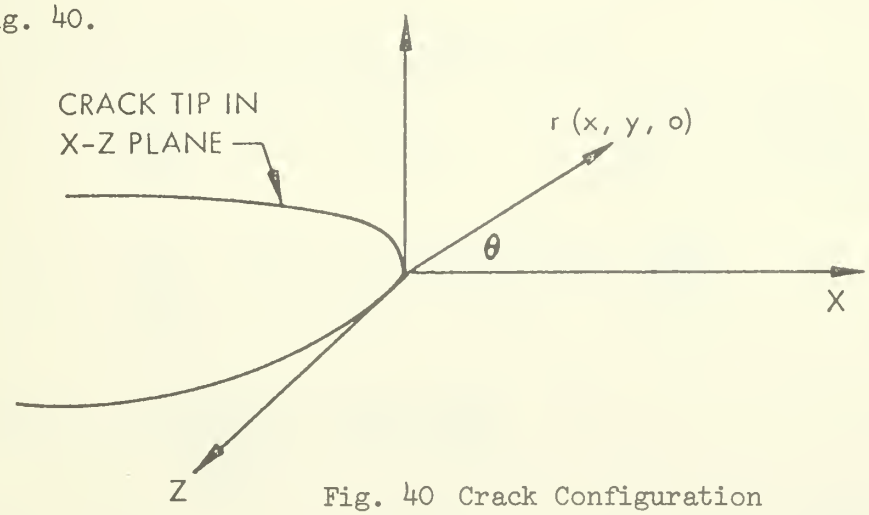

Fig. 40 Crack Configuration

Irwin[71], using Westgaard's method of solution, gives the stress field for a crack subjected to normal tension in plane strain as

$$\sigma_x = \frac{K_1 \cos\frac{\theta}{2}}{\sqrt{2r}}\left[1 - \sin\frac{\theta}{2}\sin\frac{3\theta}{2}\right] \tag{120a}$$

$$\sigma_y = \frac{K_1 \cos\frac{\theta}{2}}{\sqrt{2r}}\left[1 + \sin\frac{\theta}{2}\sin\frac{3\theta}{2}\right] \tag{120b}$$

$$\sigma_z = \nu(\sigma_x + \sigma_y) = \frac{2\nu K_1}{\sqrt{2r}}\cos\frac{\theta}{2} \tag{120c}$$

$$\tau_{xy} = \frac{K_1 \cos\frac{\theta}{2}}{\sqrt{2r}}\sin\frac{\theta}{2}\cos\frac{3\theta}{2} \tag{120d}$$

$$\tau_{yz} = \tau_{xz} = 0 \tag{120e}$$

The displacements are

$$u = \frac{K_1\sqrt{2r}}{2\mu}\cos\frac{\theta}{2}\left[(1-2\nu) + \sin^2\frac{\theta}{2}\right] \tag{121a}$$

$$v = \frac{K_1\sqrt{2r}}{2\mu}\sin\frac{\theta}{2}\left[2(1-\nu) - \cos^2\frac{\theta}{2}\right] \tag{121b}$$

$$w = 0 \tag{121c}$$

A second solution for pure shearing loads gives

$$\sigma_x = -\frac{K_2}{\sqrt{2r}}\sin\frac{\theta}{2}\left[2 + \cos\frac{\theta}{2}\cos\frac{3\theta}{2}\right] \tag{122a}$$

$$\sigma_y = \frac{K_2}{\sqrt{2r}}\sin\frac{\theta}{2}\cos\frac{\theta}{2}\cos\frac{3\theta}{2} \tag{122b}$$

$$\sigma_z = -\frac{2\nu K_2}{\sqrt{2r}}\sin\frac{\theta}{2} \tag{122c}$$

$$\tau_{xy} = \frac{K_2}{\sqrt{2r}}\cos\frac{\theta}{2}\left[1 - \sin\frac{\theta}{2}\sin\frac{3\theta}{2}\right] \tag{122d}$$

$$\tau_{yz} = \tau_{xz} = 0 \tag{122e}$$

$$u = \frac{K_2\sqrt{2r}}{2\mu} \sin\frac{\theta}{2}\left[2(1-\nu) + \cos^2\frac{\theta}{2}\right] \tag{122f}$$

$$v = -\frac{K_2\sqrt{2r}}{2\mu} \cos\frac{\theta}{2}\left[(1-2\nu) - \sin^2\frac{\theta}{2}\right] \tag{122g}$$

$$w = 0 \tag{122h}$$

For shear applied in the perpendicular direction

$$\sigma_x = \sigma_y = \sigma_z = \tau_{xy} = 0 \tag{123a}$$

$$\tau_{xz} = \frac{-K_3}{\sqrt{2r}} \sin\frac{\theta}{2} \tag{123b}$$

$$\tau_{yz} = \frac{-K_3}{\sqrt{2r}} \cos\frac{\theta}{2} \tag{123c}$$

$$u = v = 0 \tag{123d}$$

$$w = \frac{K_3}{\mu}\sqrt{2r} \sin\frac{\theta}{2} \tag{123e}$$

Now any general loading and geometry can be considered by superposing these three stress and displacement fields. To simplify the expressions the terms will be computed for special values of θ. The general stress field along the line of propagation, $\theta = 0$ is given by

$$\sigma_x = \frac{K_1}{\sqrt{2x}} \tag{124a}$$

$$\sigma_y = \frac{K_1}{\sqrt{2x}} \tag{124b}$$

$$\sigma_z = \frac{2\nu K_1}{\sqrt{2x}} \tag{124c}$$

$$\tau_{xy} = \frac{K_2}{\sqrt{2x}} \tag{124d}$$

$$\tau_{xz} = 0 \tag{124e}$$

$$\tau_{yz} = -\frac{K_3}{\sqrt{2x}} \tag{124f}$$

$$u = \frac{K_1\sqrt{2x}\,(1-2\nu)(1+\nu)}{E} \qquad x>0 \tag{125a}$$

$$v = \frac{-K_2\sqrt{2x}\,(1-2\nu)(1+\nu)}{E} \qquad x>0 \tag{125b}$$

$$w = 0 \qquad x>0 \tag{125c}$$

$$u = \pm\frac{2K_2}{E}\sqrt{-2x}\,(1-\nu^2) \qquad x<0 \tag{125d}$$

$$v = \pm\frac{2K_1}{E}\sqrt{-2x}\,(1-\nu^2) \qquad x<0 \tag{125e}$$

$$w = \pm\frac{2K_3}{E}\sqrt{-2x}\,(1+\nu) \qquad x<0 \tag{125f}$$

These expressions can be compared to Barenblatt's 1961 paper, by letting

$$\sqrt{2K_1} = 2N \qquad \sqrt{2K_2} = 2T_1 \qquad -\sqrt{2K_3} = 2T_2 \tag{126}$$

The crack with this stress field is allowed to open an amount h(z) as shown in Fig. 42.

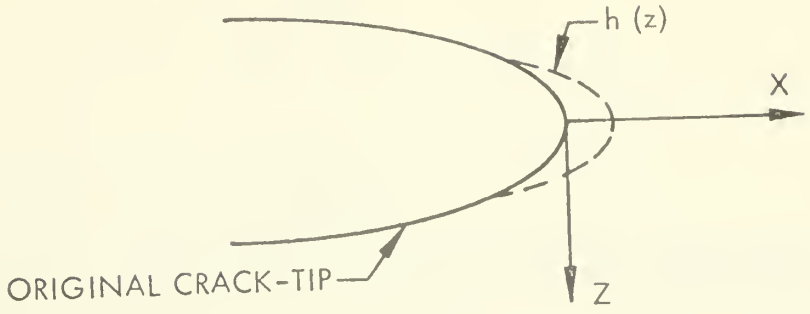

Fig. 42 Variation of Crack Surface

The work required to open this surface is

$$A = \int \bar{F} \cdot d\bar{u} = \int F_i \, du_i \tag{127}$$

where

$\bar{F}$ = force vector

$\bar{u}$ = displacement vector

If the force is linearly related to displacement $F_i = K u_i$

$$A = K \int u_i \, du_i = \frac{K u_i^2}{2} = \frac{1}{2} F_i u_i$$

and for constant force,

$$\delta A = \frac{1}{2} F_i \delta u_i \tag{128}$$

where the forces are held constant as required by the potential energy theorem.

In terms of stresses and displacements, the general expression is

$$\begin{aligned} \delta A = \frac{1}{2} \iiint \big[& \sigma_x \, dy dz \, \delta u + \sigma_y \, dx dz \, \delta v + \sigma_z \, dx dy \, \delta w \\ & + \tau_{xy} \, dy dz \, \delta v + \tau_{xy} \, dx dz \, \delta u + \tau_{xz} \, dz dy \, \delta w \\ & + \tau_{xz} \, dy dx \, \delta u + \tau_{yz} \, dx dy \, \delta v + \tau_{yz} \, dx dz \, \delta w \big] \end{aligned} \tag{129}$$

For this crack geometry (Fig. 42), there is no dy element involved in the opening or closing, so that stresses acting on dx dy and dz dy surfaces do no work.

$$\delta A = \frac{1}{2}\int\int\left[\sigma_y \delta v + \tau_{xy}\delta u + \tau_{yz}\delta w\right] dx\,dz \qquad (130)$$

Now the variation in displacement will be approximated by

$$\delta \bar{u} = \bar{u}_f - \bar{u}_i \qquad (131)$$

where

$\bar{u}_f$ = displacement after spread of crack

$\bar{u}_i$ = displacement before spread of crack

Since the displacements are referenced to the crack tip, the axes for $\bar{u}_f$ must be tanslated a distance h along the x axis (Fig. 42).

$$u_f = \pm \frac{4(1-\nu^2)}{E} T_1 \sqrt{-(x-h)} \qquad (132a)$$

$$v_f = \pm \frac{4(1-\nu^2)}{E} N \sqrt{-(x-h)} \qquad (132b)$$

$$w_f = \mp \frac{4(1+\nu)}{E} T_2 \sqrt{-(x-h)} \qquad (132c)$$

Consequently

$$\delta u = \frac{2(1+\nu)}{E}\left[\pm 2(1-\nu) T_1 \sqrt{h-x} - N(1-2\nu)\sqrt{x}\right] \qquad (133a)$$

$$\delta v = \frac{2(1+\nu)}{E}\left[\pm 2(1-\nu) N \sqrt{h-x} + T_1(1-2\nu)\sqrt{x}\right] \qquad (133b)$$

$$\delta w = \mp \frac{4(1+\nu)}{E} T_2 \sqrt{h-x} \qquad (133c)$$

Since the contributions to the energy released by the crack is the same from the lower surface as the upper surface, only one set of displacements will be used and a factor of two will be used on the energy integral.

$$\delta A = \int\int \frac{2(1+\nu)}{E}\left\{\frac{T_1}{\sqrt{x}}\left[2(1-\nu)T_1\sqrt{h-x} - N(1-2\nu)\sqrt{x}\right]\right. \tag{134}$$

$$\left. + \frac{N}{\sqrt{x}}\left[2(1-\nu)N\sqrt{h-x} + T_1(1-2\nu)\sqrt{x}\right] + \frac{T_2^2}{\sqrt{x}}2\sqrt{h-x}\right\}dx\,dz$$

Simplifying

$$\delta A = \frac{4(1+\nu)}{E}\int_A^B\int_0^h\left\{\left[(1-\nu)(T_1^2+N^2)+T_2^2\right]\sqrt{\frac{h-x}{x}}\right\}dx\,dz \tag{135}$$

The integral over x is a tabulated definite integral giving $h\pi/2$

$$\delta A = \frac{2(1+\nu)\pi}{E}\left\{(1-\nu)(T_1^2+N^2)+T_2^2\right\}\int_A^B h(z)\,dz \tag{136}$$

However the integral represents the area of new surface created. Barenblatt now states that this quantity must vanish and therefore

$$T_1 = N_1 = T_2 = 0$$

which eliminates all of the singular terms. However as mentioned earlier, if δA is equated to surface energy, δS,

$$S = \gamma\int_A^B h\,dz \tag{137}$$

A relationship is found among N_1, T_1, and T_2. For a two dimensional configuration in plane strain $T_1 = T_2 = 0$

$$\frac{2(1-\nu^2)\pi N^2}{E} = \gamma \tag{138}$$

or

$$N^2 = \frac{E\gamma}{2\pi(1-\nu^2)} \tag{139}$$

For plane stress $E/1-\nu^2$ is replaced by E

$$N^2 = \frac{E\gamma}{2\pi} \tag{140}$$

which agrees with Irwin's[71] result.

The comparison of displacements made by Barenblatt[72] for the two cases is very interesting. If the singular term remains; i.e. $N \neq 0$, the displacement of the crack surface is shown in Fig. 43a.

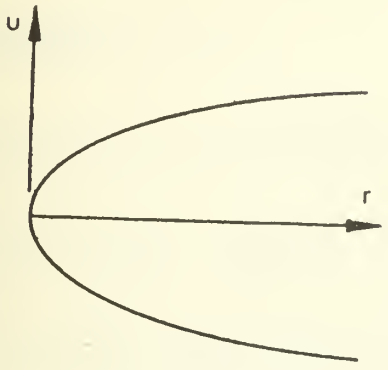

Fig. 43a

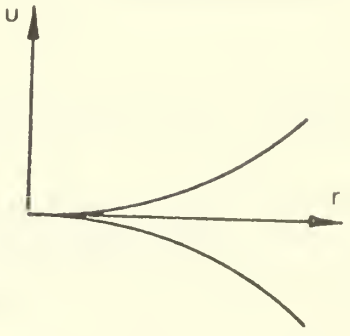

Fig. 43b

Crack Surface Contours

This corresponds to the crack contours used by Inglis and Neuber and derived by Westergaard and Williams. Figure 43b is a description of the crack contour for the nonsingular stress field $N = 0$, proposed by Barenblatt. The smoothness of closure at the tip leads him to postulate the need for inclusion of atomic cohesive forces in the energy balance for fracture prediction. To do this he subdivides the crack into two regions: one where cohesive forces are significant and one where they are not. He further assumes that the first region is small compared to the second. From this a detailed theory is fabricated, which can be extracted from his many papers[73,74].

REFERENCES

1. T. Alfrey, "Mechanical Behavior of High Polymers," Interscience Publishers, New York, 1948.

2. D. C. Drucker, Some Remarks on Flow and Fracture", in Developments in Mechanics, p. 201,

3. G. R. Irwin, "A Continium Mechanics View of Crack Propagation", Metallurgical Reviews, Vol. 10, No. 38, p. 223, 1965.

4. C. E. Inglis, "Stresses in a Plate Due to the Presence of Cracks and Sharp Corners," Proc. Institute of Naval Architects, March 14, 1913.

5. A. A. Griffith, "The Phenomena of Rupture and Flow in Solids," Phil. Trans. of Royal Society, Series A, Vol. 221, 1921.

6. A. A. Griffith, "The Theory of Rupture," Proceedings of the First International Congress for Applied Mechanics, 1924.

7. G. H. Lindsey, "Energy Criteria for Elastic Fracture," GALCIT SM 65-20, California Inst. of Tech., August 1965.

8. B. Orowan, "Energy Criteria of Fracture," J. Welding Research Supplement, March 1955, p. 157A.

9. A. L. Starr, Proceedings Cambridge Phil. Soc., Vol. 24, p. 489, 1927.

10. S. Timoshenko and J. N. Goodier, "Theory of Elasticity," McGraw-Hill, New York, 1951.

11. I. S. Sokolnikoff, "Mathematical Theory of Elasticity," McGraw-Hill, New York, 1956.

12. A. E. H. Love, "The Mathematical Theory of Elasticity," Oxford Press, London, 1927.

13. J. P. Berry, "Fracture in Glassy Polymers I," J. Poly. Sci., Vol. 50, p. 107, 1961.

14. A. M. Bueche and J. P. Berry, "The Mechanisms of Polymer Failure," Conference on Fracture, National Academy of Sciences, Swampscott, Mass, 1957.

15. J. P. Berry, "Fracture in Glassy Polymers I," J. Poly. Sci., Vol. 50, p. 107, 1961.

16. Schwarzl and Staverman
    G. H. Lindsey, "Fracture Stress and Strength of High Polymers," GALCIT SM 64-44, CIT, December 1964. Translation of article by F. Schwarzl and A. J. Staverman, Die Physik der Hochpolymeren, Vol. IV, Springer-Verlag, 1956.

17. J. P. Berry, "Fracture Processes in Polymeric Materials II," J. Poly. Sci., Vol. 50, p. 313, 1961.

18. R. P. Kambour, "Refractive Indices and Compositions ofCrazes in Several Glassy Polymers", J. Poly. Sci., p. 1159, 1964.

19. R. P. Kambour, "Refractive Index and Composition of PMM Fracture Surface Layers," J. Poly. Sci., A Vol. 2, p. 4165, 1964.

20. R. P. Kambour, "Refractive Index and Composition of PMM Fracture Surface Layers," J. Poly. Sci. A, Vol. 2, p. 4165, 1964.

21. R. P. Kambour, "Mechanism of Fracture in Glassy Polymers I", J. Poly. Sci. A, Vol. 3, p. 1713, 1965.

22. J. P. Berry, "Fracture Processes in Polymeric Materials VII, J. Poly. Sci A., Vol. 3, p. 2027, 1965.

23. R. S. Rivlin and A. G. Thomas, "Rupture of Rubber I, Characteristic Energy of Tearing," J. Poly. Sci., Vol. 10, p. 291, 1953.

24. A. G. Thomas, "Rupture of Rubber II, Strain Concentration at an Incision," J. Poly. Sci., Vol. 18, p. 177, 1955.

25. H. W. Greensmith and A. G. Thomas, "Rupture of Rubber III, Determination of Tear Properties," J. Poly. Sci., Vol. 18, p. 189, 1955.

26. H. W. Greensmith, "Rupture of Rubber IV, Tear Properties of Vulcanizates Containing Carbon Black," J. Poly. Sci., Vol. 21, p. 175, 1956.

27. A. G. Thomas, "Ripture of Rubber V," J. Poly. Sci., Vol. 31, p. 467, 1958.

28. A. G. Thomas, "Rupture of Rubber VI, Further Experiments on the Tear Criterion," J. Poly. Sci., Vol. 3, p. 168, 1960.

29. H. W. Greensmith, "Rupture of Rubber VII, Effect of Rate of Extension in Tensile Tests," J. App. Poly. Sci., Vol. 3, p. 175, 1960.

30. H. W. Greensmith, "Rupture of Rubber VIII, Comparison of Tear and Tensile Rupture Measurements," J. App. Poly. Sci., Vol. 3, p. 183, 1960.

31. H. W. Greensmith, L. Mullins, A. G. Thomas, " Rupture of Rubber," Trans. Soc. Rheology, Vol. IV, p. 179, 1960.

32. M. L. Williams and R. A. Schapery, "Spherical Flaw Instability in Hydrostatic Tension," International Journal of Fracture Mechanics, Vol. 1, 1965.

33. S. Timoshenko and J. N. Goodier, "Theory of Elasticity," McGraw-Hill, New York, 1951.

34. I. N. Sneddon, "The Distribution of Stress in the Neighborhood of a Crack in an Elastic Solid," Proc. Royal Society, Series A, Vol. 187, 1946, p. 229.

35. R. A. Sack, "Extension of Griffity's Theory of Rupture to Three Dimensions," Proc. Physical Soc. of London, Vol. 58, 1946, p. 729.

36. M. L. Williams, "Initiation and Growth of Viscoelastic Fracture," Int. J. of Frac. Mech., Vol. I, No. 4, 1965.

37. A. N. Gent and P. B. Lindley, "Internal Rupture of Bonded Rubber Cylinders in Tension," Proc. of Royal Society, Vol. 249A, 1959, p. 195.

38. M. L. Williams and R. A. Schapery, "Spherical Flaw Instability in Hydrostatic Tension", International Journal of Fracture Mechanics, Vol. 1, 1965.

39. A. E. Green and W. Zerna, "Theoretical Elasticity," McGraw-Hill, New York, 1951.

40. M. Levinson, "The Complementary Energy Theorem in Finite Elasticity," Clarkson College of Tech., Potsdam, New York.

41. G. H. Lindsey, "Hydrostatic Tensile Fracture of a Polyurethane Elastomer", Aerospace Research Laboratory Report ARL 66-0029, 1966.

42. M. Levinson, "The Finite Strain Behavior of Incompressible Hollow Cylinders and Spheres under Internal Pressure," GALCIT SM 62-48, Calif. Inst. of Tech., Dec. 1962.

43. P. J. Blatz, W. L. Ko, and A. R. Zak, "Fundamental Studies Relating to the Mechanical Behavior of Solid Rocket Motors," GALCIT 118A Progress Report No. 5, Calif. Inst. of Tech., 1962.

44. R. B. Kruse, "Laboratory Characterization of Solid Propellant Mechanical Properties", AIAA Paper No. 65-147, 6th Solid Prop. Rocket Conf., Feb 1965.

45. A. Nadai, "Theory of Flow and Fracture of Solids," McGraw-Hill, New York, 1950.

46. P. W. Bridgman, "The Physics of High Pressure," G. Bell and Sons Ltd., London 1949.

47. P. W. Bridgman, "Studies in Large Plastic Flow and Fracture," McGraw-Hill, New York, 1952.

48. S. A. Murch, Personal Communication.

49. A. C. Pipkin and R. S. Rivlin, "Mechanics of Rate - Independent Materials," ZAMP, Vol. 16, p. 313, 1965.

50. T. L. Smith, "Ultimate Tensile Properties of Elastomers," J. Poly. Sci. Part A, Vol. 1 p. 597, 1963.

51. M. L. Williams, "Engineering Analysis of Viscoelastic Media," AIAA Vol. 2, No. 5, p. 785, 1964.

52. R. Hill, The Mathematical Theory of Plasticity, Oxford Press, 1950.

53. R. F. Landel and R. F. Fedors, "Rupture of Amorphous Unfilled Polymers," in Fracture Processes in Polymeric Solids, Interscience Publishers, New York, 1964.

54. G. M. Martin, F. L. Roth and R. D. Stiekler, "Behavior of a Pure Gum Vulcanizate in Tension," Trans. Inst. of Rubber Ind. Vol. 32, p. 189, 1956.

55. M. L. Williams and R. A. Schapery, "Studies of Viscoelastic Media," Aeronautical Research Laboratories, Wright-Patterson Air Force Base, Ohio, ARL 62-366, June 1962.

56. R. E. Siron and T. H. Duerr, "An Engineering Approach to Multiaxial Failure in Solid Propellants," Bulletin of 5th Meeting, ICRPG Working Group on Mechanical Behaviors, 1966.

57. R. J. Farris, "The Character of the Stress-Strain Function for Solid Propellant", Bulletin of 5th Meeting ICRPG Working Group on Mechanical Behavior, 1966.

58. R. J. Farris, "Strain Dilatation in Solid Propellants", Bulletin of the 3rd Meeting, ICRPG Working Group on Mechanical Behavior, 1964.

59. M. A. Miner, "Cumulative Damage in Fatigue," J. Applied Mechanics, Vol. 12, p. 159, 1945.

60. M. L. Williams, P. J. Blatz and R. A. Schapery, "Fundamental Studies Relating to Systems Analysis of Solid Propellants," GALCIT Report SM 61-5, California Inst. of Tech., 1961.

61. M. L. Williams, "Fracture of Viscoelastic Materials," in Fracture of Solids, Interscience Publishers, New York, 1963.

62. K. W. Bills, R. D. Steele, and G. J. Svob, "Prediction of Useful Life of Propellant-Liner Bonds Subjected to Aerodynamic Heating," Bulletin of 5th Meeting ICRPG Working Group on Mechanical Behavior, 1966.

63. G. Kirsch, "Die Theorie der Elasticitat und die Bednirfruss der Festigkeitlehre," Zeit. des Verein Dentsches Ingenieure, Vol. 32, 1898.

64. H. Neuber, "Theory of Notch Stresses," J. W. Edwards Co., Ann Arbor, Michigan, 1946.

65. M. L. Williams, "Stress Singularities Resulting from Various Boundary Conditions in Angular Corners of Plates in Extension," Journal of Applied Mechanics, Vol. 74, 1952, p. 526.

66. Y. C. Fung, Foundations of Solid Mechanics, Prentice Hall Inc. 1965.

67. M. L. Williams, "On the Stress Distribution at the Base of a Stationary Crack," J. App. Mech., March 1957.

68. H. M. Westergaard, "Bearing Pressure and Cracks," J. Appl. Mech., Vol. 6, No. 2, 1939.

69. N. I. Muskhelishvilli, Some Basic Problems in Theory of Elasticity, Nordhoff Publishers, Holland, 1953.

70. G. I. Barenblatt, "On the Finiteness of Stresses at the Leading Edge of an Arbitrary Crack," PMM Vol. 25, No. 4, p. 752, 1961.

71. G. R. Irwin, "Fracture," in Handbuch der Physik, Vol. VI, p. 551, Springer-Verlag, Berlin, 1958.

72. G. I. Barenblatt, "On Finiteness Conditions in the Mechanics of Continuous Media. Static Problems of the Theory of Elasticity," PMM Vol. 24, No. 2, p. 311, 1960.

73. G. I. Barenblatt, "On Some General Concepts of the Mathematical Theory of Brittle Fracture," PMM Vol. 24, No. 4, p. 630, 1964.

74. G. I. Barenblatt, "The Mathematical Theory of Equilibrium Cracks in Brittle Fracture," Advances in Applied Mechanics, Vol. VII, 1962.

75. J. D. Burton and J. S. Noel, "Viscoelastic Fracture in Plane Stress and Plane Strain Fields", Bulletin of 6th Meeting, ICRPG Working Group on Mechanical Behavior, 1967.

DISTRIBUTION LIST

	Copies
Defense Documentation Center	20
Naval Weapons Center China Lake, California	10
Dr. Gerald H. Lindsey Department of Aeronautics Naval Postgraduate School Monterey, California	5
Mr. Eugene Francis United Technology Center, Bldg. 5200 1050 East Arquez Ave Sunnyvale, California	3
LT Scott Beckwith Air Force Rocket Laboratory RPMCB Edwards Air Force Base California 93523	1
Mr. Donald Saylak Air Force Rocket Laboratory RPMCB Edwards Air Force Base California 93523	1
Library Naval Postgraduate School Monterey, California	2
Dr. Robert E. Ball Department of Aeronautics Naval Postgraduate School Monterey, California	1
Dr. Ulrich Haupt Department of Aeronautics Naval Postgraduate School Monterey, California	1
Dr. Charles H. Kahr Department of Aeronautics Naval Postgraduate School Monterey, California	1

DISTRIBUTION LIST (Cont.)

	Copies
Dr. Allen E. Fuhs Department of Aeronautics Naval Postgraduate School Monterey, California	2
Dr. Louis V. Schmidt Department of Aeronautics Naval Postgraduate School Monterey, California	1

UNCLASSIFIED

Security Classification

DOCUMENT CONTROL DATA - R & D

(Security classification of title, body of abstract and indexing annotation must be entered when the overall report is classified)

1 ORIGINATING ACTIVITY *(Corporate author)*

Naval Postgraduate School
Monterey, California

2a. REPORT SECURITY CLASSIFICATION

Unclassified

2b. GROUP

3 REPORT TITLE

Viscoelastic Fracture - An Expository Treatment of Polymer Failure

4 DESCRIPTIVE NOTES *(Type of report and, inclusive dates)*

Technical Report, 1967

5. AUTHOR(S) *(First name, middle initial, last name)*

Lindsey, Gerald H.

6 REPORT DATE	7a. TOTAL NO. OF PAGES	7b. NO. OF REFS
1 November 1967	108	

8a. CONTRACT OR GRANT NO.	9a. ORIGINATOR'S REPORT NUMBER(S)
b. PROJECT NO. Work Request No. 60530	NPS-57LI7111A
c.	9b. OTHER REPORT NO(S) *(Any other numbers that may be assigned this report)*
d.	

10. DISTRIBUTION STATEMENT

This document has been approved for public release and sale; its distribution is unlimited.

11. SUPPLEMENTARY NOTES	12. SPONSORING MILITARY ACTIVITY
	Naval Ordnance Test Station

13 ABSTRACT

Fracture in viscoelastic materials is discussed here as an extension of elastic fracture. Using continuum theory, three broad approaches are treated in detail, including energy failure surfaces and cumulative damage. Typical experimental work is reported to demonstrate its impact on the theories; however much more experimental work has been omitted than has been included. The attempt and purpose has been to discuss in detail the fundamentals of the subject, and then subsequently build upon that with samplings of experimental results.

The concluding section on the classical works dealing with stress analysis of crack geometries is for the purpose of comparison and unifacation. How these analyses relate to the energy theories is the basis of comparison.

DD FORM 1 NOV 65 1473 (PAGE 1)

S/N 0101-807-6811

UNCLASSIFIED

Security Classification

A-31408

14 KEY WORDS	LINK A		LINK B		LINK C	
	ROLE	WT	ROLE	WT	ROLE	WT
Viscoelastic Fracture						
Fracture						
Failure						
Polymer Fracture						
Energy of Fracture						
Crack						